QuieterRail - A step change in prediction, mapping, acceptance testing and cost-effective mitigation for railway noise and vibration

Deliverable D4.2

Noise and vibration reductions

Project acronym:	QuieterRail
Starting date:	01/10/2024
Duration (in months):	36
Call (part) identifier:	HORIZON-ER-JU-2023-EXPLR-01
Grant agreement no:	101176865
Due date of deliverable:	Month 18
Actual submission date:	18-03-2026
Responsible/Author:	David Thompson (ISVR)
Version	1.0
Dissemination level:	PU
Status:	Issued

Reviewed: yes

This project has received funding from the European Union's Horizon Europe research and innovation programme under Grant Agreement No 101176865. UK participants are supported by UKRI grant numbers 10133356 (Cambridge) and 10139376 (Southampton). The work of the Swiss participants has received funding from the Swiss State Secretariat for Education, Research and Innovation (SERI).

Co-funded by the European Union

Document history		
Revision	*Date*	*Description*
0.1	25/02/2026	First draft for internal review
0.2	03/03/2026	Second draft for TMT review
0.3	10/03/2026	Final draft after TMT review
0.4	16/03/2026	Final draft, including revised Appendix C
1.0	18/03/2026	Final approved version submitted to ERJU

Report contributors			
Name	Beneficiary Short Name	Version	Details of contribution
David Thompson	ISVR	0.1	Report structure and writing all Sections of the main report plus Appendix A
Qianqian Li, Giacomo Squicciarini	ISVR	0.1	Writing Section 5
Qianqian Li	ISVR	0.1	All noise calculations of main report
Pieter Reumers	KU Leuven	0.1	All vibration calculations of main report
Pinar Yilmazer Rosa Casquero	UIC	0.1	Support for definition of parameters
Bart Van Damme, Slimane Ouakka, Chakib Drias	EMPA	0.1	Writing Appendix B
Mehdi Meguenni, Maurice Ammann, Joël Cugnoni	HES-SO	0.1	Writing Appendix B and C
David Thompson	ISVR	0.2	Revision after review by WP4 partners
Pascal Bouvet	Vibratec	0.2	TMT review
Geert Degrande	KU Leuven	0.2	TMT review
David Thompson	ISVR	0.3	Revision after review by TMT
Joël Cugnoni	HES-SO	0.4	Revision of Appendix C after review by TMT
Mariya Kayalova	RINA	0.4	Quality check
Jose Bertolin	UNIFE	1.0	Final review and submission

Co-funded by the European Union

Disclaimer

The information in this document is provided "as is", and no guarantee or warranty is given that the information is fit for any particular purpose. The content of this document reflects only the author's view – the Joint Undertaking is not responsible for any use that may be made of the information it contains. The users use the information at their sole risk and liability.

The content of this report does not reflect the official opinion of the Europe's Rail Joint Undertaking (EU-Rail JU). Responsibility for the information and views expressed herein lies entirely with the author(s).

Co-funded by the European Union

Table of Contents

Co-funded by the European Union

Europe's Rail
Co-funded by the European Union

Europe's Rail
Co-funded by the European Union

List of Figures

Co-funded by the European Union

Co-funded by the European Union

Co-funded by the European Union

Europe's Rail

Co-funded by the European Union

List of Tables

Co-funded by the European Union

Co-funded by the European Union

Executive Summary

This report is produced within Work Package 4 of QuieterRail, which concerns “Track optimisation for noise, vibration and life cycle costs”. The report forms Deliverable D4.2 of the project. The overall aim of WP4 is to develop a web-based tool to support the whole system optimisation of railway tracks in terms of noise, vibration and life cycle costs. To support the development of this tool, extensive calculations are carried out in WP4 of noise and vibration reductions associated with a range of abatement methods and for different combinations of track components, which will be stored in a database to be used by the tool. The calculations are performed using complementary physics-based models available to the project partners. This report summarises the input parameters and calculation results of noise and vibration source levels accounting for mitigation measures.

A set of Use Cases for track system optimisation is reported in Deliverable D4.1. These Use Cases are limited to the most common situation of straight, plain track, with trains passing at constant speed. Typical parameter values associated with them are defined here for the calculation of noise and vibration levels. Corresponding calculation results are then presented for both noise and vibration. The results for noise are determined in terms of one-third octave band spectra of sound power levels for a unit roughness, which can then be combined with roughness spectra taking account of the train speed. Similarly, the results for ground vibration are expressed as one-third octave band spectra of force density for a unit unevenness. In addition, vibration spectra on the ground surface at different distances from the track for a unit unevenness are also produced. For both noise and vibration, example results are presented in which the results are combined with example roughness/unevenness spectra to illustrate the trends.

The results allow the effect of various mitigation measures to be quantified. For noise these include rail dampers, rail shields, optimised rail pads and acoustic rail grinding. For vibration they include measures at the track, such as under-sleeper pads, under-ballast mats and track maintenance to improve track unevenness, and measures in the transmission path including heavy masses next to the track, subgrade stiffening, and stiff or soft wave barriers. An assessment of the uncertainty in the various predictions of noise and vibration has also been carried out.

A benchmark study has been performed comparing the results of the TWINS and ToPNoise models for track dynamics and radiation. The effect of various track configurations on the stresses in the ballast has also been calculated and can be used to give an indication of the effect on track settlement.

Co-funded by the European Union

Abbreviations and acronyms

Abbreviation / Acronym	Description
BEM	Boundary Element Method
EMPA	Swiss Federal Laboratories for Materials Science and Technology (Eidgenössische Materialprüfungs- und Forschungsanstalt)
ERJU	Europe's Rail Joint Undertaking
FEM	Finite Element Method
HES-SO	University of Applied Sciences and Arts Western Switzerland (Haute école spécialisée de Suisse occidentale)
ISVR	Institute of Sound and Vibration Research (University of Southampton, UK)
LCC	Life cycle costs
MAWP	Multi-Annual Work Programme
TDR	Track Decay Rate
TNE	Train Noise Expert (prediction software developed by ISVR for pass-by and stationary noise)
ToPNoise	Tool for the Prediction of Noise (prediction software developed by EMPA and HES-SO)
TWINS	Track-Wheel Interaction Noise Software (prediction model for rolling noise)
UBM	Under-ballast mats
UIC	International Union of Railways (Union Internationale des Chemins de fer)
USP	Under-sleeper pads
WP	Work Package

Co-funded by the European Union

1. Introduction

1.1 Background

The present document constitutes Deliverable D4.2 “Noise and vibration reductions” in the framework of the Exploratory Project 101176865 – QuieterRail – HORIZON-JU-ER-2023-01 as described in the EU-RAIL MAWP. It is produced in the context of Work Package 4 (WP4) “Track optimisation for noise, vibration and life cycle costs”. The overall aim of WP4 is to develop a web-based tool to support the whole system optimisation of railway tracks in terms of noise, vibration and life cycle costs (LCC). WP4 is led by ISVR, in collaboration with EMPA, HES-SO, KU Leuven and UIC.

Noise and vibration abatement methods often introduce additional costs to the railway, due to their installation costs and potentially increased maintenance costs, as well as due to effects on other parts of the system. It is therefore essential to demonstrate whether the benefits of these abatement methods outweigh these additional costs and to integrate noise and vibration abatement methods into asset management plans. Aside from traditional methods to reduce noise of the track (e.g. rail dampers), different components of the track (e.g. rail pads, sleepers) are considered as well.

To support the development of this tool, calculations are carried out in Task T4.2 to quantify noise and vibration reductions associated with a range of abatement methods and for different combinations of track components. The results of these calculations will be stored in a database to be used by the tool. The calculations in Task T4.2 are performed using complementary physics-based models available to the project partners ISVR, EMPA, HES-SO and KU Leuven.

The web-based tool itself will be developed in Task T4.4, due to commence in Month 19 (April 2026), which includes a first sub-task “Determine specifications for web-based tool”. This will include the definition of the data repository as well as the menu structure. These aspects are therefore not described here.

1.2 Objectives

The purpose of this document is to describe the calculations of noise and vibration source levels to be included in the database for the web-based tool for track optimisation. Results for a range of abatement methods are also specified. These parameters and abatement methods are aligned with the work of Task T4.1, which has defined a set of Use Cases in Deliverable D4.1 [1].

Co-funded by the European Union

2. Calculation parameters

In defining the Use Cases for WP4 in Deliverable D4.1 [1], it has been decided to concentrate on rolling noise and rolling-induced vibration on straight track. These represent the most common situation and are identified as the primary sources due to the high availability of data, mature models, and strong influence from track design parameters. They will therefore form the core of the web-based tool. Other sources can be included passively in the tool by means of user-defined datasets, but these are not discussed further here.

The parameters required to calculate rolling noise and ground-borne vibration are summarised in the following sections. The purpose is to define a typical range of parameters rather than to cover every eventuality occurring in practice.

2.1 Track parameters

2.1.1 Rail

Two common types of rail are considered: 60 kg/m and 54 kg/m. The main parameters used for the rail are listed in Table 1. It is expected that changes to the rail type (especially for nominally similar masses) will have only marginal effects on noise and vibration.

Table 1. Rail parameters

Rail type	60E2	54E1
Mass density (kg/m^3)	7850	7850
Mass per unit length (kg/m)	60.21	54.77
Second moment of area, vertical bending (cm^4)	3038.3	2337.9
Second moment of area, lateral bending (cm^4)	512.7	419.2
Shear coefficient (-)	0.4	0.4
Damping loss factor / $\tan\delta$ (-)	0.02	0.02

2.1.2 Rail pads

Example values for rail pad properties are provided in [2-4]. Based on this, five typical stiffnesses of rail pad are considered for ballasted track, which will be identified as: very soft, soft, medium, stiff and very stiff. The corresponding parameters used for the rail pad are listed in Table 2.

Table 2. Rail pad parameters

Rail pad type	Very soft	Soft	Medium	Stiff	Very stiff
Vertical static stiffness (MN/m)	50	100	150	250	700
Vertical low-frequency stiffness (MN/m)	60	120	200	350	1000
Vertical acoustic stiffness (MN/m)	100	200	400	1000	2000
Lateral acoustic stiffness (MN/m)	30	45	60	120	175
Vertical damping loss factor / $\tan\delta$ (-)	0.15	0.15	0.15	0.15	0.15
Lateral damping loss factor / $\tan\delta$ (-)	0.15	0.15	0.15	0.15	0.15

Here a distinction is made between the static stiffness (which is only included for reference), the loaded low-frequency dynamic stiffness (relevant to ground-borne vibration) and the unloaded high-frequency dynamic stiffness ('acoustic' stiffness, relevant to rolling noise). Information on lateral stiffness is less commonly available, but it is less critical to the calculated noise levels. Typically, the lateral stiffness is a factor of between 3 and 10 smaller than the vertical stiffness. In principle, to include pads with higher

Co-funded by the European Union

damping, the damping loss factor associated with the acoustic stiffness can be raised to 0.3 or 0.6. However, it should be noted that the stiffness will become more strongly frequency dependent, and consequently the ratio of acoustic stiffness to low-frequency dynamic stiffness will increase. So, for example, a 'soft' pad for vibration may become a 'medium' one for noise if the loss factor is increased.

2.1.3 Sleepers

Three types of concrete sleeper are considered for ballasted track: a lighter monobloc (B91) and a typical heavier monobloc as well as a bibloc sleeper. The parameters used for the concrete sleepers are listed in Table 3. The bibloc sleeper is represented only by its mass, whereas other sleeper types include their flexural properties.

Table 3. Parameters for concrete sleepers

Sleeper type	Monobloc (B91)	Monobloc (heavy)	Bibloc
Mass density (kg/m^3)	2436	2436	n/a
Total mass (kg)	280	330	120 [1]
Length (m)	2.6	2.6	0.84 [1]
Height at rail seat (m)	0.214	0.235	n/a
Height at centre (m)	0.175	0.210	n/a
Width of top at rail seat (m)	0.160	0.161	0.21
Width of top at centre (m)	0.173	0.150	n/a
Width of base at rail seat (m)	0.271	0.284	0.25
Width of base at centre (m)	0.220	0.220	n/a
Young's modulus (longitudinal) (GPa)	46.3	46.3	n/a
Young's modulus (transverse) (GPa)	20.0	20.0	n/a
Total support surface (m^2)	0.68	0.69	0.42 [2]
Poisson's ratio (-)	0.2	0.2	n/a
Damping loss factor / tanδ	0.016	0.016	n/a
Sleeper spacing (m)	0.6	0.6	0.6

In addition, wood, steel and composite sleepers are considered, as listed in Table 4. The steel sleepers have a hollow profile so details of the profile will be added to a model, not the dimensions in Table 4. For composite sleepers, parameters are available at ISVR for three types (Sicut, KLP and FFU); the corresponding values are listed in Table 4. A single value of sleeper spacing is considered for each sleeper type as its influence on noise and vibration is expected to be small. Note that not all rail pad stiffness values will apply for wood, steel or composite sleepers.

[1] Half sleeper
[2] Full sleeper

Co-funded by the European Union

Table 4. Sleeper parameters

Sleeper type	Wood	Steel	Composite 1 (recycled plastic)	Composite 2 (steel-reinforced polymer)	Composite 3 (fibre-reinforced foamed urethane)
Mass density (kg/m^3)	800	7850	825	1004	747
Total mass (kg)	77.4	74.3	65.4	95.8	76.8
Length (m)	2.5	2.42	2.6	2.6	2.5
Height at rail seat (m)	0.150	0.1	0.12	0.148	0.16
Height at centre (m)	0.148	0.1	0.12	0.148	0.16
Width of top at rail seat (m)	0.260	0.168	0.254	0.248	0.257
Width of top at centre (m)	0.260	0.168	0.254	0.248	0.257
Width of base at rail seat (m)	0.260	0.260	0.254	0.248	0.257
Width of base at centre (m)	0.260	0.260	0.254	0.248	0.257
Young's modulus (longitudinal) (GPa)	15.0	210	2.6	4.65	12
Shear modulus (GPa)	6.25	80.77	1.04	0.26	0.43
Total support surface (m^2)	0.65	0.63	0.66	0.65	0.64
Poisson's ratio (-)	0.2	0.3	0.25	n/a	n/a
Damping loss factor / tanδ	0.04	n/a	0.029	0.064	0.029
Sleeper spacing (m)	0.6	0.6	0.6	0.6	0.6
Rail pad vertical stiffness (MN/m)	500	1000	None	None	None
Rail pad lateral stiffness (MN/m)	177	120	None	None	None
Rail pad vertical damping loss factor	0.5	0.15	None	None	None
Rail pad lateral damping loss factor	0.5	0.15	None	None	None

For concrete monobloc sleepers, optionally under-sleeper pads (USP) can be included. Properties of three examples are listed in Table 5.

Table 5. Under-sleeper pad parameters

USP type	Soft	Medium	Stiff
Type	SLN220G	SLB2210G	Used on SBB
Thickness	20 mm	10 mm	8.5 mm
Bedding modulus, N/mm^3	0.02	0.22	0.62
Vertical low-frequency stiffness (MN/m)	14	150	420
Damping loss factor / tanδ(-)	0.1	0.2	0.25

Co-funded by the European Union

2.1.4 Ballast

For ballasted track, the parameters used for the ballast are listed in Table 6 [5-7]. Here a distinction is made between the loaded low-frequency dynamic stiffness of the ballast layer (relevant to ground-borne vibration models) and the overall foundation stiffness, including the ground (relevant to rolling noise models). To avoid having too many combinations, only the usual nominal thickness of ballast is considered for the vibration calculations – variations in the ballast thickness are expected to have negligible effect. For noise a softer variant is also considered. For the steel, wooden and composite sleepers, different values of acoustic ballast stiffness and damping are used.

Under-ballast mats (UBM) can be added beneath the ballast. The stiffness of UBM is usually expressed as a bedding modulus (stiffness per unit area). Example values are listed in Table 7 for a soft UBM (for vibration protection) and one with a moderate stiffness [8].

Table 6. Ballast parameters

Parameters for ground-vibration models				
Thickness beneath sleeper (m)	0.3			
Vertical low-frequency stiffness of ballast layer per sleeper (MN/m)	500			
Ballast mass per unit length (kg/m)	1485			
Width at the top (m)	3.0			
Width at the bottom (m)	3.6			
Damping loss factor / $\tan\delta$ (-)	0.15			
Parameters for noise models	Normal	Soft	Steel sleeper	Wood / composite sleepers
Vertical stiffness of foundation per sleeper (MN/m)	240	144	107.4	140
Vertical viscous damping coefficient per sleeper (kNs/m)	320	192	105	140
Lateral stiffness of foundation per sleeper (MN/m)	35	21	70.4	180
Lateral viscous damping coefficient per sleeper (kNs/m)	600	360	31.2	180

Table 7. Under-ballast mat parameters [8]

	Soft UBM	Medium UBM
Type	CN225	D619
Vertical static bedding modulus (MN/m^3)	15	31
Vertical low-frequency bedding modulus, 20 Hz (MN/m^3)	27	58
Damping loss factor / $\tan\delta$, assumed (-)	0.1	0.1

Co-funded by the European Union

2.1.5 Slab track

For slab track, the parameters used for the slab are listed in Table 8 [9, 10]. A single design (based on Rheda 2000) is included as slab parameters are not expected to affect vibration significantly. This consists of a concrete slab of thickness 0.24 m on a hydraulically bonded layer (HBL) of thickness 0.3 m. The noise from the slab itself will be neglected, as it has been found to be insignificant above 100 Hz [10].

Table 8. Slab track parameters [9, 10]

Slab properties	Slab	HBL	Combined
Thickness (m)	0.24	0.3	0.54
Width (m)	2.8	3.4	-
Density (kg/m^3)	2500	2000	-
Mass per unit length (kg/m)	1680	2040	3720
Young's modulus (GPa)	32	17	-
Vertical bending stiffness (MNm^2)	-	-	934
Damping loss factor / tanδ(-)	0.015	0.015	0.015

The full range of rail pad stiffnesses listed above for ballasted track does not apply to slab track. As listed in Table 9, two values of rail fastener stiffness are considered, which represent the combined stiffness of rail pads and lower pads. No separate sleepers are included. For reliable noise predictions, measured track decay rates (TDR) should be used.

Table 9. Rail fastener properties for slab track [10]

Rail fastener properties	Normal	Soft
Overall vertical static stiffness (MN/m)	25	10
Overall vertical low-frequency stiffness (MN/m)	50	15
Vertical acoustic stiffness lower pad (MN/m)	75	25
Lateral acoustic stiffness lower pad (MN/m)	35	15
Vertical damping loss factor / tanδ(-)	0.2	0.2
Baseplate mass (kg)	6.0	5.0
Vertical acoustic stiffness rail pad (MN/m)	2000	2000
Lateral acoustic stiffness rail pad (MN/m)	150	150
Vertical damping loss factor / tanδ(-)	0.2	0.2
Fastener spacing (m)	0.65	0.65

2.1.6 Ground properties

To calculate ground-borne vibration some example soil models are required. In SILVARSTAR [6] five homogeneous halfspace ground models were included. These parameters are listed in Table 10, where C_s is the shear wave velocity, C_p the dilatational wave velocity, ρ the density, and $\beta_s = \beta_p$ the material damping ratios in shear and dilatational deformation. Since the source levels for ground vibration will be determined in terms of force density levels, it is expected that they will not vary significantly between

Co-funded by the European Union

different soil conditions. It is therefore expected to be unnecessary to consider many complicated sets of ground conditions in determining the source levels.

Table 10. Dynamic soil characteristics used for homogeneous halfspace grounds [6]

	C_s (m/s)	C_p (m/s)	β_s (-)	β_p (-)	ρ (kg/m^3)
Soft	100	200	0.025	0.025	1800
Moderately soft	140	280	0.025	0.025	1800
Medium	200	400	0.025	0.025	1800
Moderately stiff	280	560	0.025	0.025	1800
Stiff	400	800	0.025	0.025	1800

2.2 Vehicle parameters

This section lists parameters defining the vehicle required to calculate rolling noise and ground-borne vibration. As the track optimisation tool is focused on track properties and costs, results will be included for only a few representative train types. In the following, parameters are specified for one passenger and one freight train.

2.2.1 Train parameters for ground-borne vibration models

A set of values for the train parameters required for ground-borne vibration models is listed in Table 11, based loosely on [6, 11].

Co-funded by the European Union

Table 11. Train parameters for ground-borne vibration models

	Passenger (unpowered)	Passenger (multiple unit)	Freight (loaded)
Car body			
Mass (kg)	32,000	32,000	80,000
Overall vehicle length (m)	25.0	25.0	15.8
Bogie			
Mass (kg)	2,500	5,000	2,100
Distance between bogie centres (m)	17.0	17.0	9.0
Wheelset			
Mass (kg)	1,200	1,800	1,400
Total axle load (kN)	108	120	220
Contact stiffness per wheel (GN/m)	1.18	1.22	1.49
Distance between axles (m)	2.5	2.5	1.8
Primary suspension			
Vertical stiffness per axle (MN/m)	2.0	2.0	5.0
Vertical viscous damping per axle (kNs/m)	40	40	40
Secondary suspension			
Vertical stiffness per bogie (MN/m)	0.5	0.5	100
Vertical viscous damping per bogie (kNs/m)	31.6	31.6	20

2.2.2 Wheel parameters for noise models

The main property affecting wheel noise is its cross-section shape. Four wheel designs are considered, as shown in Figure 1. The two for passenger rolling stock are characterised by different diameters, while for freight the conventional design is used with cast-iron brake blocks whereas the 'low-stress' wheel is used with K-blocks. Axisymmetric finite element models are produced of these wheels, with the results stored in a list of modal parameters (natural frequencies, mode shapes and damping ratios). The main wheel parameters required for the noise models are listed in Table 12. Those for Intercity passenger correspond to the unpowered vehicle in Table 11 and those for the regional passenger correspond to the multiple unit in Table 11. The properties for the freight wheels correspond to the loaded freight wagon in Table 11. The vehicle length, bogie spacing and axle spacing are as listed in Table 11.

Co-funded by the European Union

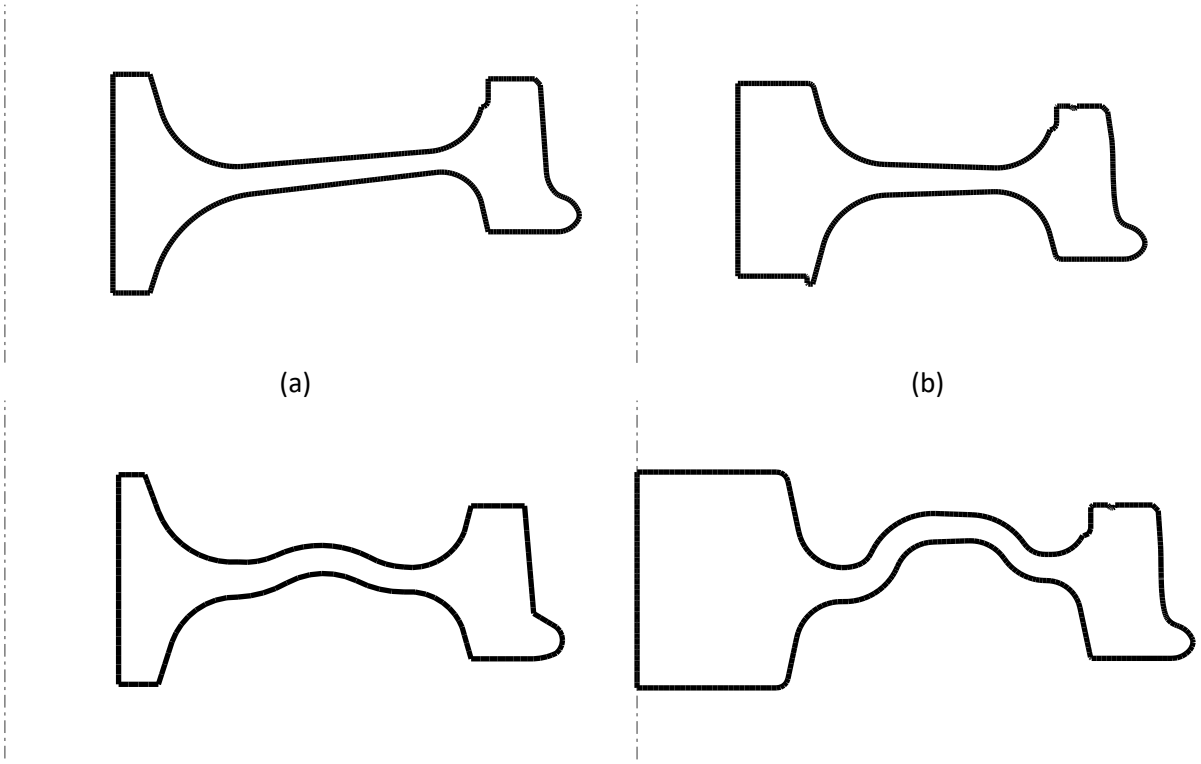

Figure 1. Wheel designs: (a) Intercity passenger (type Ba93), (b) suburban passenger (VB2N), (c) conventional freight (Ba02), (d) low-stress freight wheel (Ba319).

Table 12. Wheel parameters for rolling noise models

	Intercity Passenger	Regional Passenger	Conventional Freight	Low-stress Freight
Wheel	Ba93	VB2N	Ba02	Ba319
Radius (m)	0.475	0.42	0.46	0.461
Mass of wheel (excluding axle) (kg)	339	320	342	397
Total wheel load (kN)	54	60	110	110
Contact stiffness per wheel (GN/m)	1.18	1.20	1.49	1.49
Contact patch semi-axis length (mm)	6.0	5.8	7.4	7.4

2.3 Unevenness spectra

The noise and vibration source data will be provided in the tool in terms of a unit roughness/unevenness input. A set of predefined roughness/unevenness spectra will be provided in the tool, as listed here. The user will also be able to input their own roughness/unevenness spectra if desired. Unevenness spectra are defined in one-third octave bands separately covering low- and high-frequency regions.

For rolling noise calculations, a range of rail roughness spectra is provided from the sonRail default spectra [12], listed in Table 13. They are also plotted in Figure 2. Additionally, the limit spectrum from ISO 3095 [13] is included, which has been extrapolated to longer and shorter wavelengths (values in italics). These spectra can be augmented later with information on the effect of different rail grinding strategies on average roughness.

Co-funded by the European Union

Wheel roughness spectra used for the noise calculations are provided separately, see Table 14. They are defined depending on the braking system type as (i) cast iron tread brakes, (ii) composite brake blocks and (iii) disc brakes, for consistency with CNOSSOS-EU [14] (although the data are not those from the CNOSSOS-EU database). They were derived in [6] by applying smoothing to measured spectra presented in [15]. They are also plotted in Figure 3.

In combination with these roughness spectra, a contact filter is applied. For this, the following analytical filter is used for simplicity, see [15]:

$$|H(\lambda)|^2 = \left(1 + \frac{\pi}{4}\left(\frac{2\pi a}{\lambda}\right)^3\right)^{-1} \quad (1)$$

where λ is the roughness wavelength and $2a$ is the contact patch length in the rolling direction, which depends on the wheel radius and normal load. The filter effect in decibels is given by $10\log_{10}(|H(\lambda)|^2)$.

For the low-frequency region required for ground vibration, to cover a frequency region from 1 Hz to 250 Hz and train speeds from 36 km/h to 360 km/h, a wavelength range between 0.04 m and 100 m is required [6]. From 0.04 m to about 1.0 m this overlaps with the acoustic roughness range. However, it is proposed to allow them to be selected independently for vibration and noise to allow flexibility.

The predefined spectra for ground vibration calculations are taken from the SILVARSTAR database [6] and are listed in Table 15 for ballasted tracks and Table 16 for slab tracks. They are also plotted in Figure 4 and Figure 5. Depending on the type, rail corrugation typically affects wavelengths shorter than 0.2 m and may influence ground-borne noise but is less likely to influence feelable vibration.

The wheel roughness spectra used for ground vibration calculations are listed in Table 17. These are based on those used for noise, but with the addition of a peak due to wheel eccentricity, occurring at the wavelength corresponding to the wheel circumference. This can vary considerably [16] but here it has been allocated a value of 45 dB re 1 μm (0.5 mm peak-to-trough) for the cast-iron brake blocks at a wavelength of 3.15 m. For the other brake types, a value of 37 dB re 1 μm (0.1 mm peak-to-trough) is used, which is divided between the 2.5 m and 3.15 m bands. The levels in the bands at wavelengths 0.8 m and above are adjusted correspondingly.

Co-funded by the European Union

Table 13. Rail roughness spectra for noise calculations, dB ref. 10^{-6} m [12]

Wavelength, m	Smooth	Average	Rough	ISO 3095 limit [13]
0.63	2.3	7.0	14.3	*21.1*
0.5	1.1	6.5	13.8	*19.1*
0.4	0.6	6.0	13.3	17.1
0.31	0.1	5.5	12.8	15.0
0.25	-0.4	5.0	12.3	13.0
0.2	-0.9	4.5	11.8	11.0
0.16	-1.3	3.9	10.9	9.0
0.12	-1.5	3.6	10.1	7.0
0.1	-1.6	2.7	9.5	4.9
0.08	-2.3	2.1	9.1	2.9
0.063	-3.0	1.5	8.9	0.9
0.05	-4.4	1.0	8.5	-1.1
0.04	-6.4	-0.4	7.8	-3.2
0.0315	-7.8	-1.5	6.5	-5.0
0.025	-9.4	-3.0	4.9	-5.6
0.02	-11.2	-4.5	2.7	-6.2
0.016	-13.6	-7.5	-1.3	-6.8
0.012	-15.2	-10.1	-3.7	-7.4
0.01	-16.1	-11.8	-5.3	-8.0
0.008	-16.5	-13.0	-7.3	-8.6
0.0063	-17.0	-13.9	-8.3	-9.2
0.005	-17.3	-14.9	-9.3	-9.8
0.004	-17.5	-15.4	-10.3	-10.4
0.00315	-17.9	-16.1	-11.3	-11.0
0.0025	-18.5	-16.9	-12.3	*-11.6*
0.002	-19.5	-17.9	-13.3	*-12.2*
0.0016	-20.5	-18.9	-14.3	*-12.8*
0.00125	-21.5	-19.9	-15.3	*-13.6*
0.001	-22.5	-20.9	-16.3	*-14.2*

Co-funded by the European Union

Table 14. Wheel roughness spectra for noise calculations, dB ref. 10^{-6} m [6]

Wavelength, m	Disc-braked	Cast-iron block	K-block
0.8	2.8	7.4	-3.4
0.63	2.4	6.6	-5.3
0.5	1.9	5.8	-6.7
0.4	1.5	5.1	-7.7
0.31	0.9	4.3	-8.4
0.25	0.0	3.5	-8.9
0.2	-0.9	2.7	-9.2
0.16	-2.0	3.1	-9.3
0.12	-3.2	4.6	-9.4
0.1	-4.2	6.2	-9.4
0.08	-5.3	7.8	-9.4
0.063	-6.3	9.2	-9.4
0.05	-7.2	10.0	-9.4
0.04	-8.0	10.3	-9.5
0.0315	-8.7	10.0	-9.7
0.025	-9.3	9.2	-10.0
0.02	-9.8	8.0	-10.4
0.016	-10.1	6.4	-10.9
0.012	-10.5	4.5	-11.6
0.01	-10.7	2.6	-12.4
0.008	-11.1	0.6	-13.5
0.0063	-11.5	-1.6	-14.9
0.005	-12.1	-4.0	-16.5
0.004	-13.0	-6.5	-18.4
0.00315	-14.3	-9.9	-20.8
0.0025	-16.1	-14.1	-23.6
0.002	-18.4	-19.6	-26.8

Co-funded by the European Union

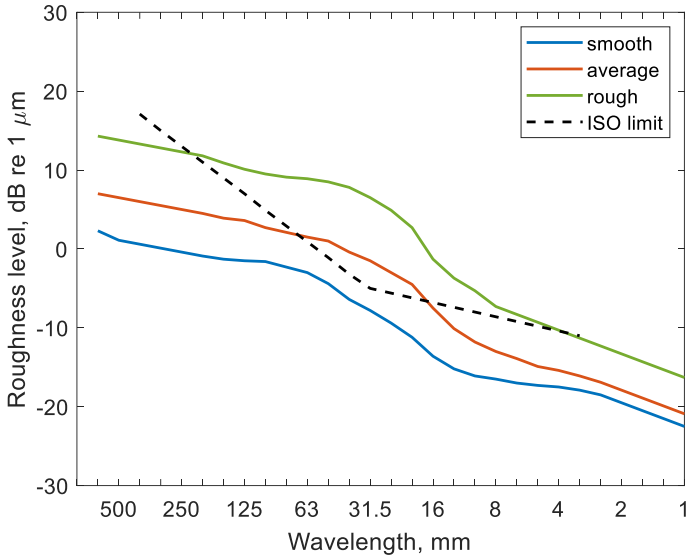

Figure 2. Acoustic rail roughness spectra

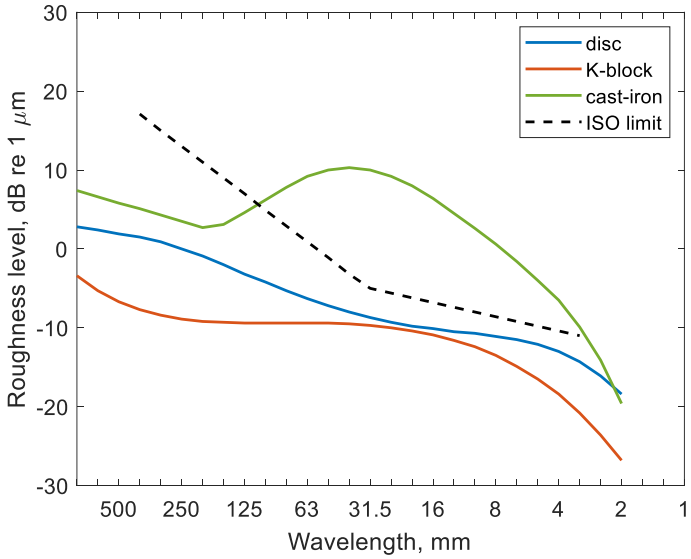

Figure 3. Acoustic wheel roughness spectra.

Co-funded by the European Union

Table 15. Ballasted track unevenness spectra for ground vibration calculations, dB ref. 10^{-6} m [6]

Wavelength m	HS or well maintained	Normally maintained	Not well maintained	Freight line	Normally maintained and corrugated	Not well maintained and corrugated
100	53.2	59.4	66.4	70.6	59.4	66.5
80	52.9	59.2	66.0	70.2	59.2	66.1
63	52.6	58.9	65.7	69.9	58.9	65.7
50	52.2	58.7	65.3	69.5	58.7	65.3
40	51.9	58.5	65.0	69.2	58.5	65.0
31.5	51.5	58.0	64.6	68.8	58.0	64.6
25	51.3	57.3	64.1	68.4	57.3	64.1
20	50.7	56.4	63.9	67.7	56.4	63.8
16	49.9	55.4	63.4	66.6	55.4	63.2
12.5	48.6	53.9	62.3	65.1	53.9	62.0
10	47.1	52.5	61.1	63.5	52.5	60.7
8	45.5	50.8	59.6	61.6	50.8	59.1
6.3	43.4	48.9	57.6	59.4	48.9	57.1
5	41.2	46.9	55.5	57.0	46.9	54.9
4	38.9	44.8	53.2	54.5	44.8	52.7
3.15	36.3	42.4	50.6	51.6	42.4	50.0
2.5	33.6	40.0	47.8	48.7	40.0	47.4
2	30.9	37.6	45.0	45.8	37.6	44.7
1.6	28.1	35.1	42.1	42.8	35.1	41.9
1.25	24.9	32.2	38.8	39.4	32.2	38.9
1	22	29.6	35.7	36.3	29.6	36.1
0.8	19	26.9	32.6	33.1	26.9	33.3
0.63	15.9	23.9	29.3	29.7	23.9	30.4
0.5	12.8	21.1	26.0	26.5	21.0	27.6
0.4	9.9	18.3	22.9	23.4	18.9	25.1
0.315	6.8	15.3	19.7	20.1	16.9	22.6
0.25	3.9	12.4	16.6	17.0	15.2	20.3
0.2	1.3	9.6	13.8	14.2	13.7	18.3
0.16	-1.3	6.9	11.0	11.4	12.5	16.5
0.125	-3.9	3.9	8.2	8.6	11.5	14.8
0.1	-6.2	1.2	5.8	6.2	10.9	13.6
0.08	-8.2	-1.4	3.6	3.9	10.7	12.7
0.063	-10.2	-4.0	1.6	1.8	10.8	12.2
0.05	-11.9	-6.5	-0.2	0.0	11.3	12.0
0.04	-13.2	-8.8	-1.6	-1.5	12.2	12.3
0.0315	-14.4	-11.2	-2.8	-2.8	13.7	13.7

Europe's Rail
Co-funded by the European Union

Table 16. Slab track unevenness spectra for ground vibration calculations, dB ref. 10^{-6} m [6]

Wavelength m	HS or well maintained	Normally maintained	Not well maintained	Normally maintained and corrugated	Not well maintained and corrugated
100	47.1	57.2	67.5	57.2	67.5
80	46.9	57.0	67.2	57.0	67.2
63	46.7	56.8	66.9	56.8	66.9
50	46.4	56.5	66.6	56.5	66.6
40	46.2	56.3	66.3	56.3	66.3
31.5	45.9	56.0	66.0	56.0	66.0
25	45.7	55.4	65.4	55.4	65.4
20	45.4	54.7	64.5	54.7	64.5
16	44.8	53.7	63.3	53.7	63.3
12.5	43.9	52.4	61.8	52.4	61.8
10	42.8	51.0	60.1	51.0	60.1
8	41.6	49.4	58.2	49.4	58.2
6.3	40.1	47.6	56.0	47.6	56.0
5	38.5	45.6	53.6	45.6	53.6
4	36.7	43.6	51.2	43.6	51.2
3.15	34.7	41.3	48.4	41.3	48.4
2.5	32.6	38.9	45.6	38.9	45.6
2	30.4	36.5	42.7	36.5	42.7
1.6	28.2	34.0	39.7	34.0	39.7
1.25	25.5	31.2	36.4	31.2	36.4
1	23.1	28.5	33.2	28.5	33.2
0.8	20.5	25.8	30.1	25.8	30.0
0.63	17.7	22.8	26.6	22.8	26.9
0.5	14.9	19.8	23.3	19.9	23.9
0.4	12.2	17.0	20.0	17.5	21.1
0.315	9.3	13.9	16.6	15.1	18.2
0.25	6.4	10.9	13.3	12.9	15.6
0.2	3.6	8.0	10.1	10.9	13.2
0.16	0.8	5.1	7.1	9.1	11.0
0.125	-2.3	1.9	3.7	7.3	8.8
0.1	-5.1	-0.9	0.8	5.8	7.1
0.08	-7.9	-3.7	-1.9	4.6	5.6
0.063	-10.8	-6.7	-4.8	3.6	4.3
0.05	-13.5	-9.4	-7.4	2.9	3.4
0.04	-16.1	-12	-9.7	2.5	2.8
0.0315	-18.8	-14.7	-12.0	2.5	2.6

Europe's Rail
Co-funded by the European Union

Table 17. Wheel roughness spectra for vibration calculations, dB ref. 10^{-6} m (based on [6])

Wavelength, m	Disc-braked	Cast-iron block	K-block
3.15	34	45	34
2.5	34	-	34
2.0	-	-	-
1.6	-	22	-
1.25	17	20	17
1.0	14	16	10
0.8	10	11	-3.4
0.63	2.4	6.6	-5.3
0.5	1.9	5.8	-6.7
0.4	1.5	5.1	-7.7
0.31	0.9	4.3	-8.4
0.25	0.0	3.5	-8.9
0.2	-0.9	2.7	-9.2
0.16	-2.0	3.1	-9.3
0.12	-3.2	4.6	-9.4
0.1	-4.2	6.2	-9.4
0.08	-5.3	7.8	-9.4
0.063	-6.3	9.2	-9.4
0.05	-7.2	10.0	-9.4
0.04	-8.0	10.3	-9.5
0.0315	-8.7	10.0	-9.7

Co-funded by the European Union

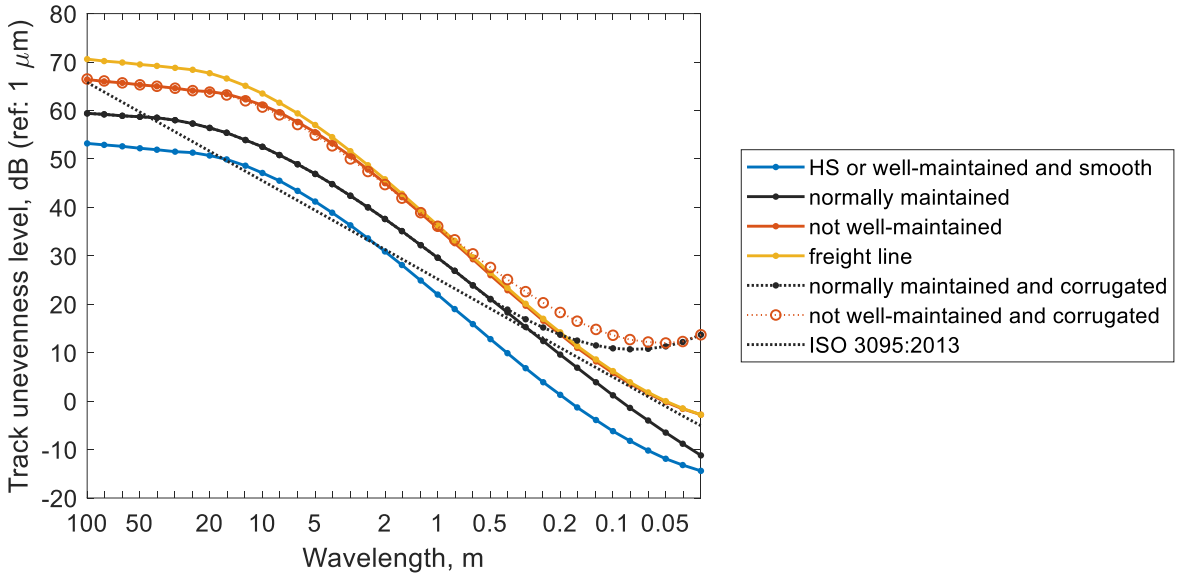

Figure 4. Track unevenness spectra for ballasted tracks.

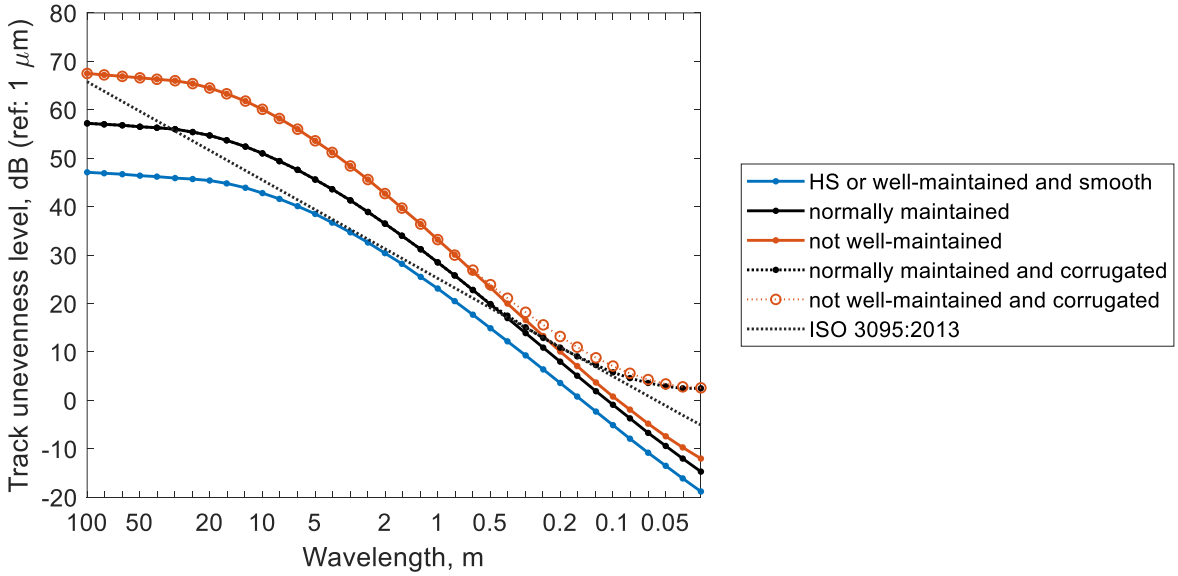

Figure 5. Track unevenness spectra for slab tracks.

Co-funded by the European Union

2.4 Noise mitigation measures

This section lists the various noise mitigation measures that will be considered within the tool and the associated parameters. The following section describes the vibration mitigation measures.

2.4.1 Optimised rail pads

The key feature of optimised rail pads is to allow a low static stiffness while maintaining a high acoustic stiffness [4]. To achieve this trend may require a higher than usual damping loss factor, leading to frequency-dependent stiffness behaviour. The associated parameters can be selected from Table 2 (although note that frequency dependence is not taken into account). However, to create an 'optimised' rail pad, the parameters used for noise and vibration should not be chosen to correspond to the same descriptor (e.g. choose stiff for noise, soft for vibration). Medium or high damping can also be selected.

2.4.2 Rail dampers

To estimate the effect of rail dampers on rolling noise, the TDR of a track fitted with the dampers is calculated by combining the decay rate of a freely suspended rail fitted with these dampers (obtained from measurements) with the TDR of the track without dampers [17].

There are many types of rail damper on the market, some with better performance than others. It is therefore important for the user to understand the relative performance of their chosen solution. Within the tool, two examples of rail damper are included, which give relatively good performance. Figure 6 shows the decay rates of a bare rail fitted with these dampers (from [17]). Damper A has a better performance for the vertical direction, while damper B has a better performance for the lateral direction. The user may also input their own decay rates if known. The effect on radiated noise depends on parameters such as the rail pad stiffness.

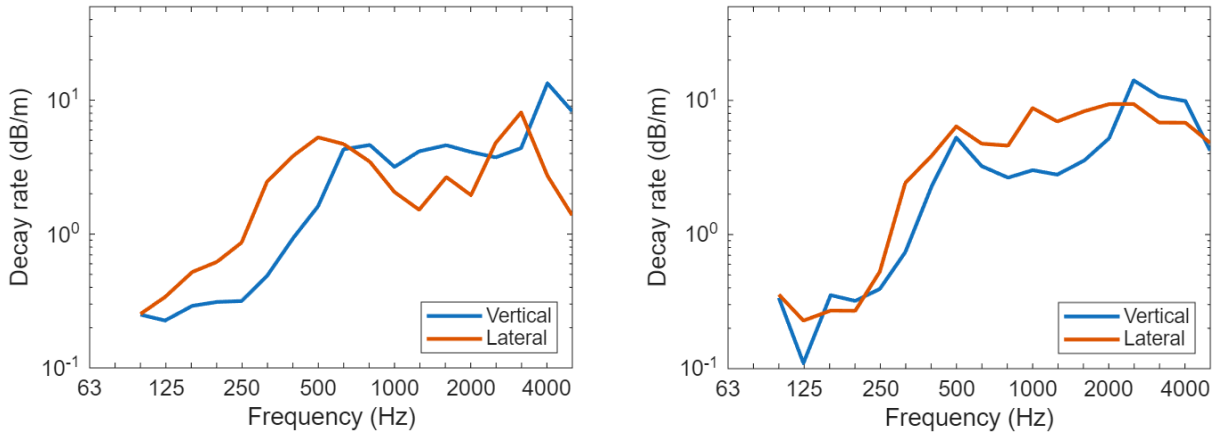

(a) (b)

Figure 6. Measured decay rate of a free rail fitted with example rail dampers. (a) Damper A, (b) damper B [17].

2.4.3 Rail shields

Rail shields can be used as an alternative to rail dampers. In this case the TDR is not affected but the sound radiation from the rail is reduced. One generic type of shield is considered, described by the insertion loss of the vertical and lateral rail noise components, calculated using a boundary element model [18]. These insertion losses are shown in Figure 7. In the tool, the vertical and lateral rail noise components, for the chosen track parameters, are modified by these insertion losses and the total noise spectrum is recalculated.

Co-funded by the European Union

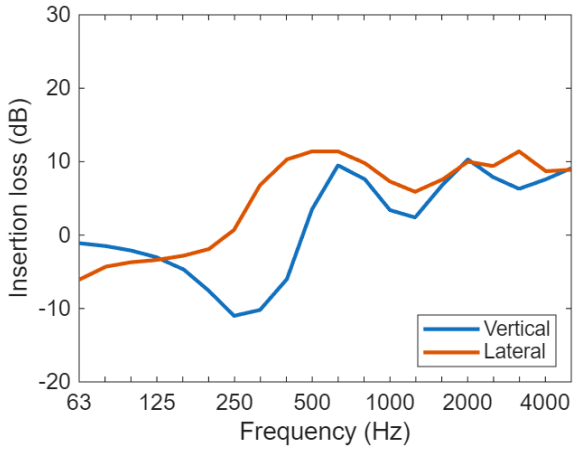

Figure 7. Predicted insertion loss of a rail fitted with generic rail shields [18].

2.4.4 Acoustic rail grinding

Rail grinding is performed routinely as part of track maintenance to remove track defects such as rolling contact fatigue and to restore the lateral rail head profile. By using an 'acoustic grinding' (or milling) technique, it is also possible to reduce wayside noise by a reduction in rail roughness. This can also be associated with onboard monitoring of the rail roughness [19].

It is also recognised that some forms of rail grinding may lead to a (temporary) increase in rail roughness levels, especially at short wavelengths due to the introduction of grinding marks on the rail [19]. It is therefore necessary to estimate the long-term average rail roughness when acoustic grinding is performed and compare this with the typical rail roughness in the absence of this noise control measure.

To represent the effect of rail grinding as a noise control measure, modified rail roughness spectra can be introduced in the calculation. At the simplest level, this could be done by replacing the 'average' rail roughness by the 'smooth' one. A comparison of this with measured rail roughness spectra is presented in Appendix A.

2.4.5 Noise barriers

The effect of noise barriers is strongly dependent on the receiver location. They affect the transmission path between source and receiver, not the source level (sound power). Established calculation methods are available in noise reception calculations (noise mapping), so the effect of barriers will be calculated using the noise reception model, not in the rolling noise source terms described here, which are based on sound power levels.

For mini-barriers installed close to the track, a similar calculation can be performed within the noise reception model.

2.5 Vibration mitigation measures

This section lists the various vibration mitigation measures that will be considered within the tool and the associated parameters.

2.5.1 Resilient track components

Various resilient track components can be introduced to increase the vibration isolation between the wheel-rail contact and the ground. These include very soft rail fasteners, under-sleeper pads and under-ballast mats.

Very soft rail fasteners can be used as a vibration control measure. These are covered in the model results using the parameters listed in Table 2. Their effect on rolling noise should also be assessed as softer fasteners can lead to increased noise levels.

Co-funded by the European Union

Under-sleeper pads are also included in the model database, using the parameters listed in Table 5. They may also have an effect on rolling noise.

Under-ballast mats can be included using the parameters listed in Table 7. Unlike the other resilient track components, under-ballast mats have negligible effect on rolling noise.

2.5.2 Track maintenance to reduce unevenness

To reduce the unevenness associated with the excitation of ground vibration, rail grinding is not effective as it targets shorter wavelengths than are relevant. However, maintenance activity such as track tamping can lead to an improvement in track geometry at longer wavelengths.

A change from 'normally maintained' to 'well maintained' track unevenness (see Figure 4) can lead to significant reductions in vibration. These spectra are based loosely on measured data for a typical mainline track and a well-maintained high-speed line. However, they do not correspond to the same track before and after such maintenance activity. Where the user has such data available, this is to be preferred.

2.5.3 Mitigation in the transmission path

Additionally, insertion loss results for various mitigation measures in the transmission path that were studied in the RIVAS project are provided. As the results depend heavily on the soil properties, these results are recalculated to correspond to three of the five homogeneous ground types considered here (soft/medium/stiff). The following mitigation measures studied in the RIVAS project are considered:

- Stiff soil barrier [20]
- Sheet pile wall [21]
- Soft-filled trench [22]
- Heavy masses beside the track [23]
- Subgrade stiffening [24]

To calculate the insertion loss of these mitigation measures, a coupled finite element / boundary element (FE-BE) model is used. At least 10 quadratic elements per shear wavelength are used in the computations. The track is not modelled, but instead the transfer functions are computed for a set of vertical forces applied to the soil at the position where the centre of the track would be. A line source is simulated using point forces arranged at spacing 10 m over a length of 100 m, centred around a position $y = 0$ m. Receivers are located at $y = 0$ m and at lateral distances of $x = 8$, 16, 24, 32, 48 and 64 m from the line of forces. Logarithmic frequency sampling is used (5 samples per one-third octave band), covering centre frequencies between 1 and 250 Hz. Example results are contained in Section 4.4 for heavy masses beside the track and subgrade stiffening.

The heavy masses represent a Gabion wall with a width of 1 m and a height of 2 m. It has a density of 1700 kg/m³, shear wave velocity 300 m/s, Poisson's ratio 0.2, and material damping ratio 0.02 (loss factor 0.04). The distance between the line of forces (i.e. the centreline of the track) and the centre of the Gabion wall is 4 m.

The subgrade stiffening has a width of 6 m, a thickness of 0.5 m (embedded at the ground surface), and is centred around $x = 0$ (the centre of the track). It has a density of 2400 kg/m³, shear wave velocity 1400 m/s, Poisson's ratio 0.25, and material damping ratio 0.05 (loss factor 0.10).

The stiff wall barrier has a width of 1 m and a depth of 3 m. It has a density of 2400 kg/m³, Young's modulus of 30 GPa, Poisson's ratio 0.2, and no material damping. The distance between the line of forces (i.e. the centreline of the track) and the centre of the stiff wall barrier is 6 m.

The soft wall barrier (soft-filled trench) has a width of 0.05 m and a depth of 3 m. It has a density of 700 kg/m³, Young's modulus of 1 MPa, Poisson's ratio 0.4, and no material damping. The distance between the line of forces (i.e. the centreline of the track) and the centre of the soft wall barrier is again 6 m.

These results for these mitigation measures in the transmission path are obtained in the form of an insertion loss, which is independent of the track and vehicle but depends on lateral receiver distance. It

Co-funded by the European Union

relies on the assumption that the force density is not affected by these mitigation measures in the transmission path.

Co-funded by the European Union

3. Rolling noise results

3.1 Calculation cases

Rolling noise sound power spectra for a unit roughness are calculated using the TWINS/TNE model of ISVR [25, 26]. The model used includes the effect of the discrete support provided by the sleepers. The input parameters used are listed in Section 2. These results will be stored in a database and combined with wheel and rail roughness spectra for the chosen train speed in the web-based tool.

Table 18 lists the variants included in the noise calculations. A reference case is selected (shown highlighted in the table) for the purpose of illustrating the results in this report. Not all combinations are considered: for example, 54E1 rail is only considered for one sleeper type, one value of rail pad damping and one value of ballast thickness (the reference values in each case). Similarly, the range of rail pads associated with wood, steel and composite sleepers is limited to stiffer pads with low damping. Sound power spectra for unit roughness have been calculated for a total of 776 combinations.

At this stage, the results focus on tracks with concrete sleepers in ballast, which represents the most common configuration. Results for other sleeper types and for slab track will be added later.

Results for different cases are shown in the next section, in which one parameter at a time is varied while the others retain their reference value. Train speed can be set arbitrarily, but for the purpose of illustration, five values are considered here, with 120 km/h selected as the reference value.

Table 18. Summary of variants considered for noise calculations (reference case is shown shaded)

Component	Variants				
Wheel type	Intercity Passenger	Regional Passenger	Conventional Freight	Low-stress Freight	
Rail type	60E2		54E1		
Rail pad stiffness	Very soft	Soft	Medium	Stiff	Very stiff
Rail pad damping	Low		Medium		High
Sleeper type	Concrete monobloc B91	Conc monobloc (heavy)	Concrete bibloc	Wood	
	Steel	Composite 1	Composite 2	Composite 3	
Under-sleeper pad	None	Stiff	Medium	Soft	
Ballast thickness	0.3 m		0.5 m		Slab track
Rail roughness	Smooth		Average		Rough
Wheel roughness	Disc-braked		Cast-iron braked		Composite braked
Train speed (km/h)	50	80	120	160	200

3.2 Example results for parameter variations

3.2.1 Reference case

For the reference case indicated in Table 18, the unweighted sound power spectra are shown in Figure 8 for the noise radiated by the wheel, rail and sleeper as well as their combined total. The rail noise is the dominant component in the important mid-frequency region and has an overall level of 101.8 dB(A). The sleeper noise dominates the low-frequency region below 250 Hz, with an overall level of 91.1 dB(A),

Co-funded by the European Union

whereas the wheel noise is the dominant component at 2.5 kHz and above, with an overall level of 96.4 dB(A), i.e. 5.4 dB lower than the rail component.

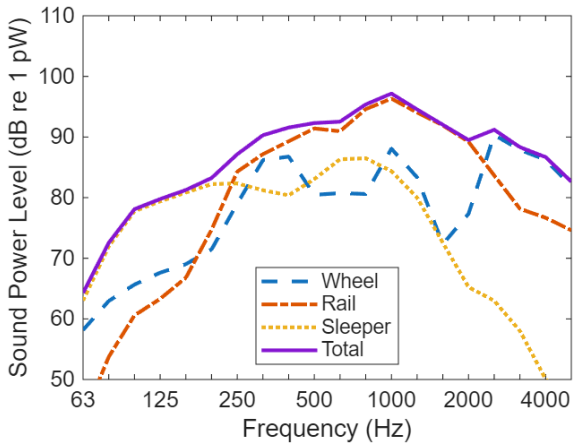

Figure 8. Component sound power spectra for reference case (120 km/h).

3.2.2 Train speed

Figure 9(a) shows the total noise spectra for five train speeds, with other parameters set to correspond to the reference case indicated in Table 18. The overall A-weighted levels are shown in Figure 9(b), including the contributions from the wheel, rail and sleeper. As speed increases, the noise at high frequencies increases more than that at low frequencies. Consequently, the relative importance of the wheel component (which is predominant at high frequencies) increases – it is only 2.4 dB(A) lower than the rail component at 200 km/h whereas the difference is 5.3 dB(A) at 50 km/h and 5.4 dB(A) at 120 km/h. Figure 9(c) shows the trend of overall A-weighted level plotted against speed V; the slope is close to 30 $\log_{10}V$ as expected [15].

Co-funded by the European Union

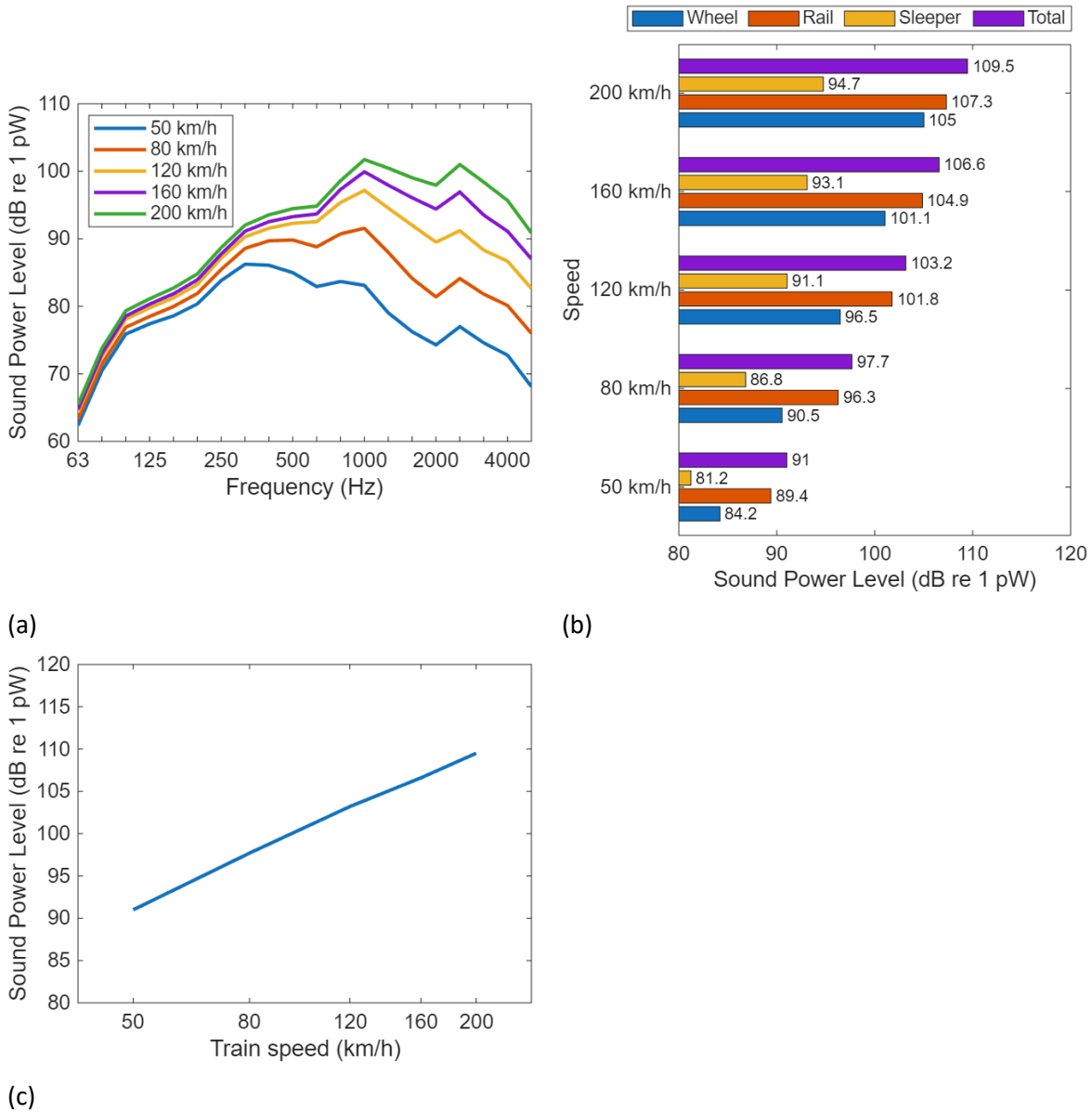

Figure 9. Effect of train speed: (a) total sound power spectra, (b) overall A-weighted sound power levels of each component, (c) overall A-weighted sound power levels plotted against speed.

3.2.3 Wheel type

Figure 10 shows results for the four types of wheel considered, with other parameters set to correspond to the reference case as indicated in Table 18. Details of these wheels are given in Section 2.2.2. The total noise spectra are shown in Figure 10(a), while the overall A-weighted levels are shown in Figure 10(b), including the contributions from the wheel, rail and sleeper. Figure 10(c) shows the sound power spectra for the wheel component (other components have only small variations).

There are differences in wheel component of up to 4.5 dB(A) (overall level) between the various wheels. The reference wheel (Regional passenger) has the lowest wheel contribution due to its straight web and smaller diameter, while the low-stress wheel is 1.4 dB(A) noisier than the conventional freight wheel due to its highly curved web. The Intercity passenger wheel has the highest noise level due to its thin web (see also [15]). The differences in total noise level are at most 1.2 dB(A) due to the dominance of the track in the reference case. For stiffer rail pads, or higher speeds, where the rail contribution is lower, the differences between the total noise levels for the different wheel types will be greater.

Co-funded by the European Union

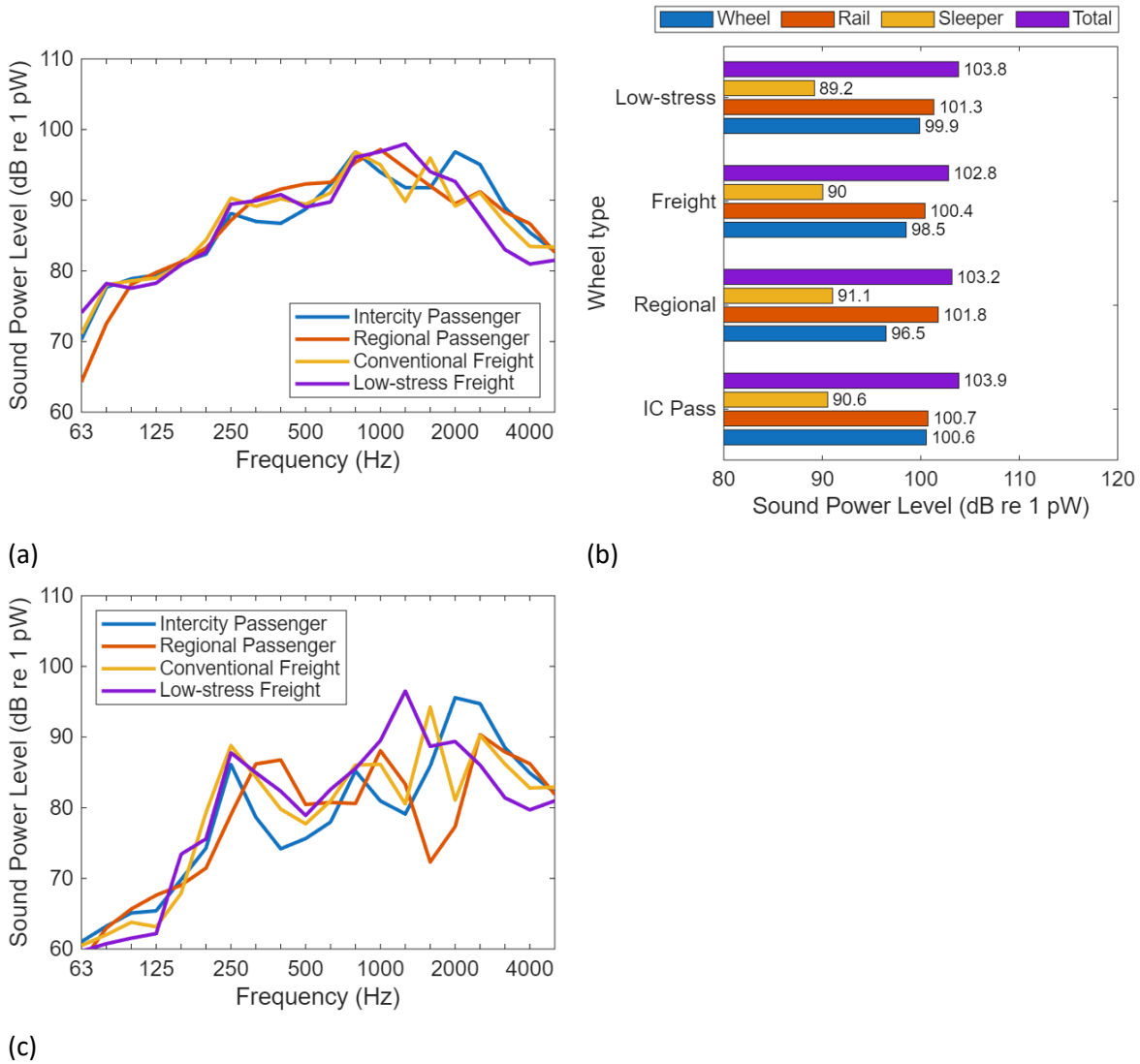

Figure 10. Effect of wheel type: (a) total sound power spectra, (b) overall A-weighted sound power levels of each component, (c) wheel sound power spectra.

3.2.4 Rail type

Figure 11 shows results for the two types of rail, with other parameters set to correspond to the reference case as indicated in Table 18. The total noise spectra are shown in Figure 11(a), while the overall A-weighted levels are shown in Figure 11(b), including the contributions from the wheel, rail and sleeper. The differences between the two types of rail are small (0.4 dB(A) in rail component and in total noise level), which confirms the decision not to calculate the full range of parameters for the second rail type.

Co-funded by the European Union

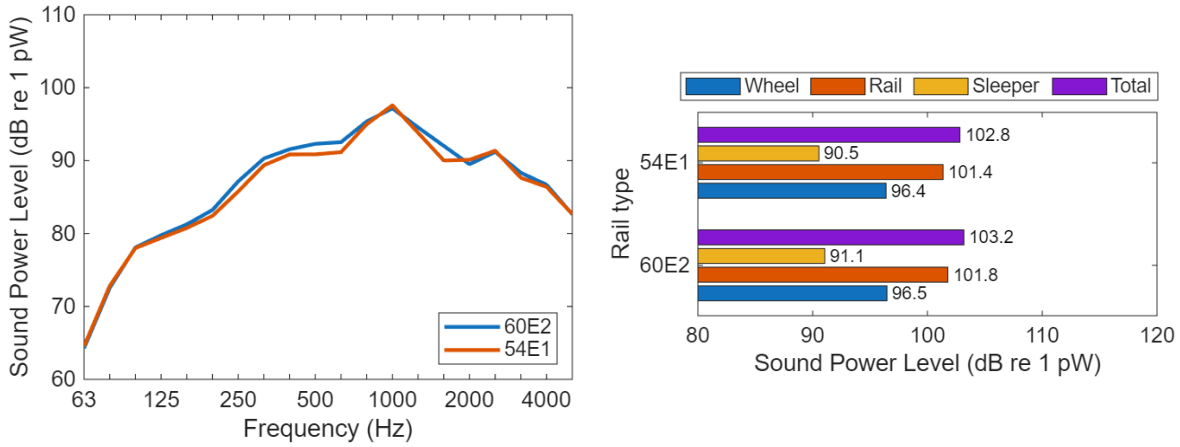

(a) (b)

Figure 11. Effect of rail type: (a) total sound power spectra, (b) overall A-weighted sound power levels of each component.

3.2.5 Rail pad stiffness and damping

Figure 12 shows results for the five different values of rail pad stiffness listed in Section 2.1.2, with other parameters corresponding to the reference case as indicated in Table 18. The total sound power spectra are shown in Figure 12(a), which indicates that the largest variations are in the important mid-frequency region where the rail is the dominant component, see Figure 8. The overall A-weighted levels of each component are shown in Figure 12(b); these values are also plotted in Figure 12(c), from which it is clear that the rail pad stiffness has a large effect on the rail component of noise, with variations of up to 8.4 dB(A), whereas the effect on the sleeper is less than 2 dB and the influence on the wheel component is at most 0.6 dB(A). The total noise level reduces by 6 dB between the very soft and very stiff rail pads.

The dependence on rail pad stiffness is mainly associated with the track decay rates (TDR). Figure 13 shows the TDRs for vertical and lateral vibration, both of which are increased significantly as the rail pad stiffness is increased, as expected.

The influence of rail pad damping is shown in Figure 14. This shows a range of overall noise levels of up to 2.4 dB(A) for the same (medium) stiffness. The corresponding track decay rates are shown in Figure 14(c) for the vertical direction and Figure 14(d) for the lateral direction, which show the expected trends.

Co-funded by the European Union

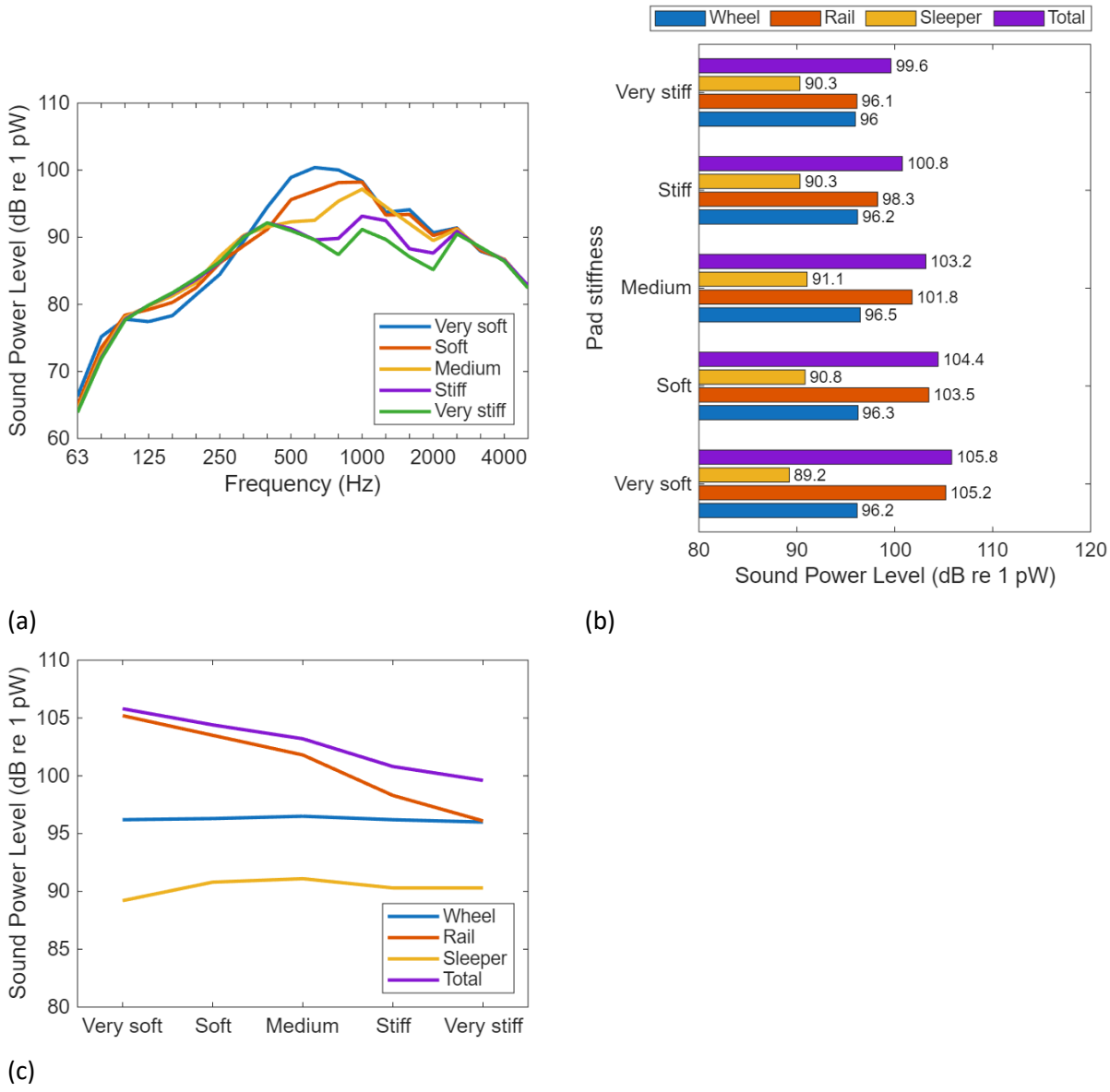

Figure 12. Effect of rail pad stiffness: (a) total sound power spectra, (b) overall A-weighted sound power levels of each component, (c) overall A-weighted sound power levels plotted against rail pad stiffness.

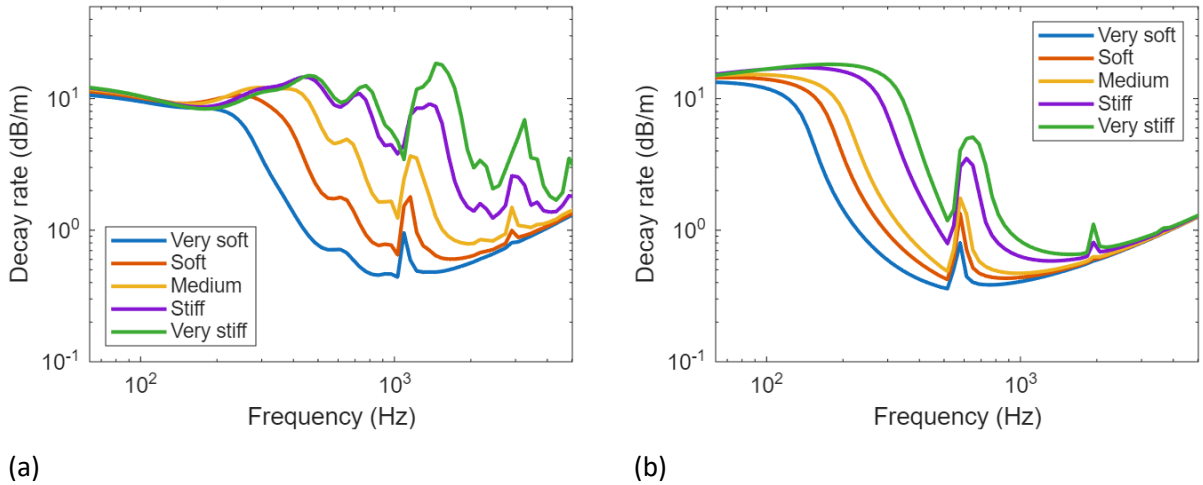

Figure 13. Effect of rail pad stiffness on track decay rates: (a) vertical TDR, (b) lateral TDR.

Co-funded by the European Union

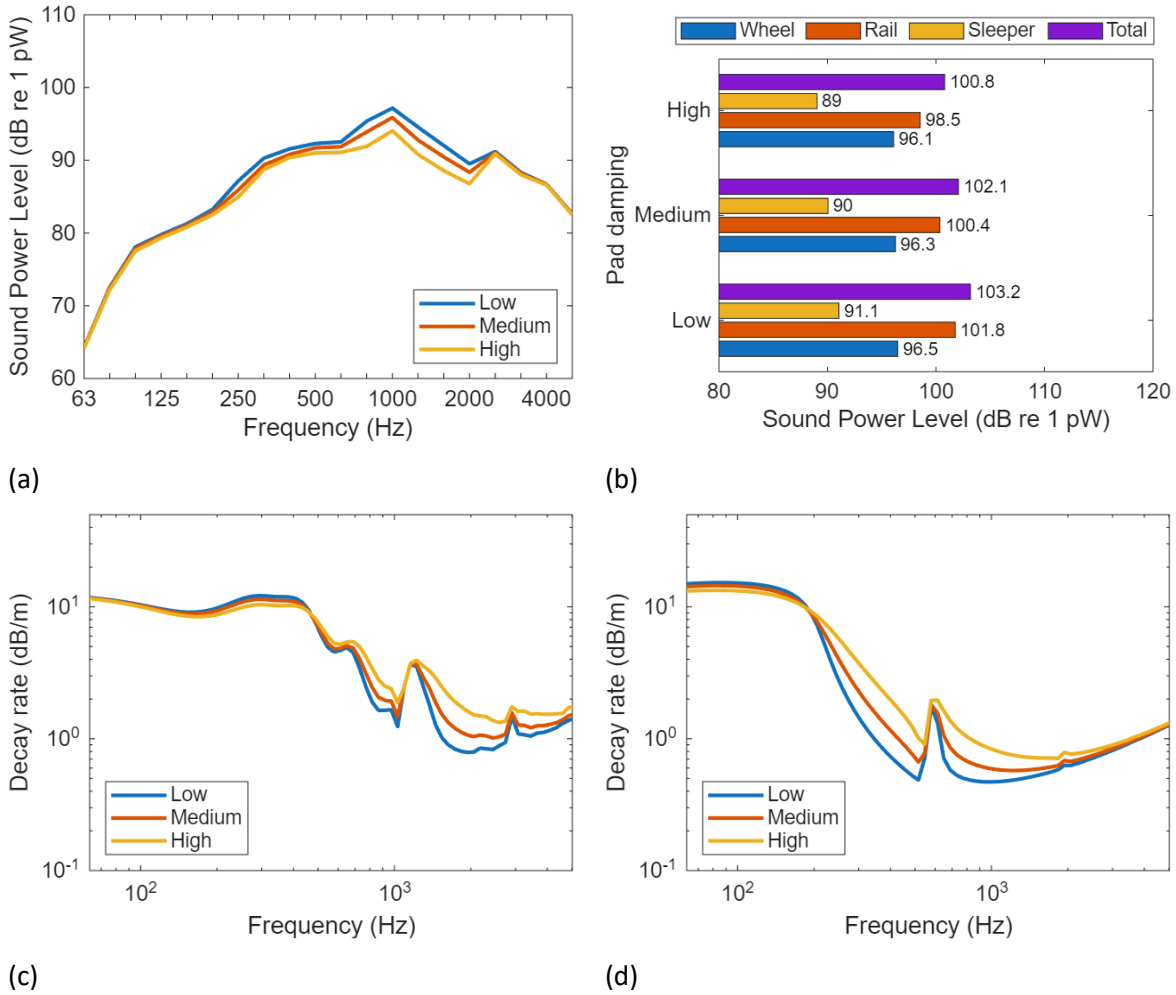

Figure 14. Effect of rail pad damping: (a) total sound power spectra, (b) overall A-weighted sound power levels, (c) vertical TDR, (d) lateral TDR.

3.2.6 Sleeper type

Figure 15 compares the results for three different types of concrete sleeper, with other parameters corresponding to the reference case indicated in Table 18. The total sound power spectra are shown in Figure 15(a), while the overall A-weighted levels of each component are shown in Figure 15(b). There is negligible difference between the two monobloc concrete sleepers, with the heavier sleepers producing 0.5 dB(A) less noise than the lighter B91, but the total noise level being unaffected. For the bibloc sleepers, the sleeper contribution is 6 dB(A) lower than the monobloc sleepers, but the rail contribution is slightly higher, leading to an increase in total level of 0.6 dB(A).

Results for the other sleeper types (wood, composite and steel) are shown in Figure 16. Unlike the concrete sleepers, the results for these sleepers have a high sleeper component, similar to or exceeding that of the rail. The overall noise with wooden sleepers (101.6 dB(A)) is greater than concrete monobloc with stiff (100.8 dB(A)) or very stiff rail pads (99.6 dB(A)), see Figure 12, although it is less than concrete sleepers with medium rail pads (103.2 dB(A)). The steel sleepers give overall levels that are 4 dB(A) greater than wooden sleepers. These results for steel sleepers are based on stiff rail pads, but it is found that using medium or very stiff rail pads gives very similar overall levels (differences less than 0.5 dB(A)). The three types of composite sleeper give very similar overall noise levels (differences less than 0.5 dB(A)); these are around 1 dB(A) higher than the results for wooden sleepers.

Co-funded by the European Union

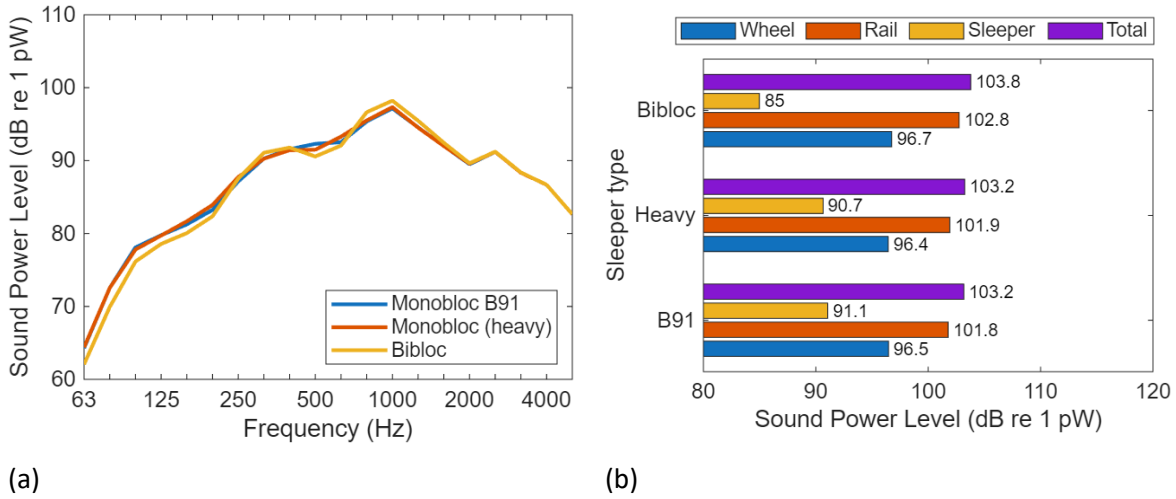

(a) (b)

Figure 15. Effect of sleeper type (concrete sleepers): (a) total sound power spectra, (b) overall A-weighted sound power levels.

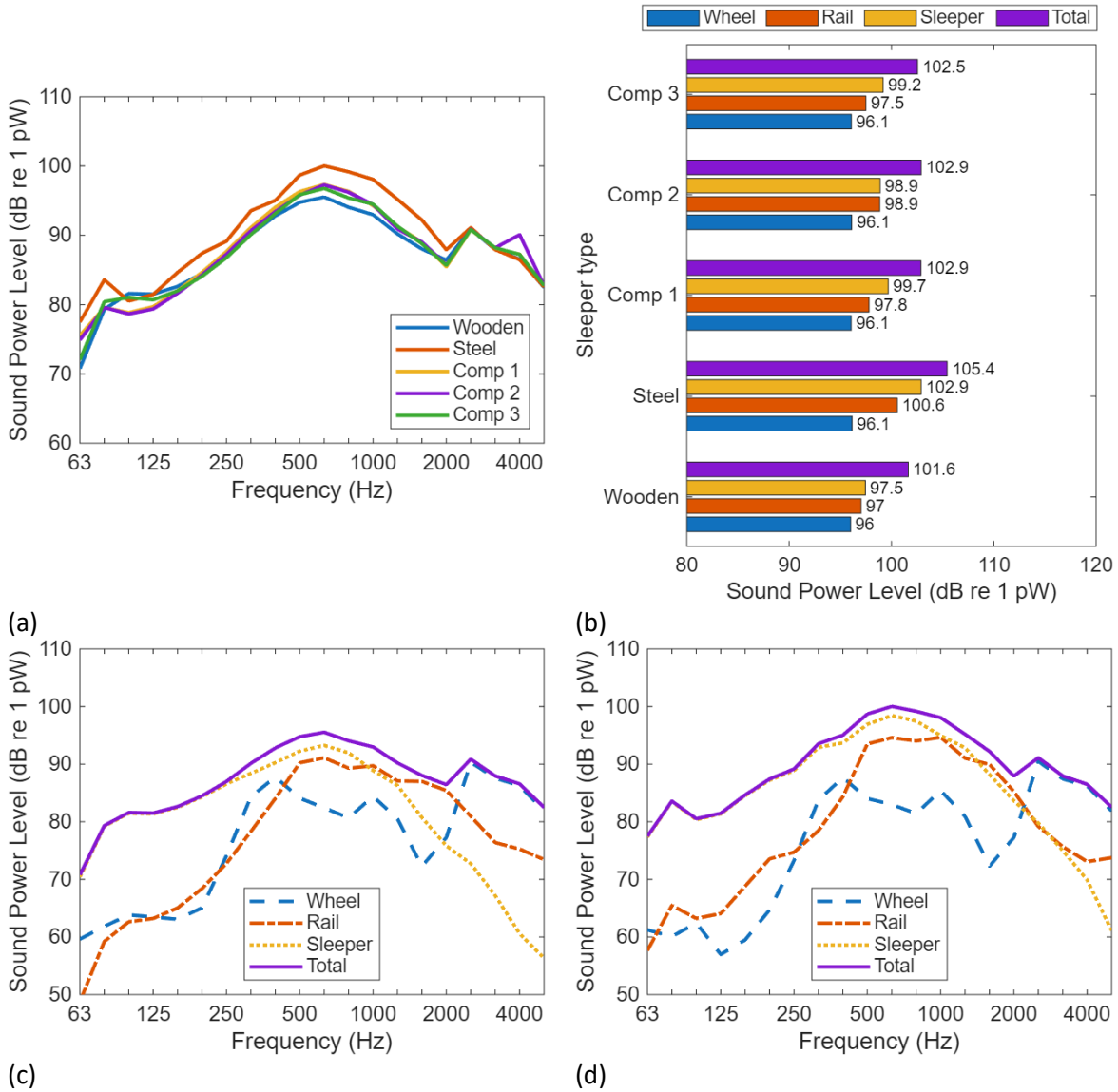

(a) (b)

(c) (d)

Figure 16. Effect of sleeper type (other types): (a) total sound power spectra, (b) overall A-weighted sound power levels, (c) component sound power spectra for wooden sleepers, (d) component sound power spectra for steel sleepers.

Co-funded by the European Union

3.2.7 Ballast stiffness

Varying the ballast stiffness leads to differences in low frequency noise radiated by the sleeper. However, as shown in Figure 17, although the noise from the sleepers is increased by 1.8 dB(A), the effect on the total noise levels is negligible.

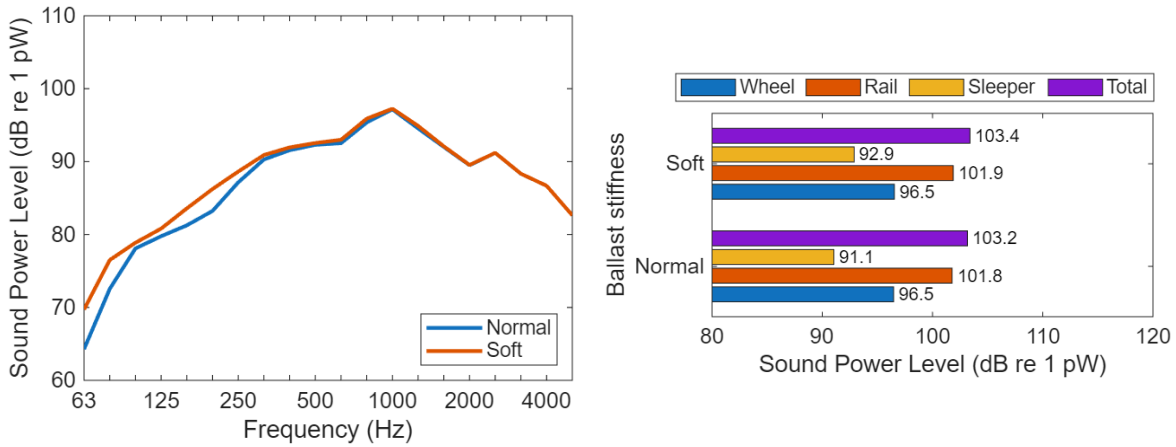

(a) (b)

Figure 17. Effect of ballast stiffness: (a) total sound power spectra, (b) overall A-weighted sound power levels.

3.2.8 Slab track

Using the selected parameters for slab track in the model, the decay rates are very low in the mid-frequency range. This has the effect of overpredicting noise radiated by the rail. Figure 18 compares the predicted TDR, for the two values of fastener stiffness, with measurements from [27, 28, 29] (measured according to EN 15461 [30]). The drop from around 10 dB/m at low frequency to values below 1 dB/m occurs at a frequency that is determined by the fastener stiffness. The measured curves all correspond to slab tracks with 'normal' fastener stiffness, although a range of rail pad stiffness values is represented. However, in the mid-frequency region 400-1600 Hz the predicted TDR is generally lower than the measured curves, especially for the vertical direction.

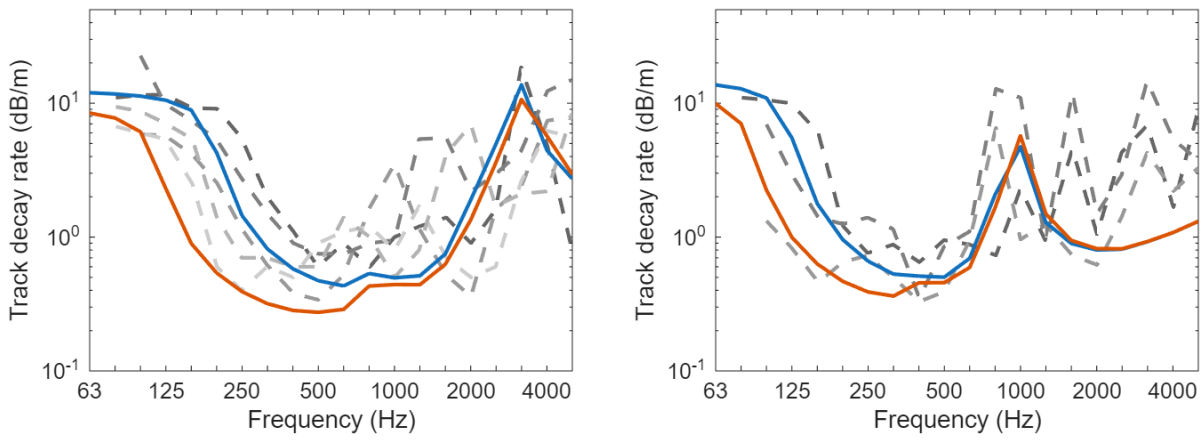

(a) (b)

Figure 18. Track decay rates for slab tracks: (a) vertical TDR, (b) lateral TDR. Blue: normal fastener stiffness; red: soft fastener stiffness; grey: measured.

Co-funded by the European Union

As shown in Figure 19, this would lead to an overall sound power level of 107.1 dB(A) for the reference conditions, compared with 103.2 dB(A) for ballasted track with medium stiffness rail pads, an increase of 3.9 dB. For the slab track with soft fasteners the predicted increase is 5.3 dB. Compared with a track with stiff rail pads (100.8 dB(A), see Figure 12), the differences are predicted as 6.3 and 7.7 dB.

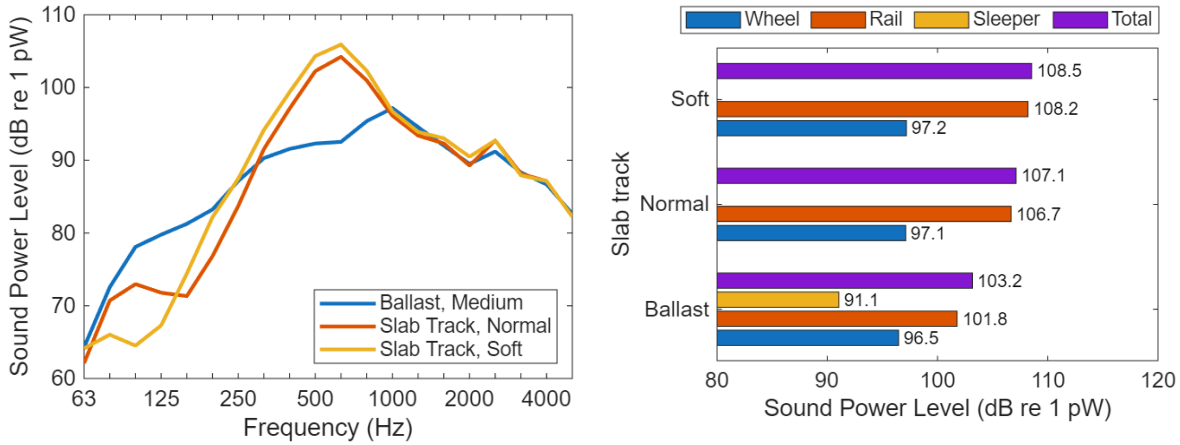

(a) (b)

Figure 19. Comparison of ballasted track (medium pad stiffness) and slab tracks (using calculated TDR): (a) total sound power spectra, (b) overall A-weighted sound power levels.

The differences in noise level between mainline slab tracks and ballasted tracks found in practice are often around 3 dB. The predicted noise levels in Figure 19 therefore seem unrealistically high. This is a direct result of the low predicted TDR in Figure 18. Although it has been shown recently [31] that there are systematic differences between the results of decay rates measured according to EN 15461 and the predicted decay rates of the principal wave, nevertheless it appears justified to moderate the difference between slab and ballasted track by increasing the predicted TDR in Figure 18. This could be achieved by using measured TDR spectra in the predictions. As a simple alternative, the TDR are here limited by adding a constant value, chosen as 0.3 dB/m. These modified TDR spectra are shown in Figure 20, which align better with the measured values. The resulting noise predictions are shown in Figure 21. The increases compared with the reference ballasted track are now 2 and 3 dB, which is more reasonable.

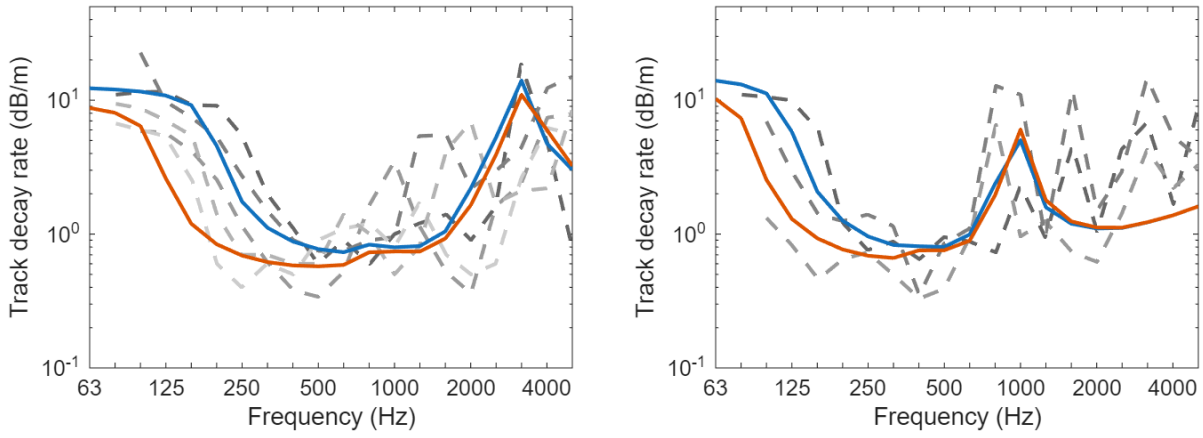

(a) (b)

Figure 20. Modified track decay rates for slab tracks: (a) vertical TDR, (b) lateral TDR. Blue: normal fastener stiffness; red: soft fastener stiffness; grey: measured.

Co-funded by the European Union

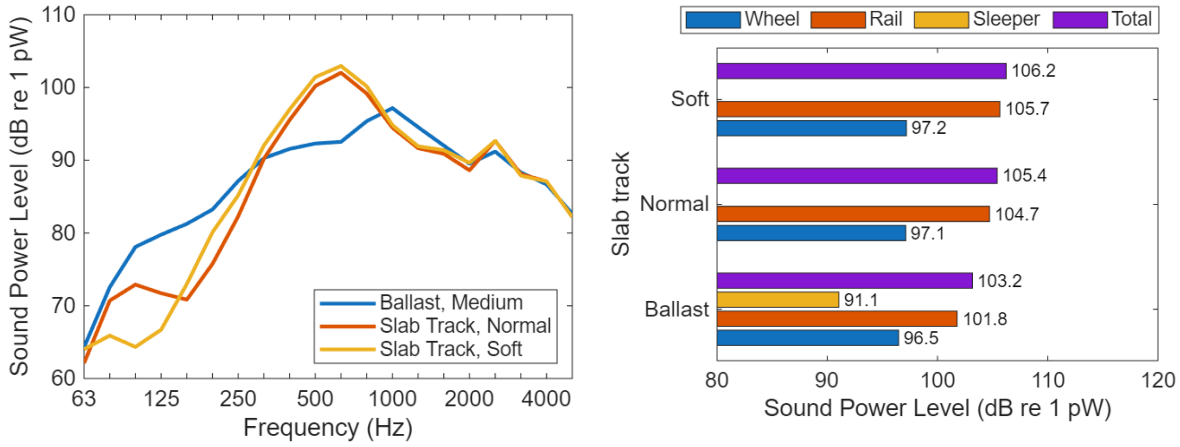

(a) (b)

Figure 21. Comparison of ballasted track (medium pad stiffness) and slab tracks (based on modified TDR): (a) total sound power spectra, (b) overall A-weighted sound power levels.

3.2.9 Rail and wheel roughness

Figure 22 compares the results for three different rail roughness spectra, with other parameters corresponding to the reference case indicated in Table 18. Compared with the 'average' rail roughness used in the reference case, the 'smooth' rail leads to a reduction of 3.7 dB(A) while the 'rough' rail leads to an increase of 6.7 dB(A). These roughness spectra are defined in Section 2.3.

The corresponding results for the different wheel roughness spectra are shown in Figure 23. The roughness spectra, and hence noise levels, of composite and disc braked vehicles are similar, whereas a noise reduction of 10-11 dB(A) can be observed by replacing cast-iron braked vehicles by composite brake blocks. This trend agrees with practical experience [15].

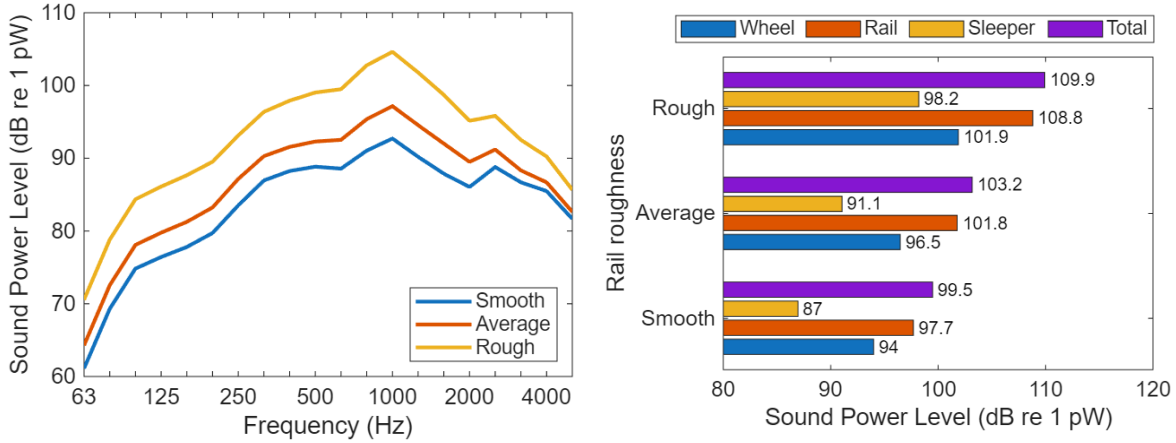

(a) (b)

Figure 22. Effect of rail roughness: (a) total sound power spectra, (b) overall A-weighted sound power levels.

Co-funded by the European Union

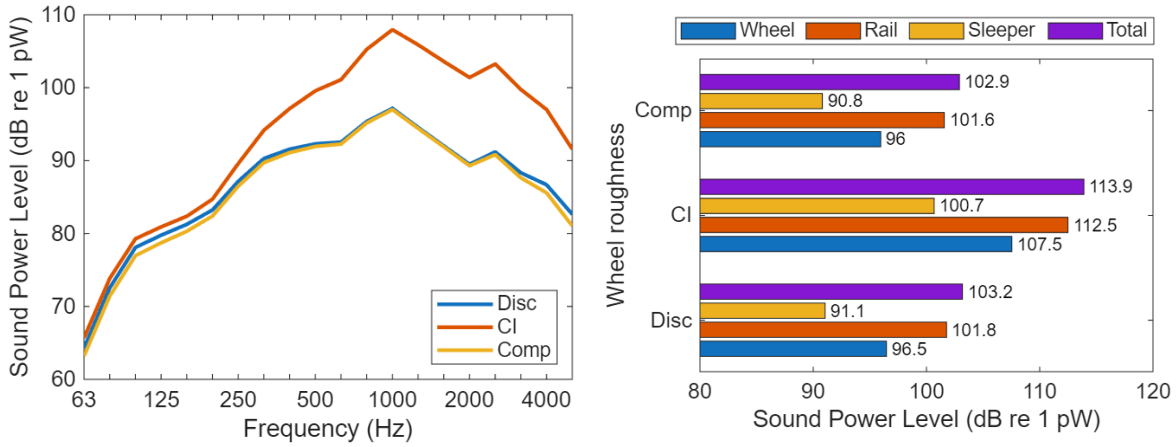

(a) (b)

Figure 23. Effect of wheel roughness: (a) total sound power spectra, (b) overall A-weighted sound power levels.

3.3 Example results for mitigation measures

3.3.1 Rail dampers and rail shields

Rail dampers are designed to increase the track decay rate. A variety of designs are commercially available, but for the purpose of illustration, a single example is included here, damper B from [17]. It should be noted, however, that other types of rail damper may give smaller benefits.

To estimate the effect on the rolling noise, the TDR of a track fitted with the dampers is calculated by combining [17]:

- the decay rate of a bare rail fitted with these dampers (obtained from measurements [17], see Section 2.4.2)
- the TDR of the untreated track (obtained from the TWINS/TNE calculation model and stored in the database).

According to this method, the effect of rail dampers fitted to any track can be estimated. Results are shown in Figure 24 for the reference parameters for both dampers from [17]. The total noise spectrum is reduced between 315 and 2000 Hz, where the rail is the dominant component, see Figure 8. The overall level is reduced by 3.9 dB(A) for damper B and 3.6 dB(A) for damper A. The influence on the sleeper and wheel components is negligible. The effect of the rail damper on the vertical and lateral TDR is shown in Figure 24(d) for damper B, from which it is seen that the TDR for both directions is increased at frequencies above 315 Hz.

Co-funded by the European Union

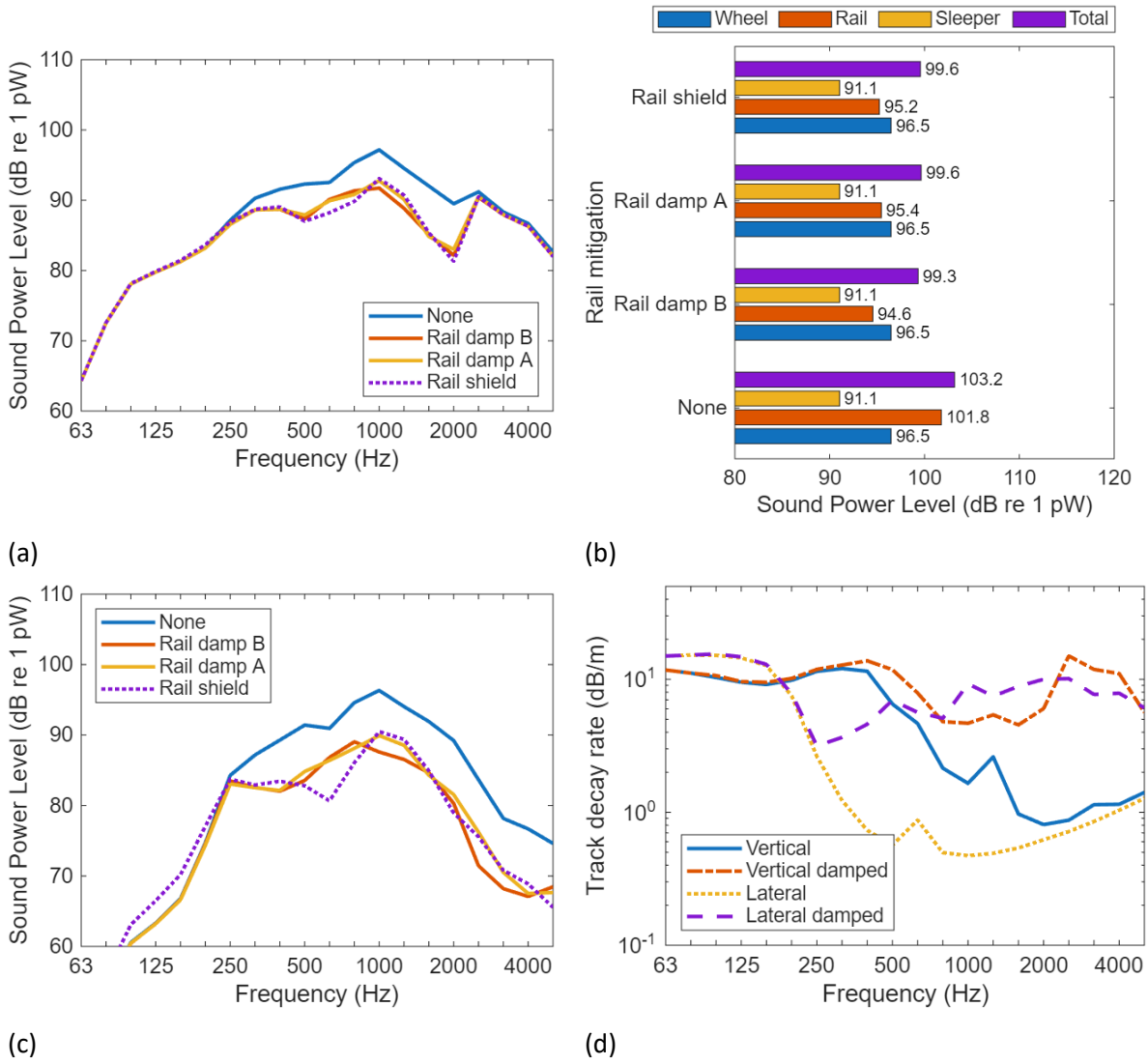

Figure 24. Effect of rail mitigation measures: (a) total sound power spectra, (b) overall A-weighted sound power levels, (c) rail sound power spectra, (d) track decay rates for rail damper B.

As an alternative to a rail damper, a rail shield can be used that encloses the rail web and foot. This does not affect the track decay rate but reduces the sound radiation from the rail. The insertion loss of such a shield has been estimated using numerical methods in [18], see Section 2.4.3. Based on these results, the change in noise levels due to the use of a rail shield is shown in Figure 24. The effect on the total noise level in this reference case (which has a relatively quiet wheel design) is shown as 3.7 dB(A). This is consistent with measured noise reductions, which have been reported between 2 and 4 dB depending on the wheel type, train speed and rail pad stiffness [32, 33]; for very soft rail pads and quiet wheels a reduction of up to 5.4 dB has been found [34].

Rail dampers are more effective for soft rail pads and less effective for stiff ones where the TDR is already high (Figure 13) [35]. Figure 25 shows the overall effect of rail dampers for different values of rail pad stiffness. Figure 25(a) shows the total sound power levels, Figure 25(b) the sound power levels from the rail, and Figure 25(c) the reduction in total sound power levels due to introduction of the mitigation measures. The reduction in total noise level due to the use of rail damper B is 6.3 dB(A) for very soft pads, reducing to 1.6 dB(A) for very stiff pads; for damper A the reductions are 0.3 dB(A) less in each case. The noise level shows a much weaker dependence on rail pad stiffness as a result.

Co-funded by the European Union

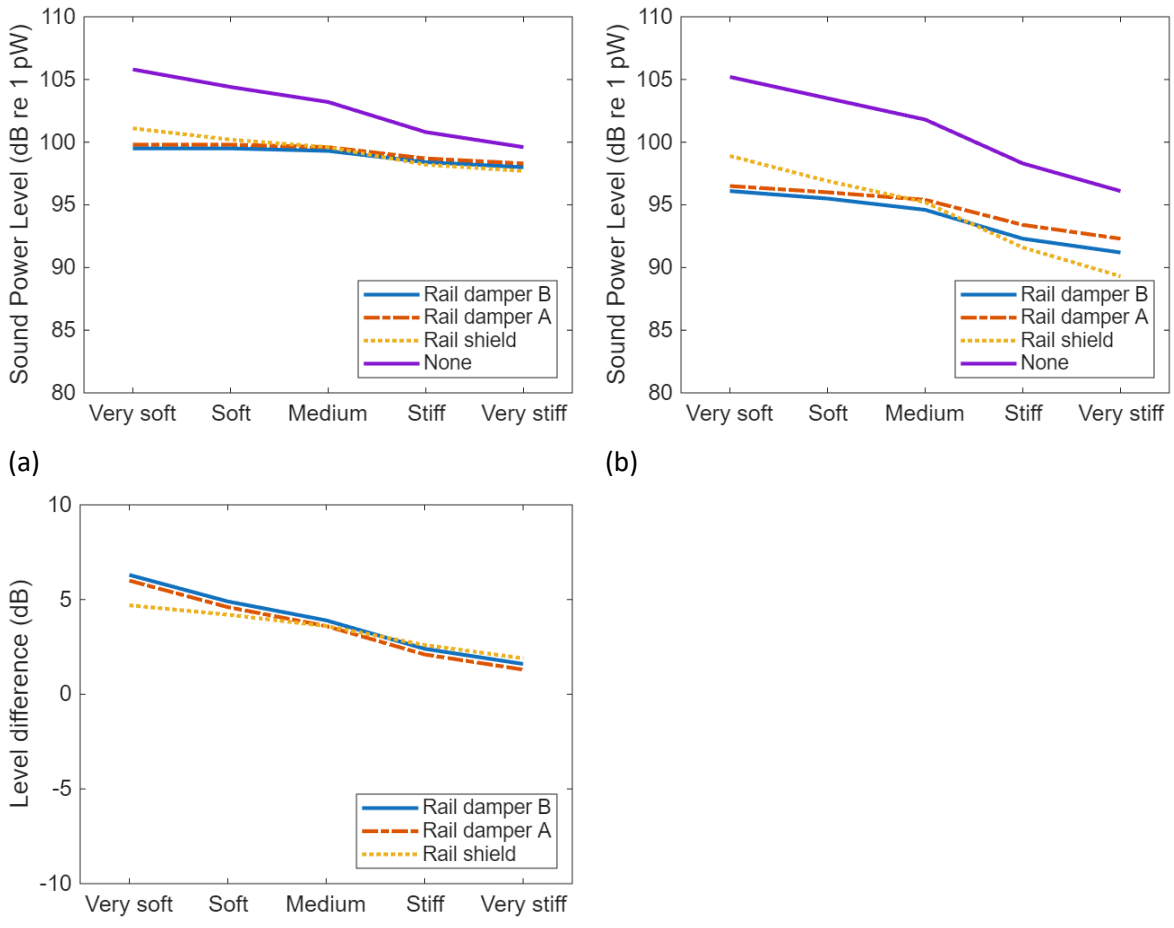

Figure 25. Effect of rail mitigation measures for different rail pad stiffness values: (a) total A-weighted sound power levels with and without mitigation measures, (b) A-weighted sound power levels from rail with and without mitigation measures, (c) effect of mitigation measures on total A-weighted sound power levels.

For the rail shields, the reduction in the rail component is largely independent of the rail pad stiffness. Consequently, for the very soft pad the overall benefit is 4.8 dB(A), which is lower than for the rail damper, whereas for the very stiff pad it is 2.1 dB(A) which is slightly better than the rail damper.

Note that the effect of both rail dampers and rail shields on the total noise levels shown here has been calculated for the Regional passenger wheel type; the effect will be smaller for other wheel designs, as these have a larger wheel component of noise, see Figure 10. As an example, Figure 26 shows the results for the low-stress freight wheel. In this case, the higher wheel contribution means that the reduction in total noise is 2.7 dB(A) for the rail damper and 2.5 dB(A) for the rail shield.

Co-funded by the European Union

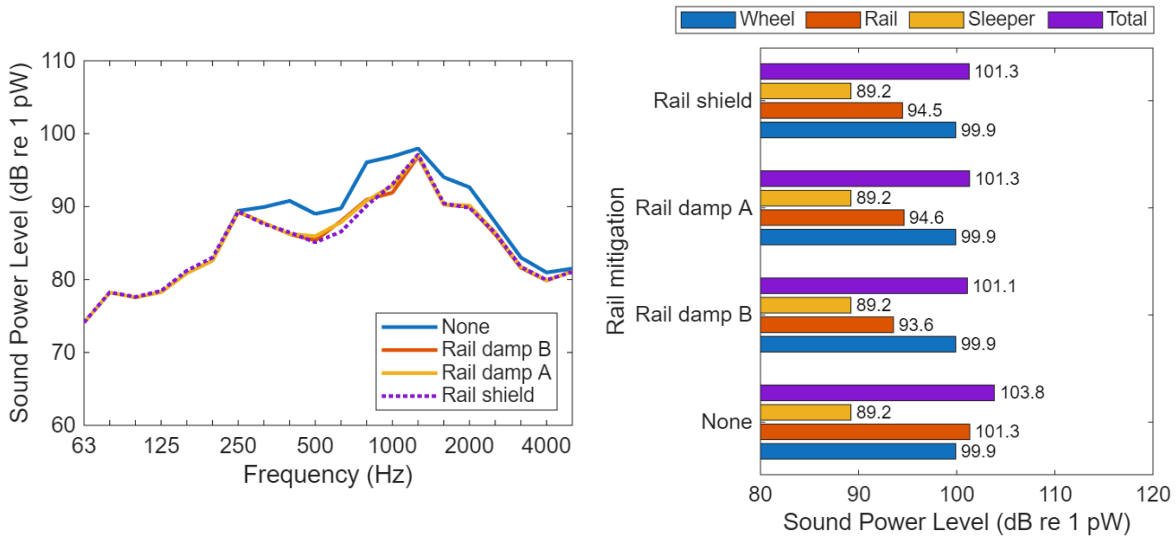

(a) (b)

Figure 26. Effect of rail mitigation measures for low-stress freight wheel: (a) total sound power spectra, (b) overall A-weighted sound power levels.

3.3.2 Optimised rail pads

Optimised rail pads have been developed and tested in the UIC LOWNOISEPAD project [4]. A key feature of these optimised pads is their ability to increase the TDR while maintaining a moderate level of static and low-frequency dynamic stiffness. The dependence of TDR and noise on rail pad stiffness and damping has been presented in Section 3.2.5. The user should therefore select a high value of acoustic stiffness and a lower value of low-frequency dynamic stiffness. Changes to the pad damping have a smaller effect. Alternatively, measured TDRs can be entered by the user where these are available.

By way of example, the measured vertical and lateral TDRs from a track with optimised rail pads and another with stiff EVA pads from [36] are shown in Figure 27. Two measured results are shown for each rail pad, corresponding to the left and right rails at the same site. There is no significant difference between the vertical TDRs for the EVA pad and the optimised pad; in the lateral direction the optimised pad has a higher TDR at high frequencies.

These measured TDRs are compared in Figure 27 with predicted TDRs for the ‘stiff’ and ‘very stiff’ rail pads as defined in Section 2.1.2. For the vertical direction, it appears that a stiffness close to the ‘very stiff’ value (2000 MN/m) would be appropriate and should give good agreement with the measurements. For the lateral direction the ‘stiff’ rail pad gives reasonable agreement at low and mid frequencies but above 1.6 kHz the measured TDR increases considerably.

The effect of introducing an ‘optimised’ rail pad will depend on the stiffness of the original rail pad as well as on the properties of the particular ‘optimised’ rail pad to be used. If this is already stiff the difference will be small, whereas if it is soft a much larger effect can be expected, as seen in the results in Section 3.2.5. It is proposed that it is left to the user to select the most appropriate values of rail pad stiffness (and damping).

Co-funded by the European Union

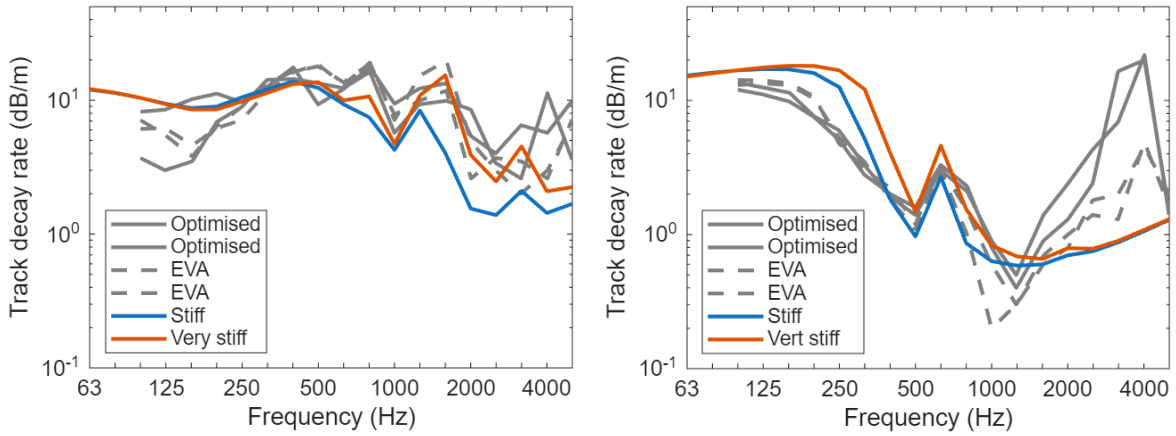

(a) (b)

Figure 27. TDR for stiff and optimised pads, comparison with measurement results from [36]: (a) vertical, (b) lateral.

3.3.3 Under-sleeper pads

Three different values of under-sleeper pad (USP) stiffness are defined in Section 2.1.3. USPs introduce a flexible layer between the sleeper and the ballast. Consequently, the damping of the sleeper that is normally provided by contact with the ballast is reduced. Prediction results are shown in Figure 28. As the USP stiffness is reduced, the sleeper contribution increases significantly, as seen in Figure 28(b,c). The TDR is also affected by the introduction of USPs in some frequency bands, as seen in Figure 28(d). However, the total noise spectrum is only affected below 1 kHz, as seen in Figure 28(a) and the overall level varies by between 1 and 2 dB(A). In reality, it is possible that the effect is smaller than these results indicate.

Co-funded by the European Union

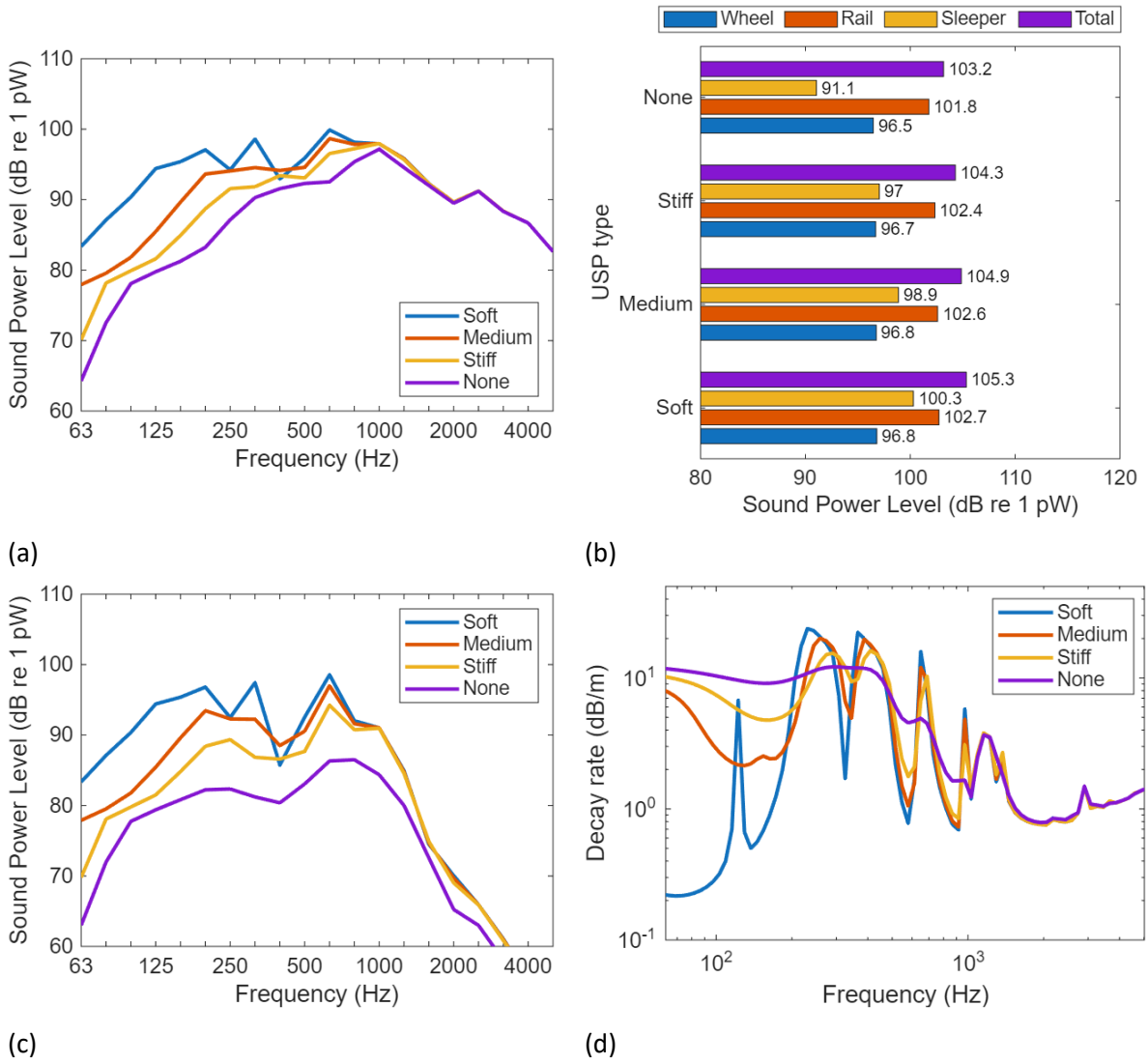

Figure 28. Effect of USP: (a) total sound power spectra, (b) overall A-weighted sound power levels, (c) sleeper sound power spectra, (d) vertical TDR.

3.3.4 Acoustic rail grinding

Rail grinding affects the rail roughness spectrum. Where rail roughness spectra are available to represent the effect of acoustic rail grinding, these can be introduced into the tool. In the absence of specific data, the 'smooth' rail roughness spectrum in the database can be used to represent the outcome from acoustic rail grinding. Figure 22 shows an example of the effect of this change in roughness on the noise for the reference case, giving a predicted reduction of 3.7 dB(A) at 120 km/h compared with the 'average' rail roughness.

This analysis could be refined by including typical roughness spectra, representative of the average situation after implementation of an acoustic grinding strategy. In Appendix A a comparison is given of various measured rail roughness spectra and their effect on noise levels. This study indicates that the sonRail 'average' and 'smooth' spectra used here are reasonably representative of normal and ground track. The alternatives listed in Appendix A could be used if preferred, or the user could enter their own spectra.

Co-funded by the European Union

3.3.5 Wheel braking system

As observed in Figure 23, a noise reduction of 10-11 dB(A) can be obtained by replacing cast-iron braked vehicles by composite brake blocks. This is an established noise control measure.

3.3.6 Noise barriers

The effects of noise barriers, both conventional lineside barriers and mini-barriers, are expected to be dependent on receiver location, both height and distance from the track. They will therefore be considered within the noise reception calculations, rather than in the source data generated in Task T4.2.

3.4 Cross-checking of models and calculation of ballast stresses

The main noise prediction results described above are based on the TWINS/TNE models of ISVR. A benchmarking exercise has been carried out to cross-check these models against the Swiss ToPNoise models of EMPA and HES-SO. These comparisons are described in Appendix B.

In addition, ToPNoise has been used by HES-SO to predict the effect of different track components on the stresses applied to the ballast, allowing a qualitative estimate of the effect on track settlement. This is described in Appendix C.

Co-funded by the European Union

4. Vibration results

4.1 Calculation cases

Ground vibration is calculated in the form of force densities and vibration levels at different distances from the track using the TRAFFIC model of KU Leuven [37] for a unit roughness spectrum. The input parameters used are listed in Section 2. These results will be stored in a database and combined with wheel and rail unevenness spectra for the chosen train speed in the web-based tool.

Table 19 lists the variants included in the vibration calculations. A reference case is selected (shown highlighted in the table) for the purpose of illustrating the results in this report. Similar to the noise calculations, not all combinations are considered. For example, under-sleeper pads are only considered for concrete monobloc sleepers and stiff ballast as they are not applied in practice on other sleeper types. For concrete sleepers (monobloc and bibloc), the very soft, soft and medium rail pads are considered, whereas for steel and wooden sleepers the stiff rail pads are used. Vibration level spectra for unit unevenness have been calculated for a total of 1155 combinations. Line source transfer mobilities are also provided which can be used in combination with the velocity levels to derive force densities [40].

Vibration level spectra at 16 m from the track are shown in the next section, for cases in which one parameter at a time is varied while the others retain their reference value. Train speed can be set arbitrarily, but for the purpose of illustration, five values are considered here, with 120 km/h selected as the reference value. In addition, force density spectra are also shown, which are derived from the vibration velocity levels minus the corresponding line source transfer mobility (in dB).

Table 19. Summary of variants considered for vibration calculations (reference case is shown shaded)

Component	Variants				
Vehicle type	Passenger (unpowered)	Passenger (multiple unit)	Freight		
Rail type	60E2				
Rail pad stiffness	Very soft	Soft	Medium	Stiff	
Rail pad damping	Low				
Sleeper type	Conc monobloc (heavy)	Concrete bibloc	Wood	Steel	
Under-sleeper pad	None	Stiff	Medium	Soft	
Ballast	Stiff	Soft	Slab track		
Under-ballast mat	None	Medium	Soft		
Ground	Soft	Moderately soft	Medium	Moderately stiff	Stiff
Distance	8 m	16 m	32 m	64 m	
Rail unevenness (ballasted track)	HS or well-maintained	Normally maintained	Not well maintained		
	Freight line	Normally maintained and corrugated	Not well maintained and corrugated		
Wheel roughness	Disc-braked	Cast-iron braked	Composite braked		
Train speed (km/h)	50	80	120	160	200

Co-funded by the European Union

4.2 Example results for parameter variations

4.2.1 Reference case: effect of distance

Results are stored in the database for distances from 4 m to 32 m at 1 m intervals, and to 64 m at 4 m intervals. For the reference case indicated in Table 19, the vertical vibration velocity spectra are shown in Figure 29(a) at four different distances from the track. Higher frequencies are attenuated to a greater extent with increasing distance than low frequencies. Consequently, the peak in the vibration spectrum shifts from 63 Hz at 8 m from the track to 32 Hz at 64 m.

The force density spectra in Figure 29(b) show a much weaker dependence on the distance, at least above 10 Hz. The peak at 63 Hz is stronger in the force density evaluated from the vibration at 8 m than for larger distances.

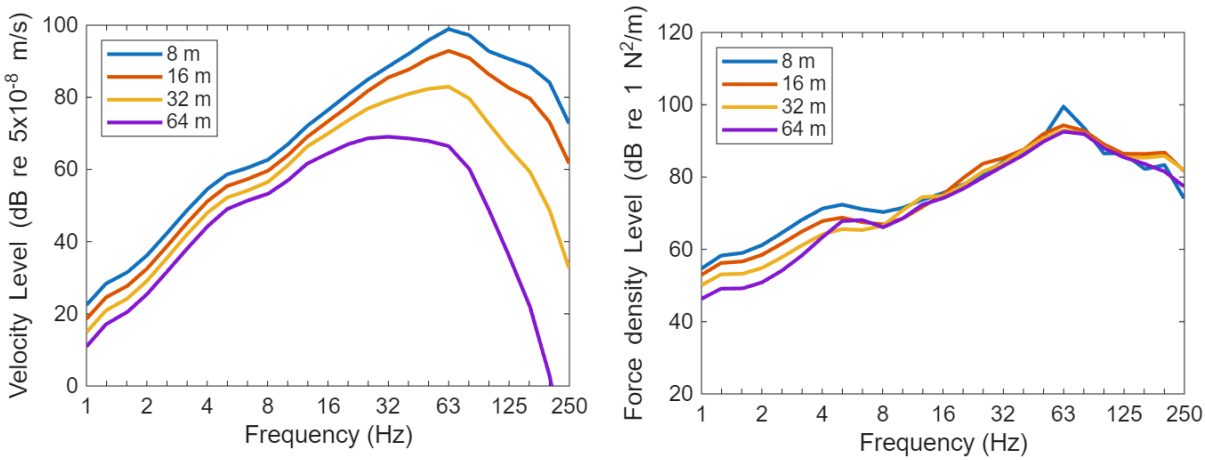

(a) (b)

Figure 29. (a) Vertical vibration velocity spectra for reference case (120 km/h) at different distances from the track, and (b) corresponding force densities.

4.2.2 Ground stiffness

Five different homogeneous ground types are considered, as described in Section 2.1.6. For the reference case indicated in Table 19, the vertical vibration velocity spectra are shown in Figure 30(a). The vibration at frequencies below about 40 Hz is greater for softer ground conditions, whereas at high frequencies the opposite is true.

The force density spectra in Figure 30(b) have a much weaker dependence on ground stiffness below 50 Hz, but there are differences at higher frequencies due to the influence of the ground properties on the track mobility.

Co-funded by the European Union

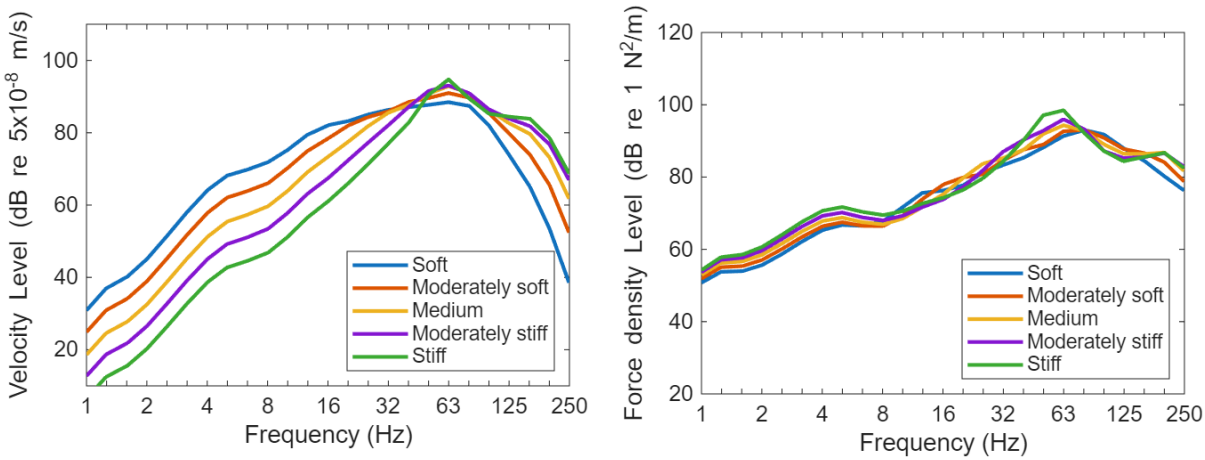

(a) (b)

Figure 30. (a) Vertical vibration velocity spectra for different ground types (at 16 m from the ballasted track and a speed of 120 km/h), and (b) corresponding force densities.

4.2.3 Train speed

Figure 31(a) shows the vibration spectra for five train speeds, with other parameters set to correspond to the reference case indicated in Table 19. As speed increases, the vibration at higher frequencies increases more than that at low frequencies. Similar trends are seen in the force density spectra in Figure 31(b). This is a consequence of the shape of the unevenness spectra, plotted in Figure 31(c) against frequency. The main peak remains at 63 Hz and is related to the 'P2 resonance' in which the unsprung mass of the vehicle bounces on the stiffness of the track and ground.

In practice, peaks will occur in the vibration spectrum corresponding to harmonics of the vehicle passing frequency [38]. However, these peaks do not appear in the current results as they are based on incoherent axle loads. Although this omission affects the detailed spectrum shape the overall level is hardly affected [39].

Co-funded by the European Union

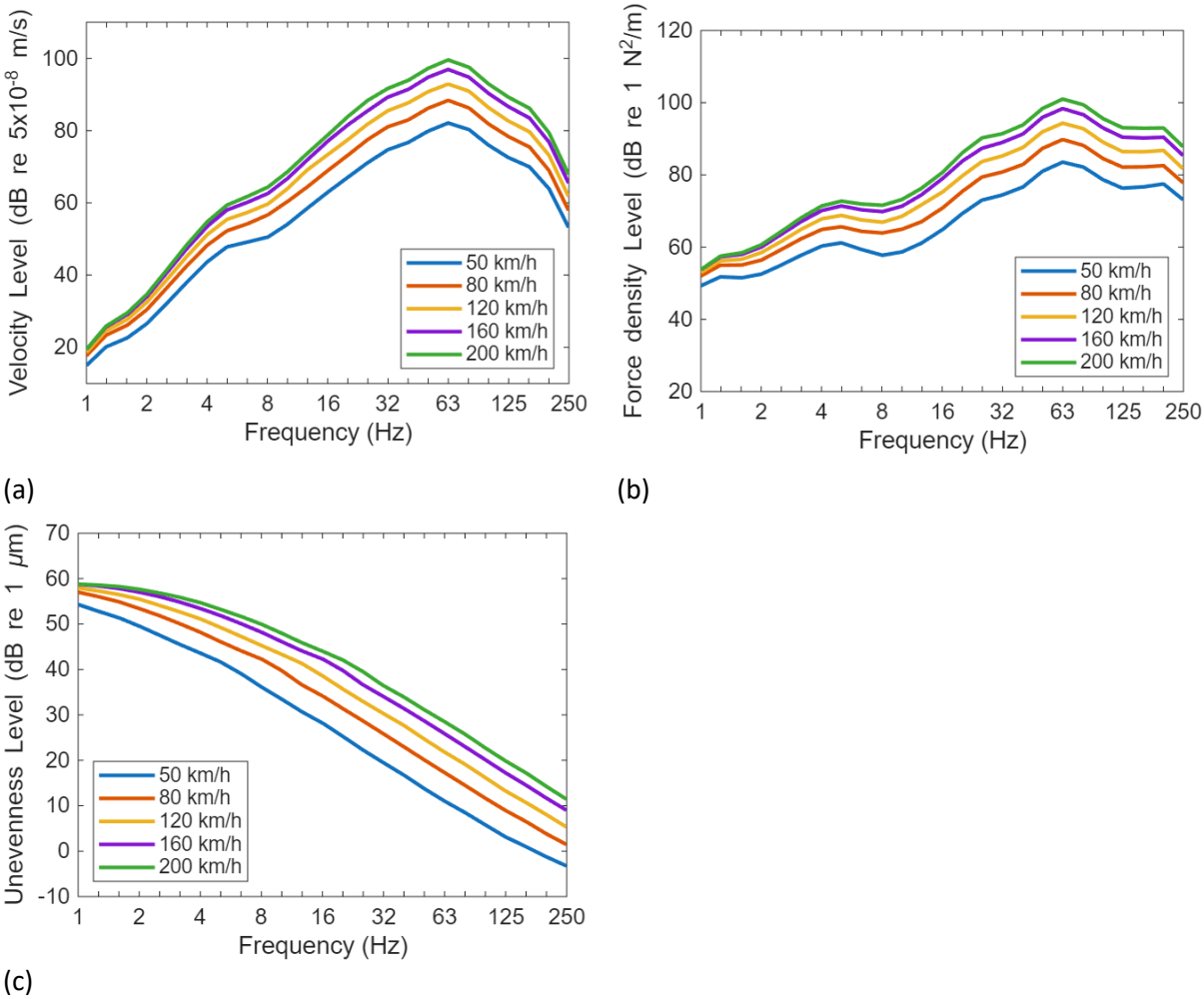

Figure 31. Effect of train speed (a) effect on vibration spectra at 16 m from the track, (b) force density spectra, (c) unevenness levels plotted against frequency.

4.2.4 Train type

Figure 32 shows vibration and force density spectra for the three types of vehicle considered, with other parameters (including the unevenness spectra) set to correspond to the reference case as indicated in Table 19. Details of these vehicles are listed in Section 2.2.1. The differences between the results for these vehicles is mainly related to their unsprung mass, which is larger for the multiple unit passenger vehicle (1800 kg) and smaller for the unpowered Intercity vehicle (1200 kg), whereas it is 1400 kg for the freight vehicle. The peak at 5 Hz for the freight vehicle is related to its much higher secondary suspension stiffness.

Co-funded by the European Union

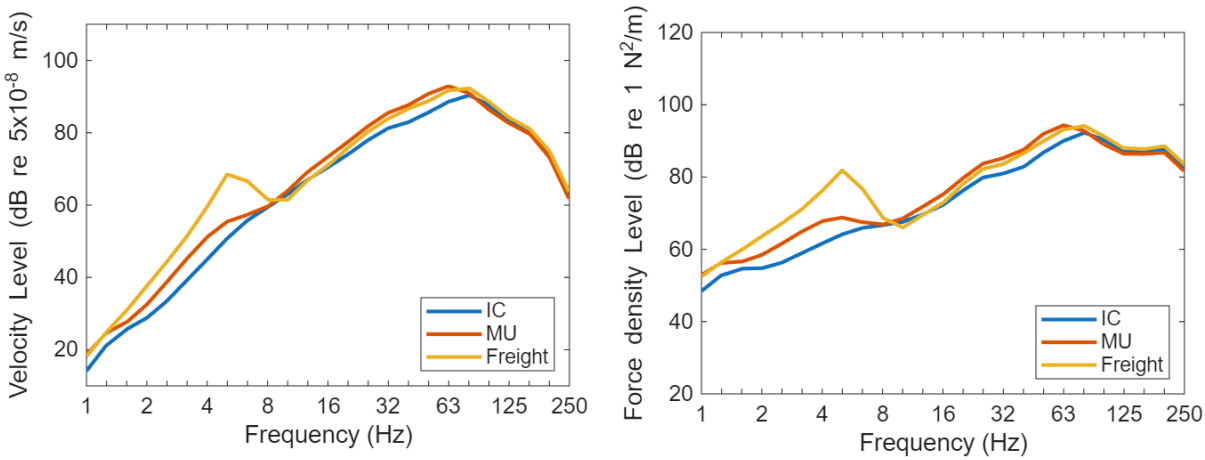

(a) (b)

Figure 32. Effect of vehicle type on (a) vertical vibration spectra at 16 m from the track and a speed of 120 km/h, (b) force density spectra.

4.2.5 Rail pad stiffness

Figure 33(a) shows the vibration spectra for three different values of rail pad stiffness, with other parameters set to correspond to the reference case indicated in Table 19. Of the five values of rail pad stiffness defined in Section 2.1.2, the two stiffest pads are not considered in the ground vibration calculations for concrete sleepers as the effect of changing from medium to stiff or very stiff pads is expected to be small.

Softer rail pads lead to lower vibration levels above 50 Hz, whereas there is a slight increase around 40 Hz. These changes are also largely reflected in the force densities shown in Figure 33(b), although the changes at high frequency are greater. The insertion loss (vibration level difference) relative to the reference case (medium rail pad stiffness) is shown in Figure 33(c).

Co-funded by the European Union

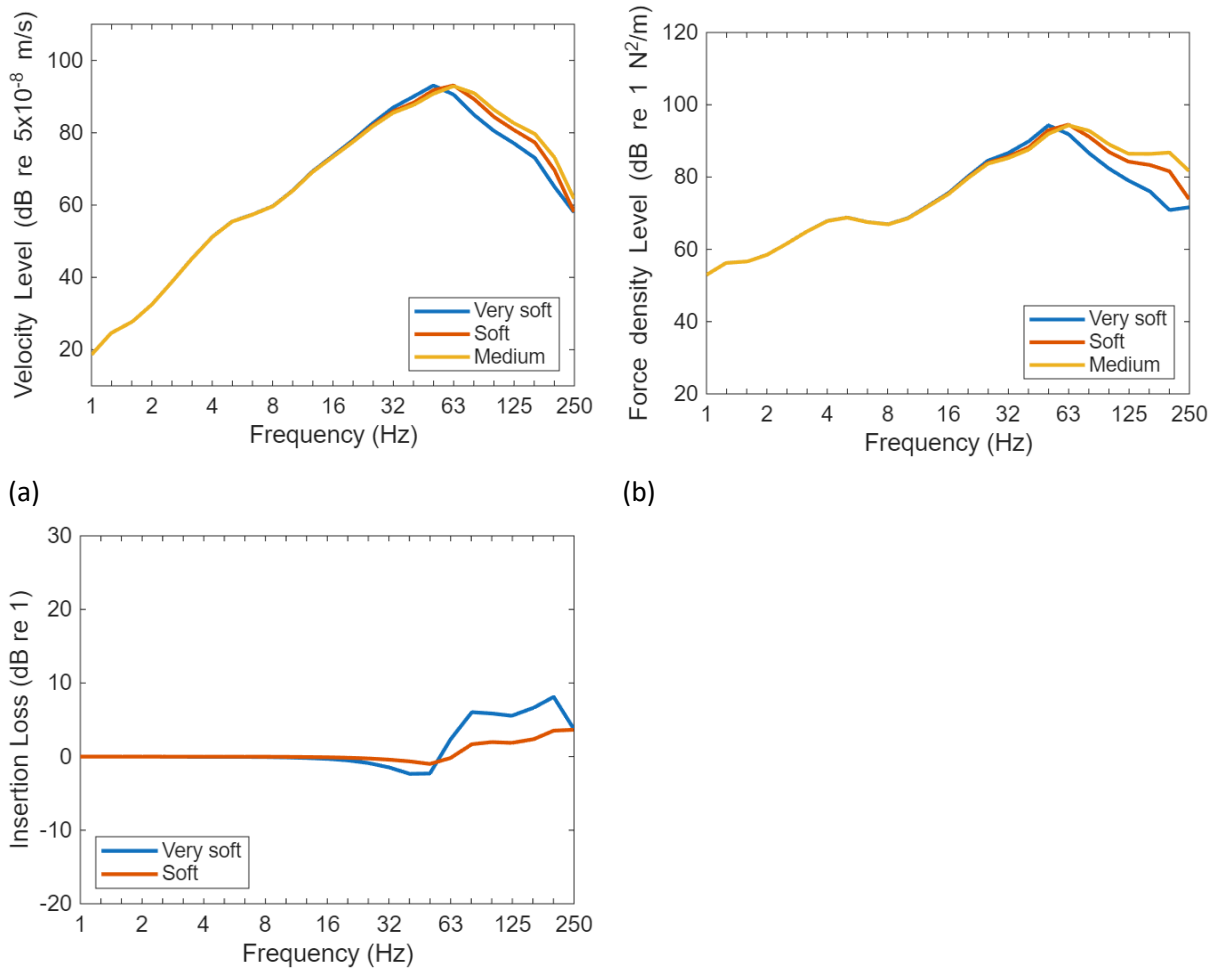

Figure 33. Effect of rail pad stiffness: (a) effect on vibration spectra at 16 m from the track and a speed of 120 km/h, (b) force density spectra, (c) insertion loss relative to medium rail pads.

4.2.6 Sleeper type

Figure 34 shows the vibration and force density spectra for four different sleeper types, with other parameters set to correspond to the reference case indicated in Table 19. The differences are negligible, which justifies neglecting other sleeper types. The sleepers differ in their masses, but this only affects the vibration above 200 Hz.

Co-funded by the European Union

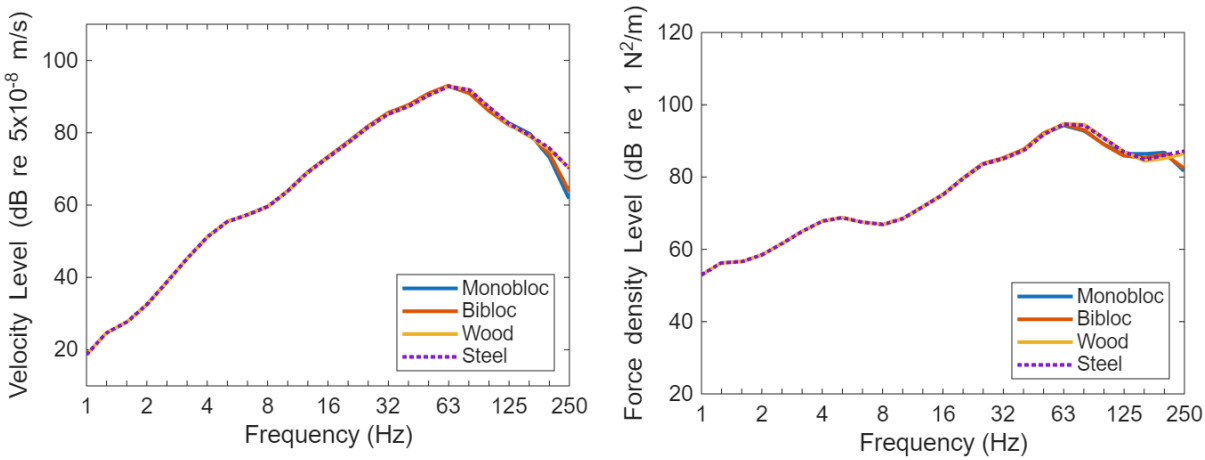

(a) (b)

Figure 34. Effect of sleeper type on (a) vibration spectra at 16 m from the track and a speed of 120 km/h, (b) force density spectra.

4.2.7 Ballast stiffness

Figure 35 shows the vibration and force density spectra for two different values of ballast stiffness, with other parameters set to correspond to the reference case indicated in Table 19. There is no strong systematic effect and there are negligible differences below 63 Hz; the softer ballast causes a small reduction in the vibration around 80 Hz and above 200 Hz, but the level is increased at other frequencies.

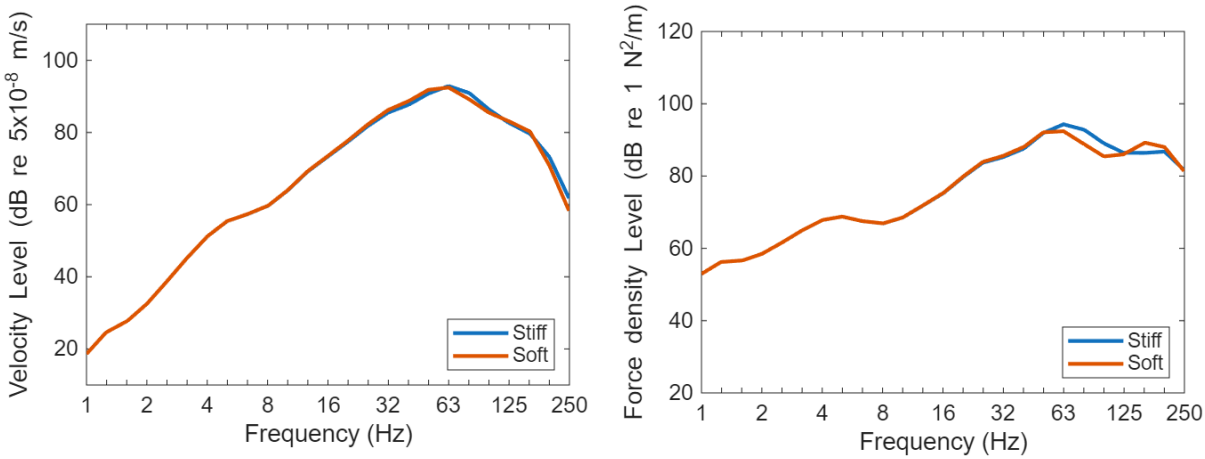

(a) (b)

Figure 35. Effect of ballast stiffness on (a) vibration spectra at 16 m from the track and a speed of 120 km/h, (b) force density spectra.

4.2.8 Slab track

Figure 36 shows the vibration and force density spectra for slab track with two different values of fastener stiffness, with other parameters set to correspond to the reference case indicated in Table 19. The results for ballasted track with two values of rail pad stiffness are shown for comparison. As both rail fasteners used on the slab track are softer than the medium rail pads, used in the reference ballasted track, the main peak in the vibration and force density (the "P2 resonance") shifts down from 63 Hz for the ballasted track to 50 Hz for the normal fastener and 31.5 Hz for the soft one. The vibration is attenuated at frequencies above these peaks. The ballasted track with very soft rail pads, also shown, has a similar P2 resonance

Co-funded by the European Union

frequency to the slab track with normal fasteners. However, compared with this result, the vibration amplitude for the slab track is reduced above 25 Hz; the difference at the peak at 50 Hz is about 3 dB and at 160 Hz it exceeds 10 dB. The differences in force density between these two cases are much smaller, indicating that the vibration attenuation for the slab track is due to the effect of the mass (and bending stiffness) of the slab in the transmission path.

The results for slab track (with the normal fastener stiffness) on different ground types are shown in Figure 37. These show similar trends to those for ballasted track in Figure 30.

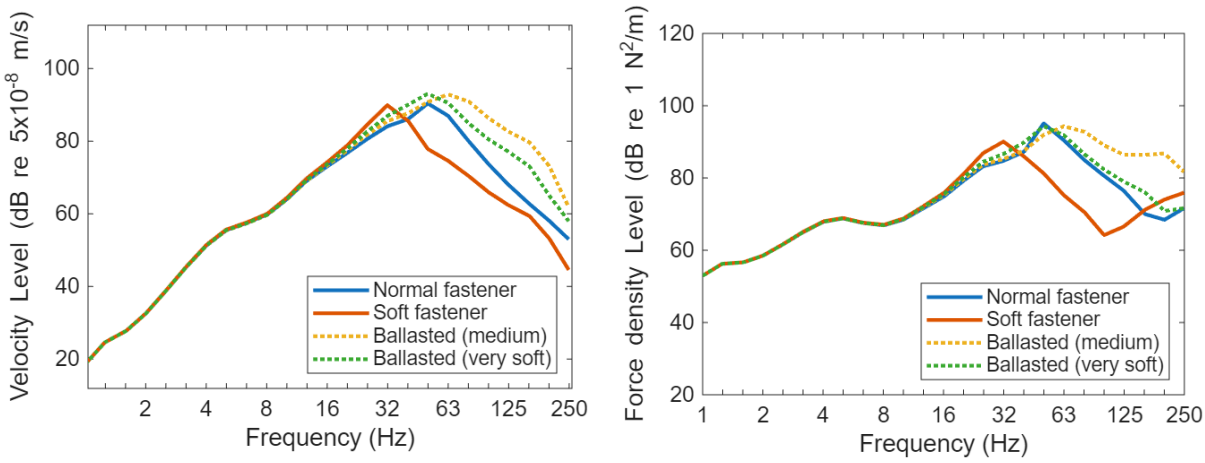

(a) (b)

Figure 36. Comparison of slab track with ballasted track. (a) Vibration spectra at 16 m from the track and a speed of 120 km/h, (b) force density spectra.

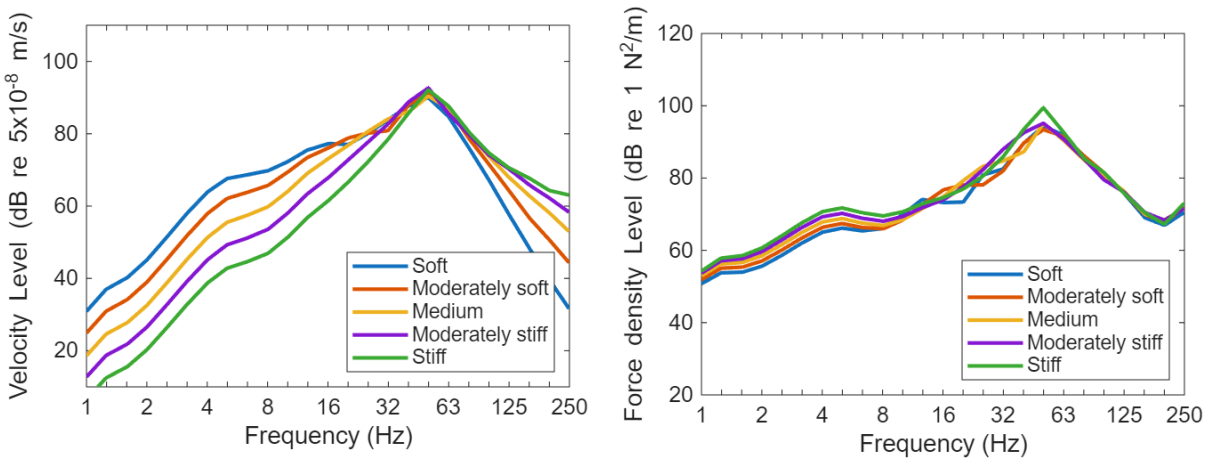

(a) (b)

Figure 37. (a) Vertical vibration velocity spectra for slab track on different ground types (at 16 m from the ballasted track and a speed of 120 km/h), and (b) corresponding force densities.

4.2.9 Unevenness

Figure 38(a) shows the vibration spectra for three different rail unevenness spectra, in each case in combination with the disc-braked wheel roughness. Figure 38(b) shows the corresponding force density spectra. The combined unevenness spectra are shown in Figure 38(c). A small peak is evident at 12.5 Hz (for 120 km/h) for the well-maintained rail unevenness, which corresponds to wheel eccentricity, i.e. at a wavelength corresponding to the wheel circumference (2.8 m).

Co-funded by the European Union

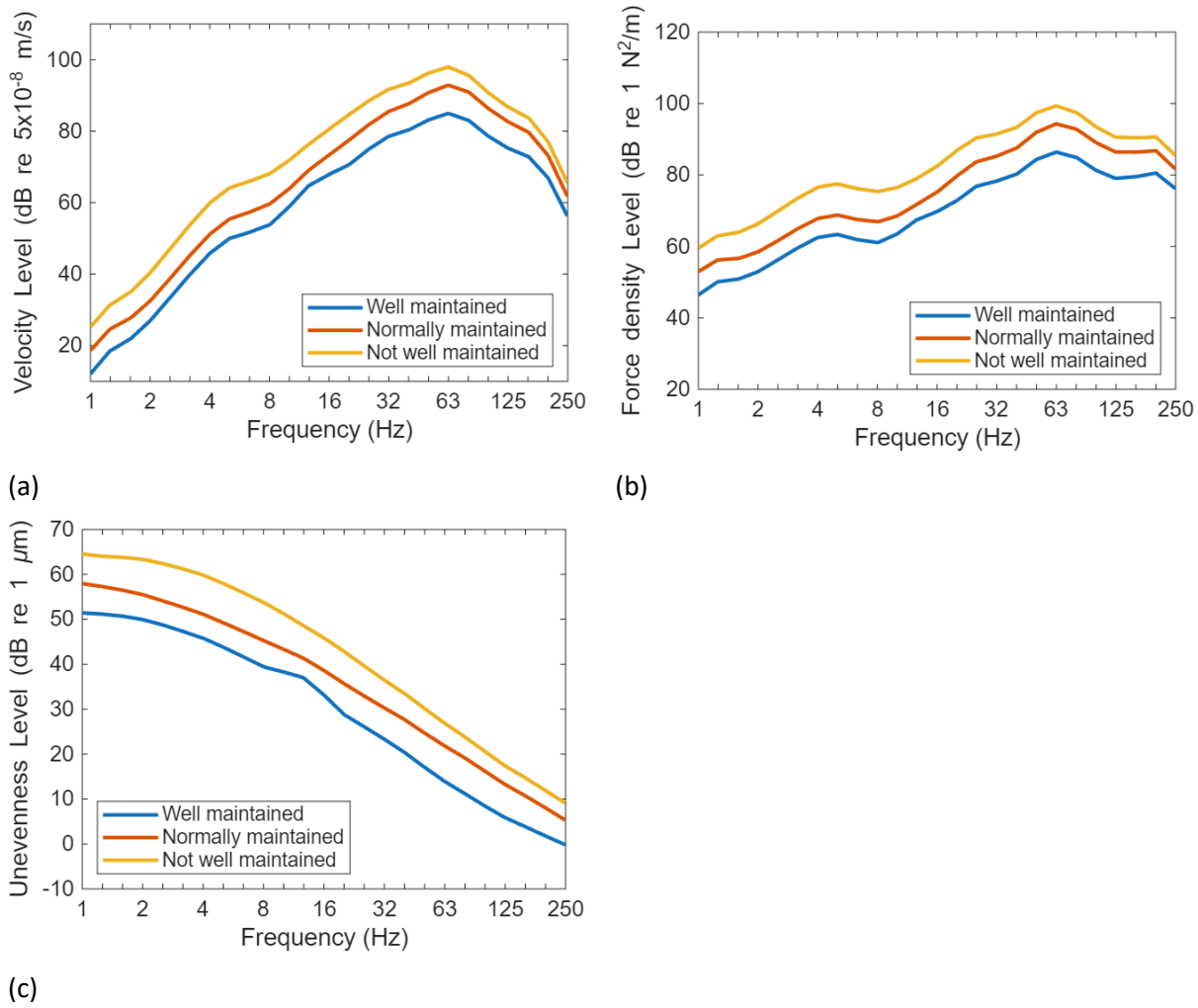

Figure 38. Effect of rail unevenness: (a) effect on vibration spectra at 16 m from the track and a speed of 120 km/h, (b) force density spectra, (c) combined wheel/rail unevenness spectra for disc-braked wheels.

The effect of varying the wheel roughness in combination with the normally maintained rail unevenness is shown in Figure 39. Equivalent results in combination with the well-maintained rail unevenness are shown in Figure 40, which highlight the differences in wheel roughness more clearly. Generally, the rail unevenness has a higher level than the wheel roughness, apart from the peak due to wheel eccentricity occurring at the wavelength corresponding to the wheel circumference, 3.15 m and/or 2.5 m, see Table 17. This wavelength corresponds to a frequency of 10-12.5 Hz at this speed.

Wheel roughness associated with the cast-iron brake blocks is higher than the other spectra at frequencies above 100 Hz (for this speed) and this increases the vibration spectrum when applied in combination with well-maintained rail unevenness. Unlike the effects on rolling noise seen in Figure 23, however, the wheel roughness has a limited effect on vibration levels.

Co-funded by the European Union

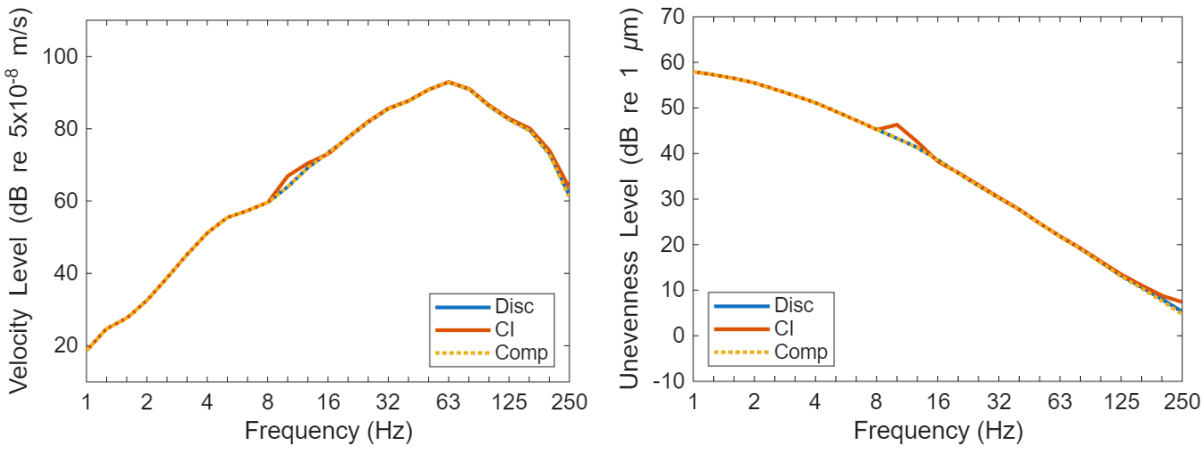

(a) (b)

Figure 39. Effect of wheel unevenness for normally maintained rail unevenness: (a) effect on vibration spectra at 16 m from the track and a speed of 120 km/h, (b) combined wheel/rail unevenness spectra.

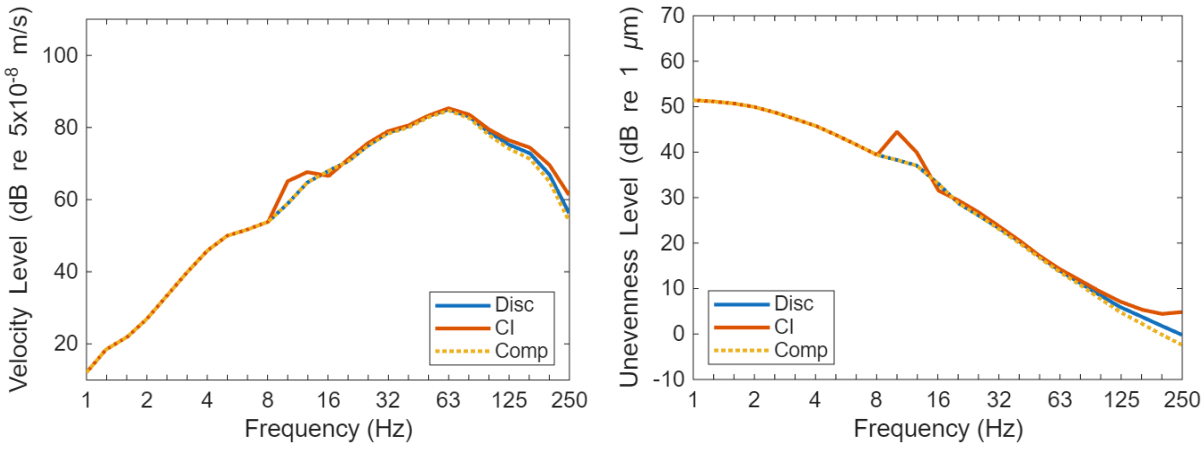

(a) (b)

Figure 40. Effect of wheel unevenness for well-maintained rail unevenness: (a) effect on vibration spectra at 16 m from the track and a speed of 120 km/h, (b) combined wheel/rail unevenness spectra.

4.3 Example results for mitigation measures at the track

4.3.1 Under-sleeper pads

The effect of under-sleeper pads (USP) with different values of stiffness is shown in Figure 41 for the medium ground stiffness. The stiff USP that is commonly used has a small effect on the vibration. The medium stiffness USP has a larger effect on the vibration around 63-80 Hz, similar to the effect of the soft rail pad seen in Figure 33. Meanwhile, the soft USP has a large effect at frequencies above 31.5 Hz and a detrimental effect around 20 Hz. The force density spectra in Figure 41(b) show a different dependence at high frequency, especially above 100 Hz, due to the effect of the USP on the track mobility. The insertion losses, based on the vibration spectra, are shown in Figure 41(c). The insertion loss for the soft USP has a dip around 20 Hz and an increasing benefit at frequencies above 31.5 Hz, whereas for the stiffer USPs the effects are more moderate. The shape of these curves is typical of resilient elements in the track [15].

Co-funded by the European Union

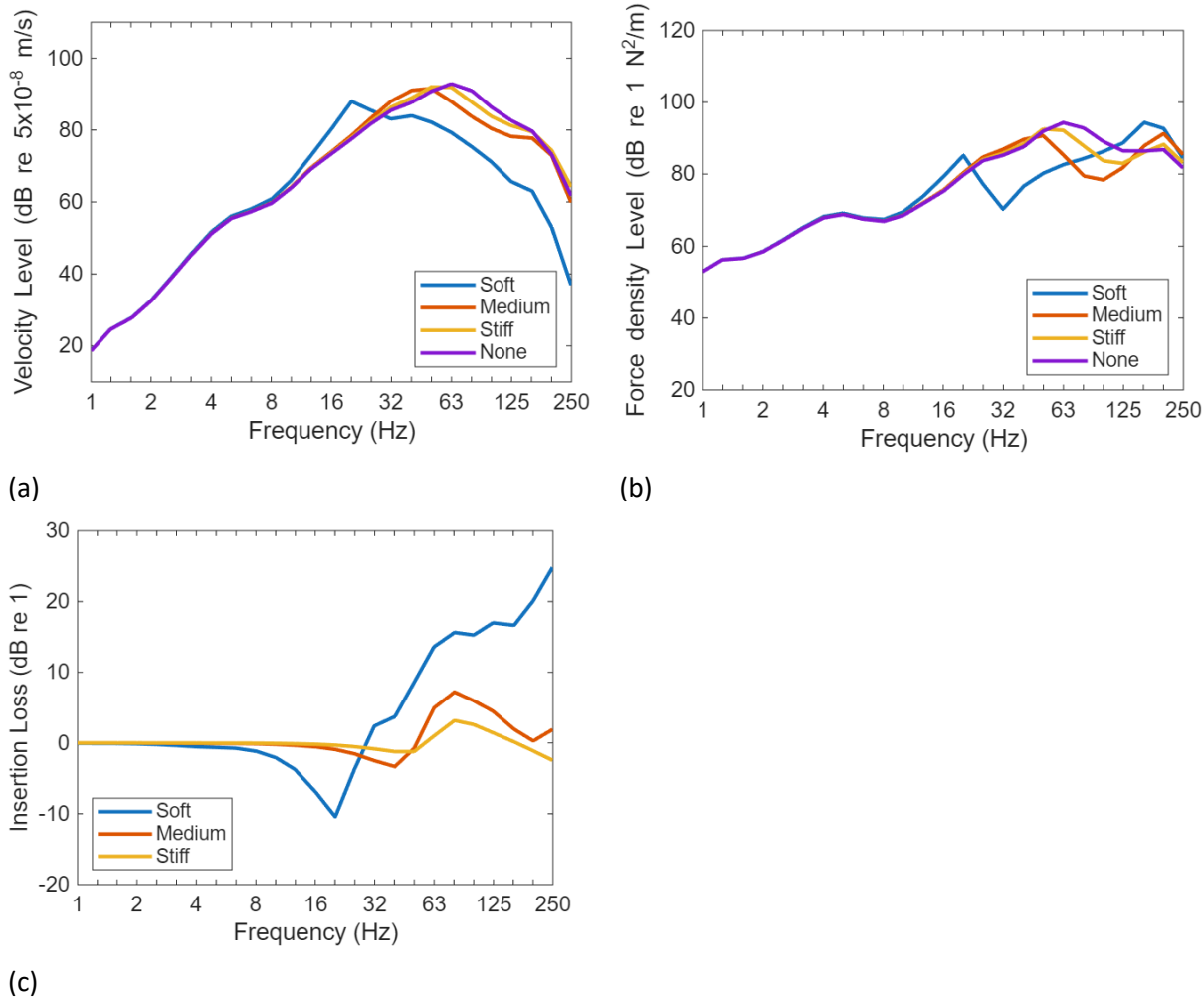

Figure 41. Effect of under-sleeper pads: (a) effect on vibration spectra at 16 m from the track and a speed of 120 km/h, (b) force density spectra, (c) insertion loss relative to no USP based on vibration spectra.

4.3.2 Under-ballast mats

The effect of under-ballast mats (UBM) with different values of stiffness is shown in Figure 42 for the medium ground stiffness. Both stiffness values of UBM lead to a reduction in the vibration above 40/50 Hz and a detrimental effect around 25 or 31.5 Hz. Again, the force density spectra in Figure 42(b) show a different dependence at high frequency, especially above 100 Hz, due to the effect of the UBM on the track mobility. The insertion losses, based on the vibration spectra, are shown in Figure 42(c). The insertion loss increases considerably at higher frequencies. Similar to the USPs in Figure 41(c), the shape of these curves is typical of resilient elements in the track [15].

Co-funded by the European Union

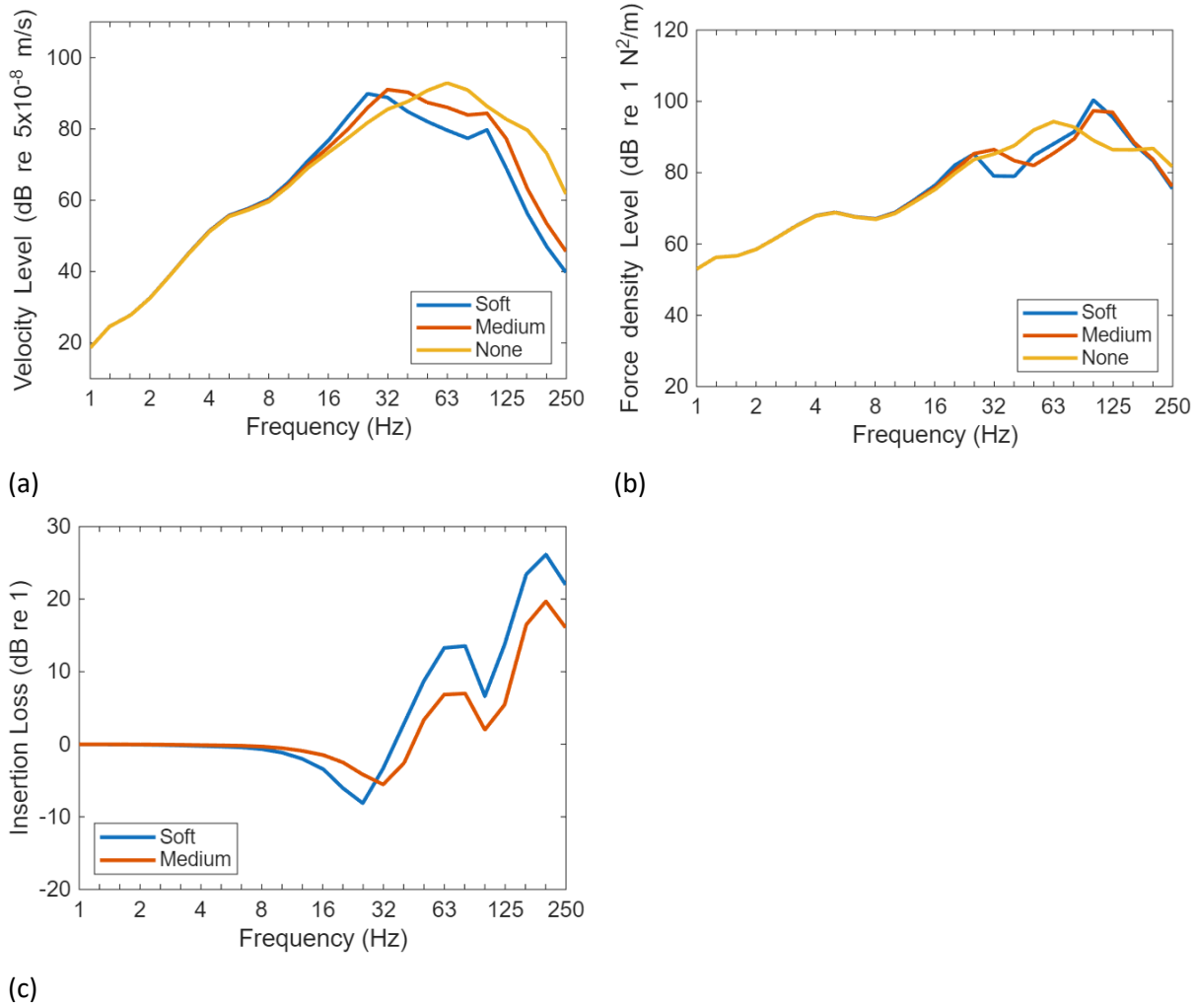

Figure 42. Effect of under-ballast mats: (a) effect on vibration spectra at 16 m from the track and a speed of 120 km/h, (b) force density spectra, (c) insertion loss relative to no UBM.

4.3.3 Rail pad stiffness

Changes to rail pad stiffness are assessed in Section 4.2.5. The insertion loss (vibration level difference) relative to the reference case (medium rail pad stiffness) is shown in Figure 33(c), which indicates that the effect is minimal unless a very soft rail fastener is introduced.

4.3.4 Unevenness

Predictions for a range of unevenness spectra are included in the database, see Section 4.2.9. Unlike rolling noise, changes to the vehicle braking system have negligible effect on the ground vibration. A change from 'normally maintained' to 'well maintained' track unevenness can lead to significant reductions in vibration. The corresponding insertion losses are plotted in Figure 43.

These spectra are based loosely on measured data for a typical mainline track and a well-maintained high-speed line. The results imply that, by suitable track construction and maintenance, the vibration can be reduced considerably; however, to increase confidence in this result, measurements of vibration before and after maintenance activity, such as tamping, would be required.

Co-funded by the European Union

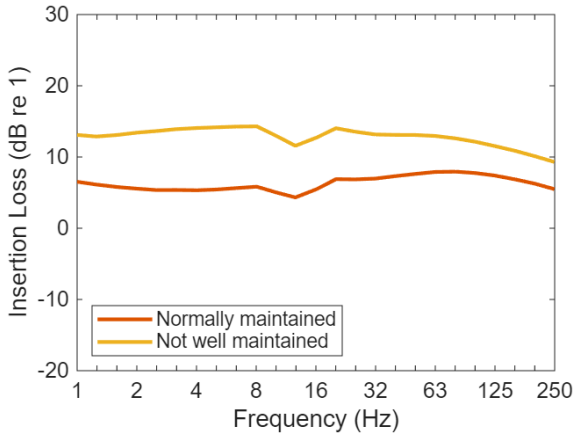

Figure 43. Effect of changing track unevenness to 'well maintained'.

4.4 Mitigation measures in the transmission path

The various mitigation measures in the transmission path that were studied in the RIVAS project are considered, as described in Section 2.5.3. As the results depend heavily on the soil properties, these results have been recalculated as insertion loss spectra corresponding to three of the five homogeneous ground types considered here (soft/medium/stiff). Example results are presented here for heavy masses beside the track and subgrade stiffening. Others, such as stiff or soft wave barriers will be added to the database as the results become available.

4.4.1 Heavy masses beside the track

The heavy masses represent a Gabion wall with a width of 1 m and a height of 2 m, located at a distance of 4 m from the track centreline. The insertion loss, for a line source along the track centreline, is shown in Figure 44 for the three types of homogeneous ground. The insertion loss shows a peak of up to 5 dB, located at about 50 Hz for the medium and stiff soils. For the soft soil, the peak is broader and located between 20 and 50 Hz. The frequencies of these peaks are determined by the combination of the added mass and the effective soil stiffness [23]. At higher frequencies and larger distances, the insertion loss drops.

Co-funded by the European Union

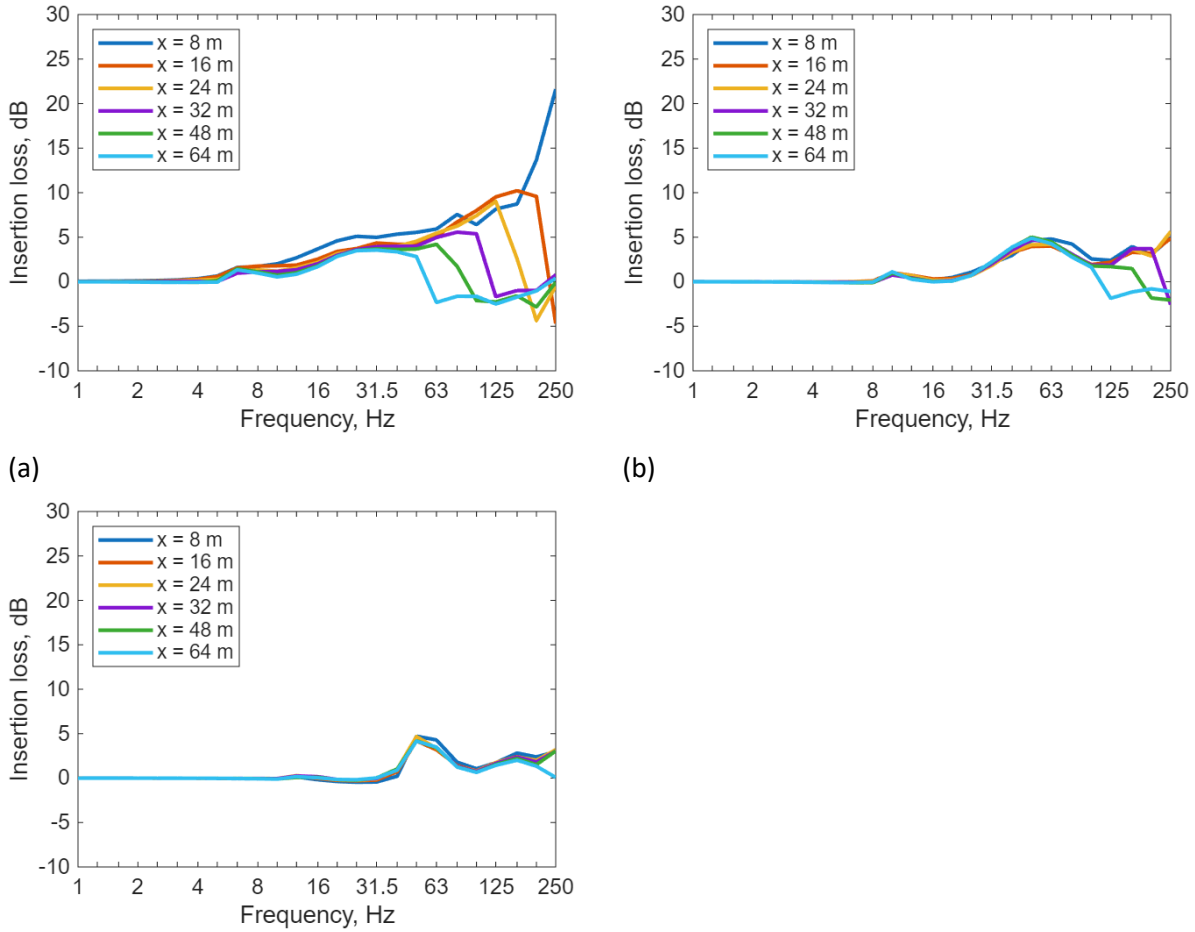

Figure 44. Effect of heavy masses beside the track for receivers at different distances from the track: insertion loss for (a) soft, (b) medium, and (c) stiff soil.

Figure 45 shows the effect of combining these results with the vibration predictions due to train traffic, for a regional train at a train speed of 120 km/h and a receiver distance of 16 m. The choice of mass leads to vibration reductions of between 3 and 5 dB at the peak frequency of the vibration in each case.

Co-funded by the European Union

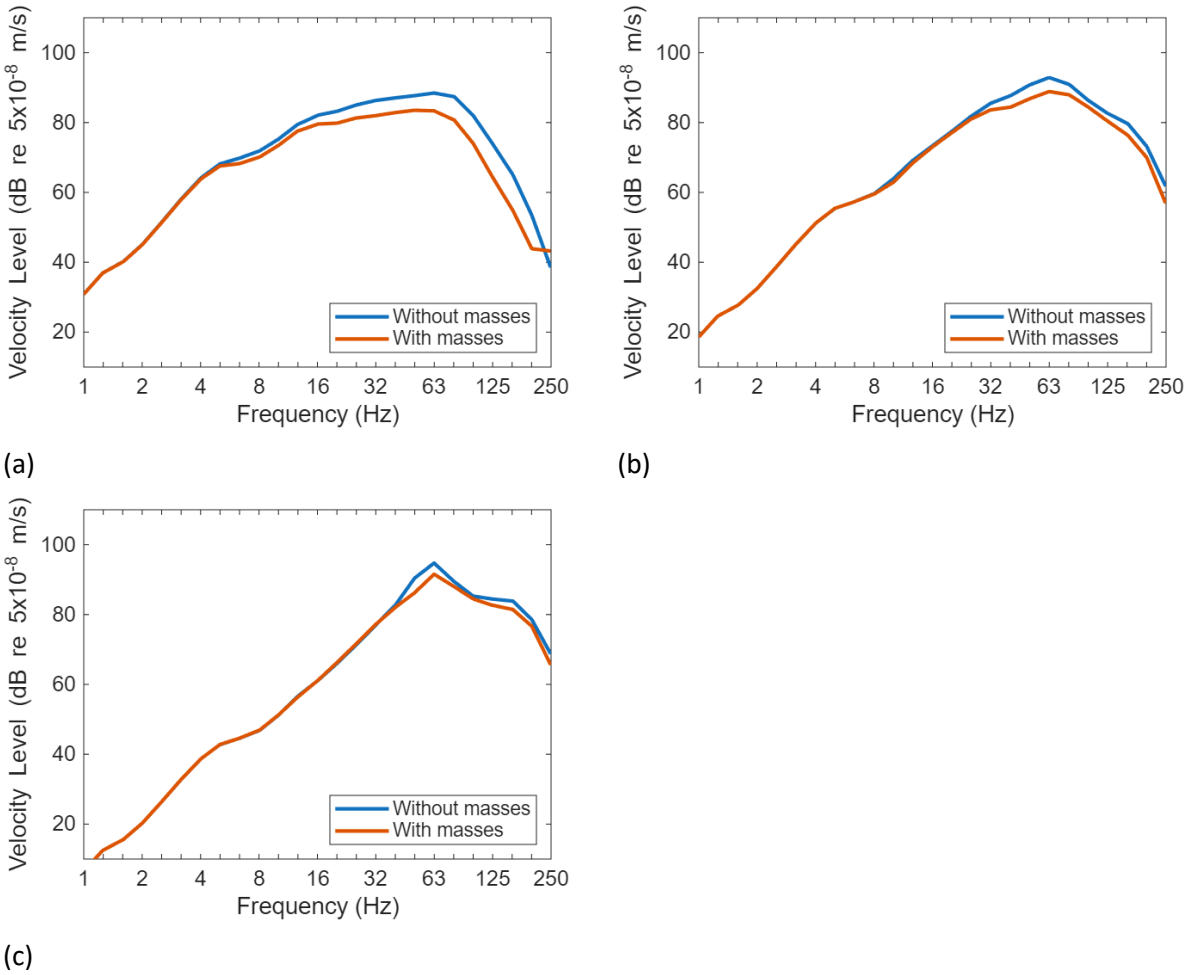

Figure 45. Effect of heavy masses beside the track on vibration spectra at 16 m from the track and a speed of 120 km/h: (a) soft, (b) medium, and (c) stiff soil.

4.4.2 Subgrade stiffening beneath the track

The subgrade stiffening has a width of 6 m, a thickness of 0.5 m (embedded at the ground surface), and is centred around $x = 0$ (the centre of the track). The insertion loss, for a line source along the track centreline, is shown in Figure 46 for the three types of homogeneous ground. The insertion loss shows an increasing trend with increasing frequency which is largely independent of distance. The frequency above which the mitigation becomes effective is around 8 Hz for the soft soil, 20 Hz for the medium soil and 63 Hz for the stiff soil.

Co-funded by the European Union

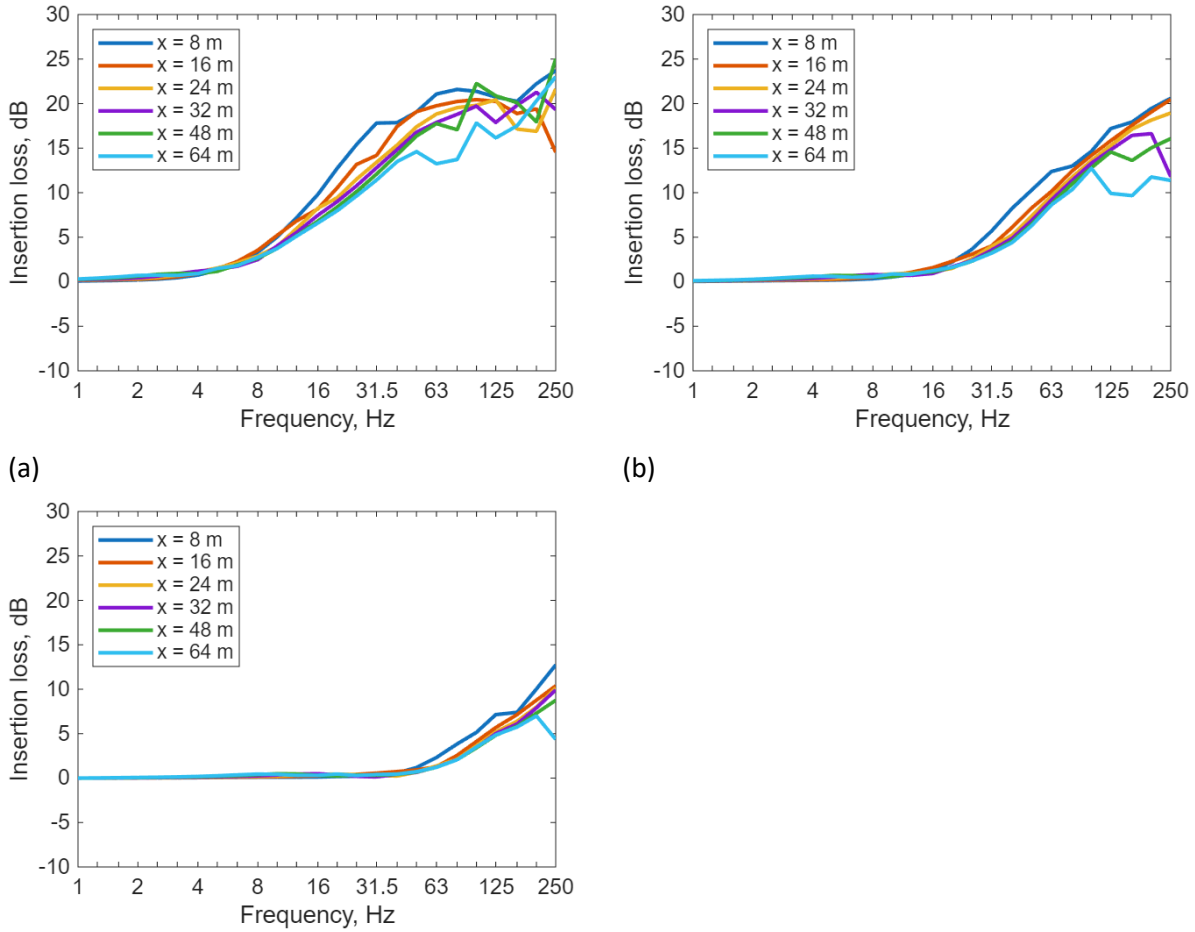

Figure 46. Effect of subgrade stiffening beneath the track for receivers at different distances from the track: insertion loss for (a) soft, (b) medium, and (c) stiff soil.

Figure 47 shows the effect of combining these results with the vibration predictions due to train traffic, for a regional train at a train speed of 120 km/h and a receiver distance of 16 m. As expected, subgrade stiffening gives a much larger vibration reduction for the soft soil than for the stiff soil.

It has been assumed in this analysis that the force density is not affected by the introduction of subgrade stiffening. Although there could be an effect, it is likely to be small, as seen from the results for different soil stiffnesses in Figure 30(b).

Co-funded by the European Union

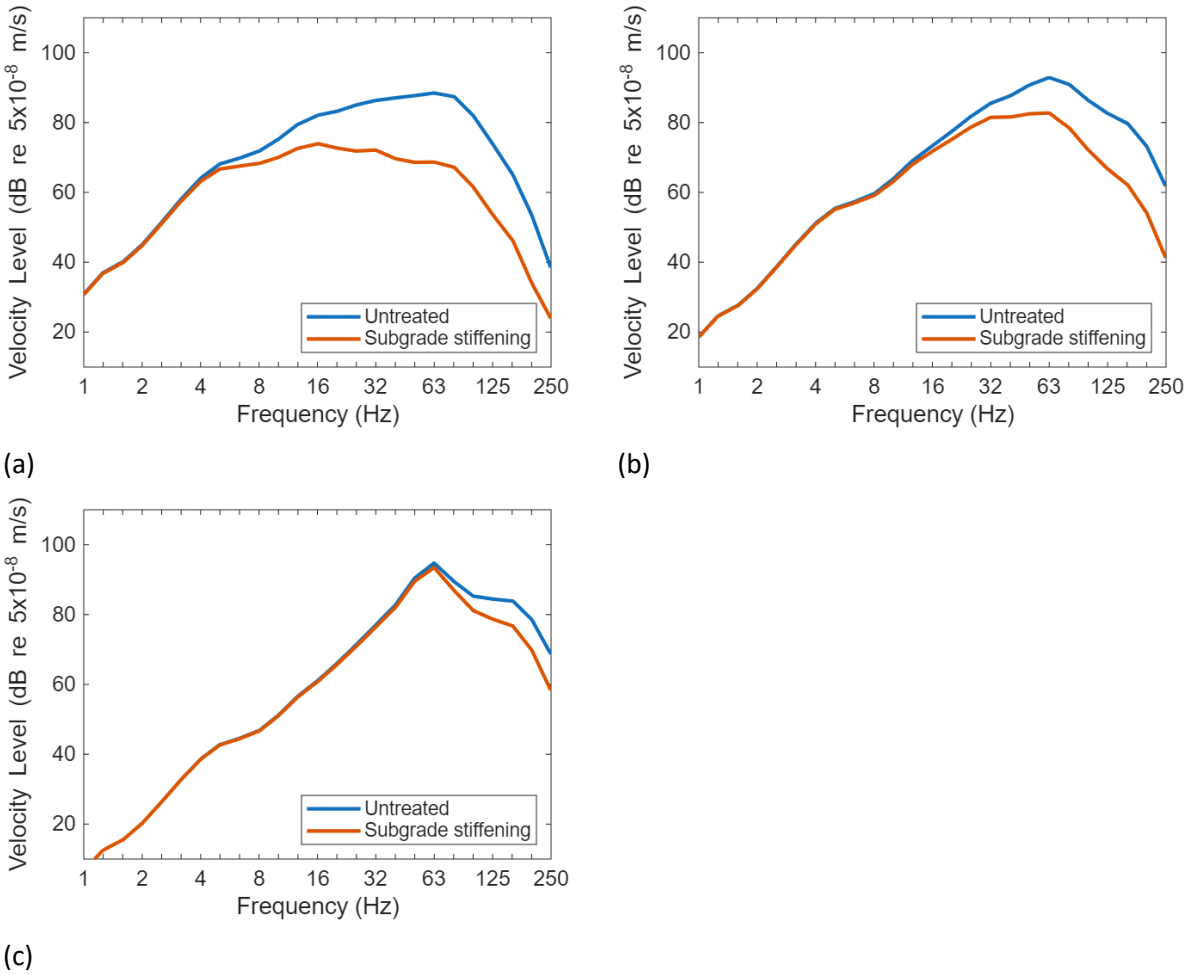

Figure 47. Effect of subgrade stiffening beneath the track on vibration spectra at 16 m from the track and a speed of 120 km/h: (a) soft, (b) medium, and (c) stiff soil.

4.4.3 Stiff wall barrier

The stiff wall barrier has a thickness of 1 m, a depth of 3 m, and is centred at a distance of 6 m from the centre of the track. The insertion loss, for a line source along the track centreline, is shown in Figure 48 for the three types of homogeneous ground. The insertion loss shows an increasing trend with increasing frequency which is largely independent of distance but drops again at high frequency, above a frequency that depends on distance. Apart from this, the effectiveness is similar to the subgrade stiffening. For the soft soil, results were computed up to 125 Hz.

Co-funded by the European Union

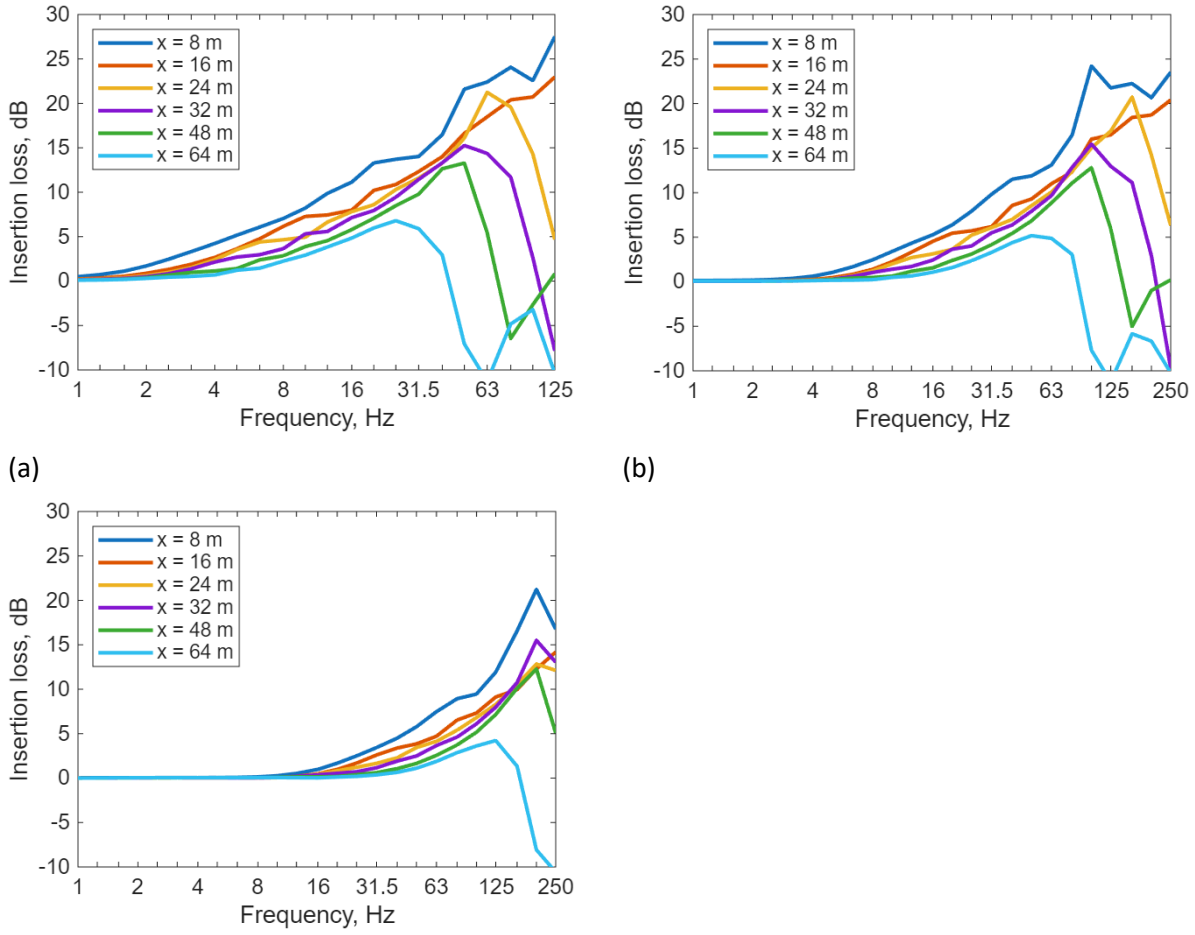

Figure 48. Effect of stiff wall barrier for receivers at different distances from the track: insertion loss for (a) soft, (b) medium, and (c) stiff soil.

Figure 49 shows the effect of combining these results with the vibration predictions due to train traffic, for a regional train at a train speed of 120 km/h and a receiver distance of 16 m. It has been assumed in this analysis that the force density is not affected by the introduction of the barrier, which is reasonable as it is located far from the track. As expected, the stiff barrier gives a much larger vibration reduction for the soft soil than for the stiff soil. At the peak, the reduction for the soft soil is around 15 dB; for the medium soil it is 11 dB and for the stiff soil it is 5 dB.

Co-funded by the European Union

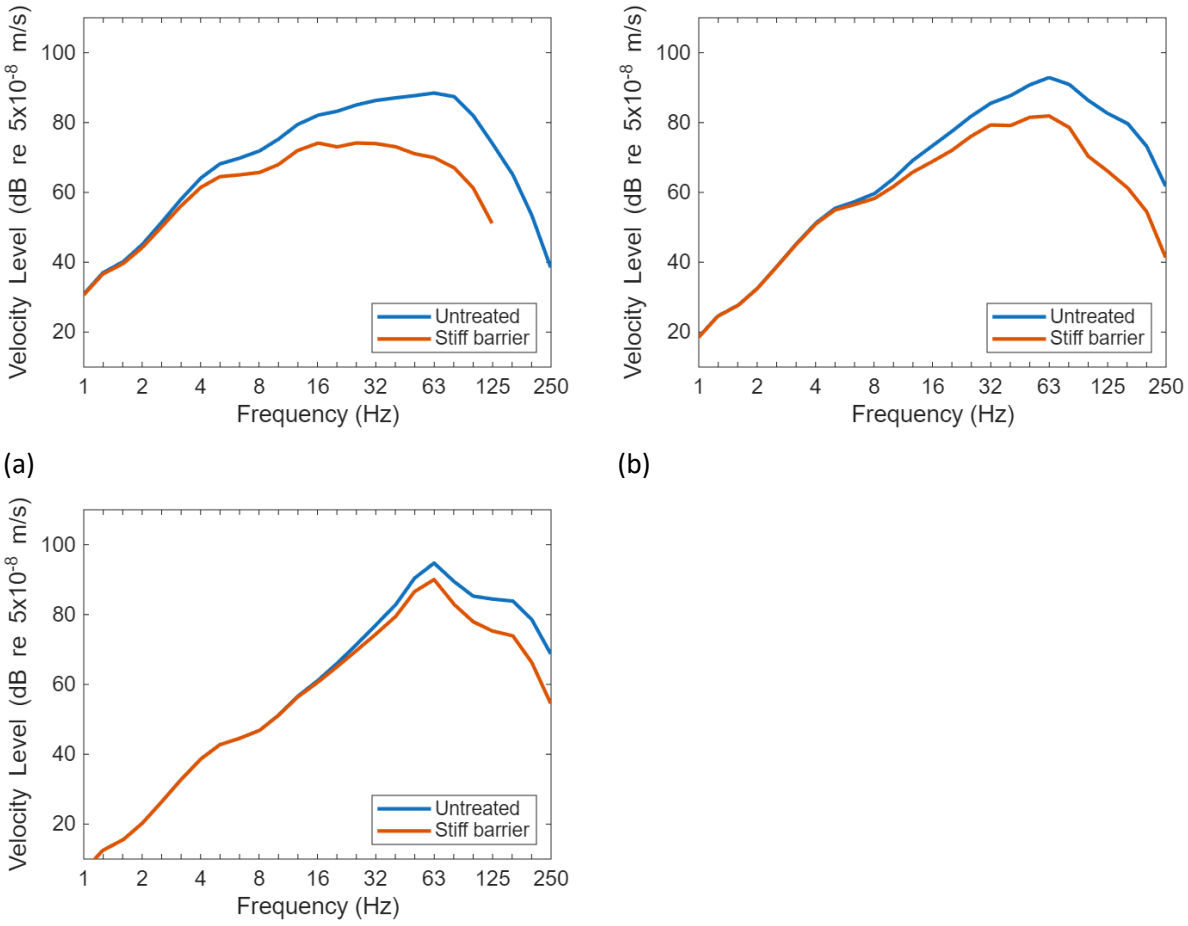

Figure 49. Effect of stiff wall barrier on vibration spectra at 16 m from the track and a speed of 120 km/h: (a) soft, (b) medium, and (c) stiff soil.

4.4.4 Soft wall barrier

The soft wall barrier has a thickness of 0.05 m, a depth of 3 m, and is centred at a distance of 6 m from the centre of the track. The insertion loss, for a line source along the track centreline, is shown in Figure 50 for the three types of homogeneous ground. The insertion loss shows an increasing trend with increasing frequency which is largely independent of distance but again drops at high frequency, above a frequency that depends on distance. The soft wall barrier is less effective than the stiff barrier (for the chosen parameter values). For the soft and medium soil, results were computed up to 125 Hz.

Co-funded by the European Union

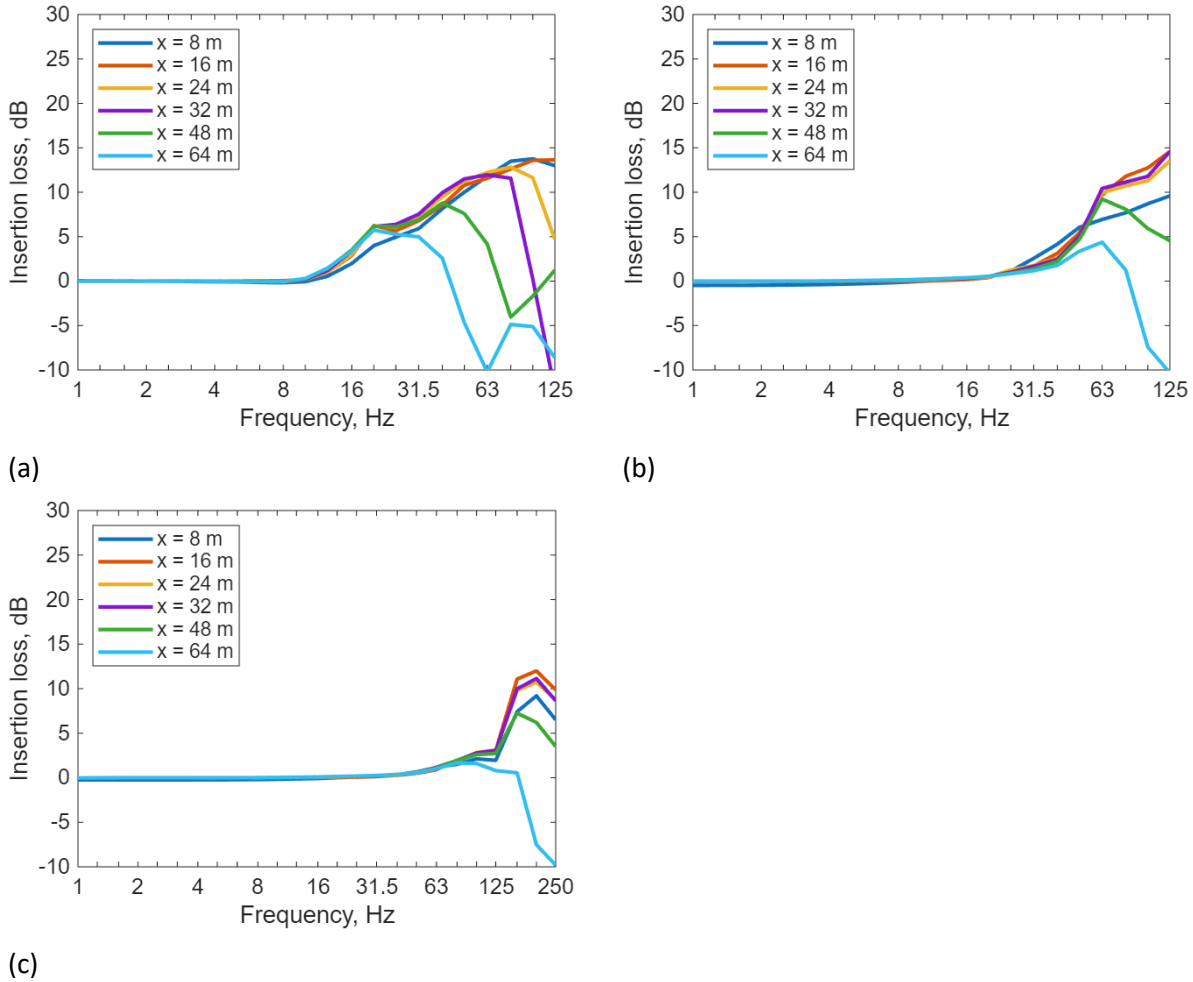

Figure 50. Effect of soft wall barrier for receivers at different distances from the track: insertion loss for (a) soft, (b) medium, and (c) stiff soil.

Figure 51 shows the effect of combining these results with the vibration predictions due to train traffic, for a regional train at a train speed of 120 km/h and a receiver distance of 16 m. It has been assumed in this analysis that the force density is not affected by the introduction of the barrier, which is reasonable as it is located far from the track. As expected, the soft wall barrier gives a much larger vibration reduction for the soft soil than for the stiff soil. At the peak, the reduction for the soft soil is around 9 dB; for the medium soil it is 7 dB whereas for the stiff soil it is negligible. An open trench in a half-space would be effective (attenuation of at least 12 dB) for frequencies at which the depth of trench is greater than 0.6 times the Rayleigh wavelength. For the current ground properties this is expected at 19 Hz for the soft soil, 37 Hz for the medium soil and 75 Hz for the stiff soil. As the soft barrier is quite thin the performance is reduced compared with an open trench [22].

Co-funded by the European Union

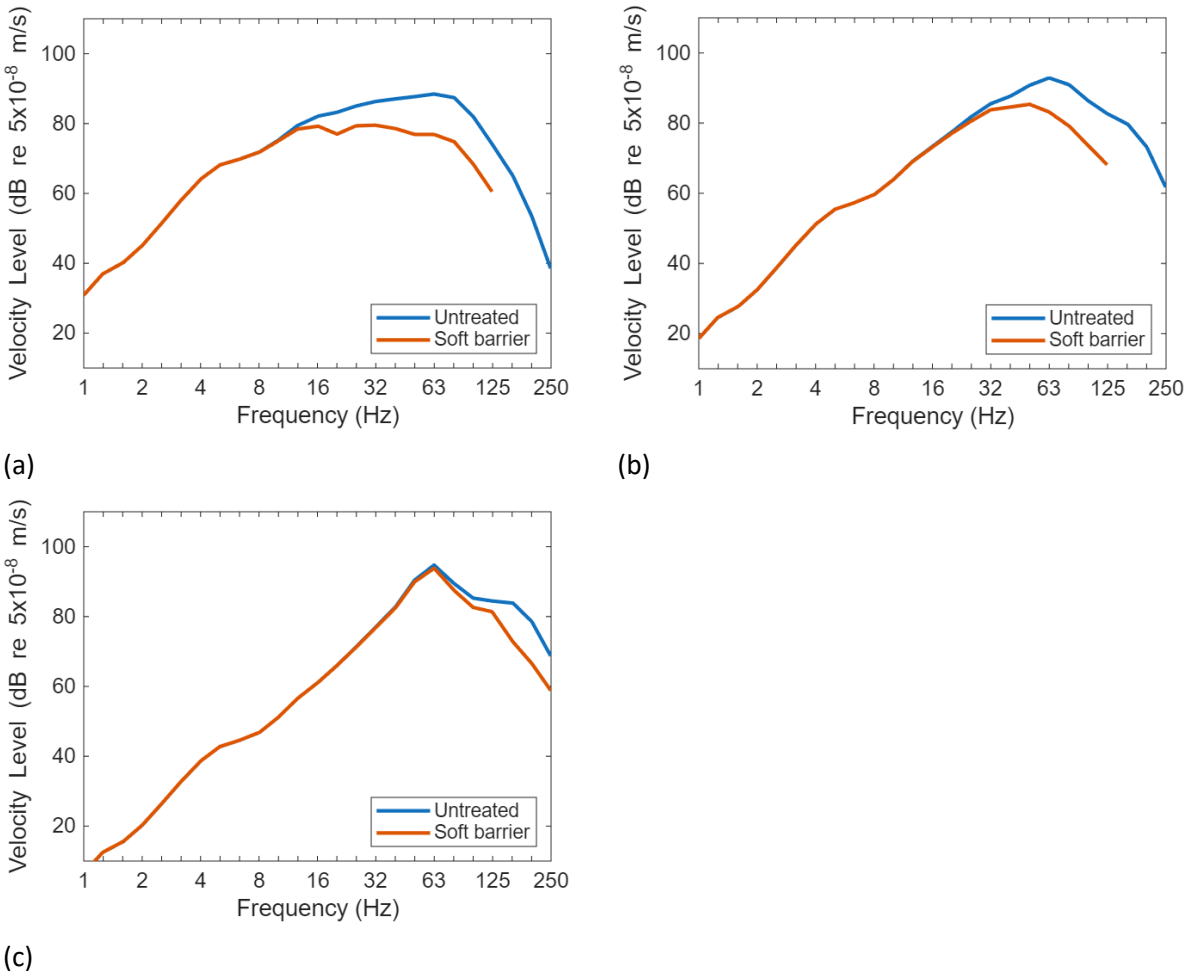

Figure 51. Effect of soft wall barrier on vibration spectra at 16 m from the track and a speed of 120 km/h: (a) soft, (b) medium, and (c) stiff soil.

Co-funded by the European Union

5. Uncertainty assessment

This section provides an assessment of the uncertainty associated with the estimates of noise and vibration reductions given in this report.

5.1 Noise mitigation measures

The uncertainty assessment is performed by assuming an uncertainty range of the key parameters related to the noise mitigation measures and evaluating the influence on the mitigation effect. For rail dampers, rail shields, and optimised rail pads, the influence is assessed for all rail pads listed in Table 18, given that the mitigation effects vary with the pad stiffness and damping (see Section 3.3), while all other track and vehicle parameters corresponding to the reference case as indicated in the same Table.

5.1.1 Rail dampers

The rail dampers mitigate the rolling noise by increasing the TDR, and the uncertainty of the decay rate of a free rail fitted with a rail damper can be up to a factor of 3 [17] (a factor of 3 in the final TDR would correspond to +/-5 dB in noise emission from the rail). Figure 52 shows the nominal decay rate of a free rail fitted with the rail damper B (see Section 2.4.2) in vertical and lateral directions, and the values after applying an uncertainty factor of 1/3 or 3.

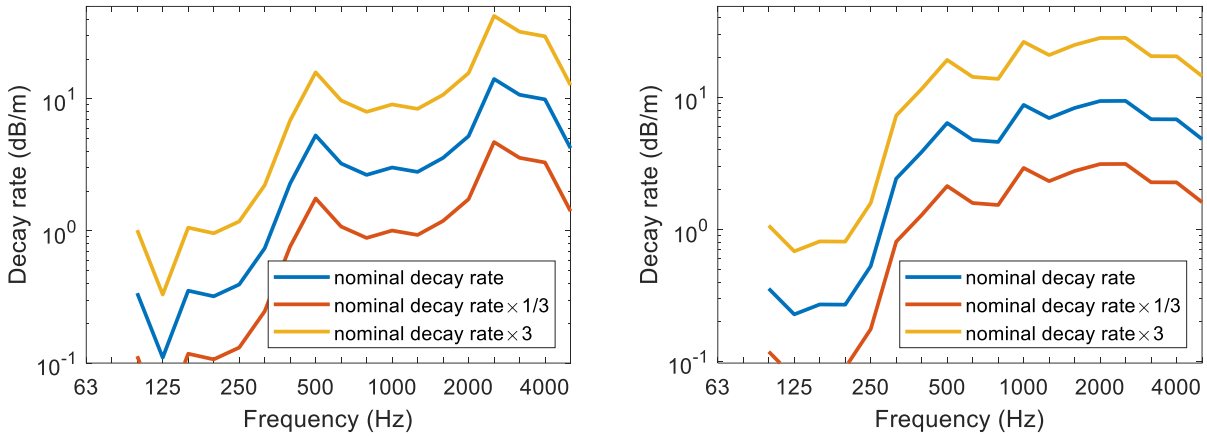

Figure 52. Decay rate of a free rail fitted with rail damper B considering an uncertainty factor of 3: (a) vertical direction, (b) lateral direction.

Rolling noise is calculated assuming the uncertainty factor varying from 1 to 3 with increments of 0.5. Results calculated with the medium rail pad stiffness are presented in Figure 53. Figure 53(a) shows the spectra of the vertical component of rail noise, Figure 53(b) shows that of the lateral component and Figure 53(c) shows that of total noise. Equivalent results calculated with the very stiff rail pad are presented in Figure 54.

The influence on rail noise is pronounced in the frequency range above 250 Hz for both vertical and lateral directions, while the effect on total noise is evident in the mid-frequency range, where rail noise dominates. The influence is more noticeable for the medium rail pad than the very stiff pad, consistent with the trend in the mitigation effect with increasing rail pad stiffness (see Figure 25).

Co-funded by the European Union

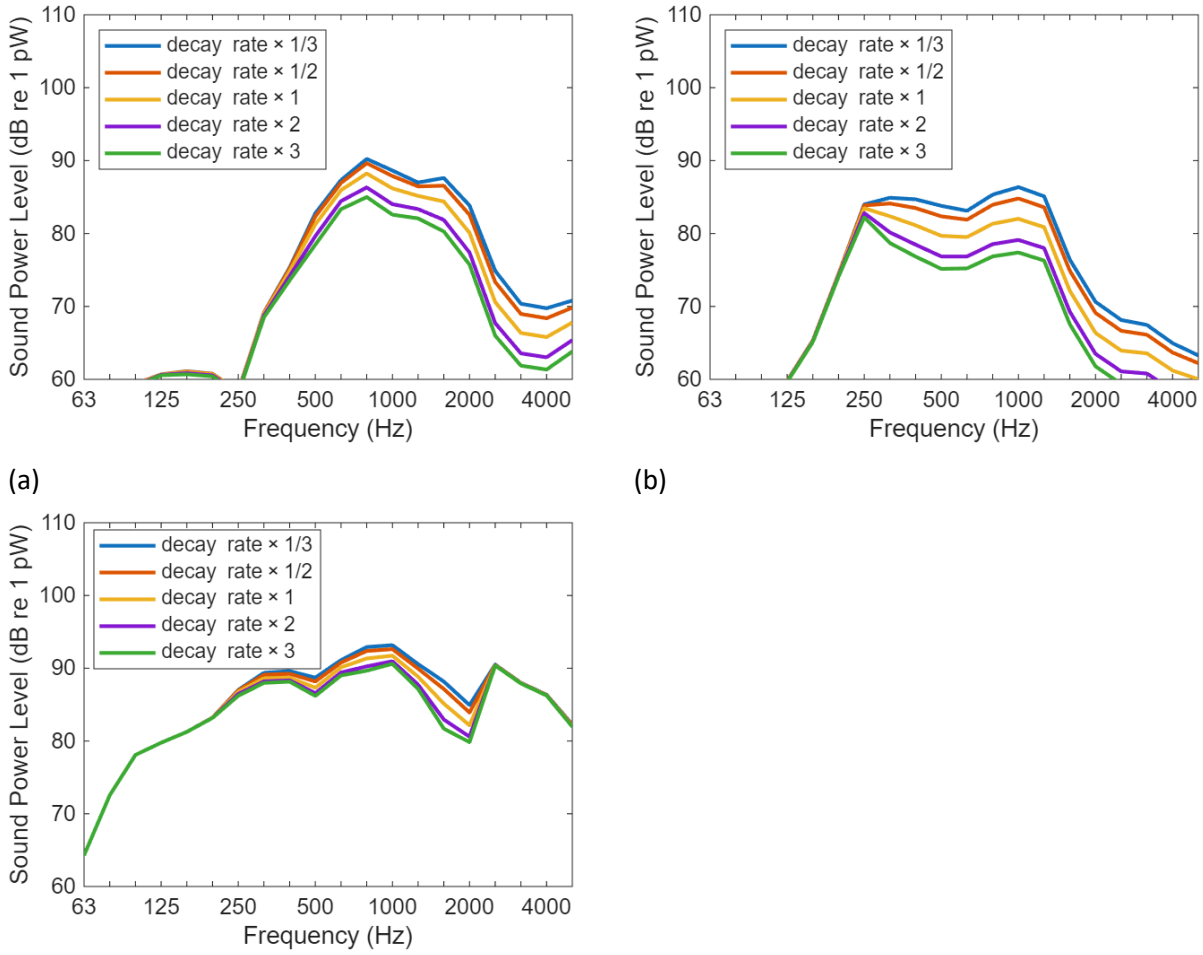

Figure 53. Influence of uncertainty of decay rate with rail damper on sound power levels, calculated with medium rail pad: (a) rail vertical, (b) rail lateral, (c) total.

Co-funded by the European Union

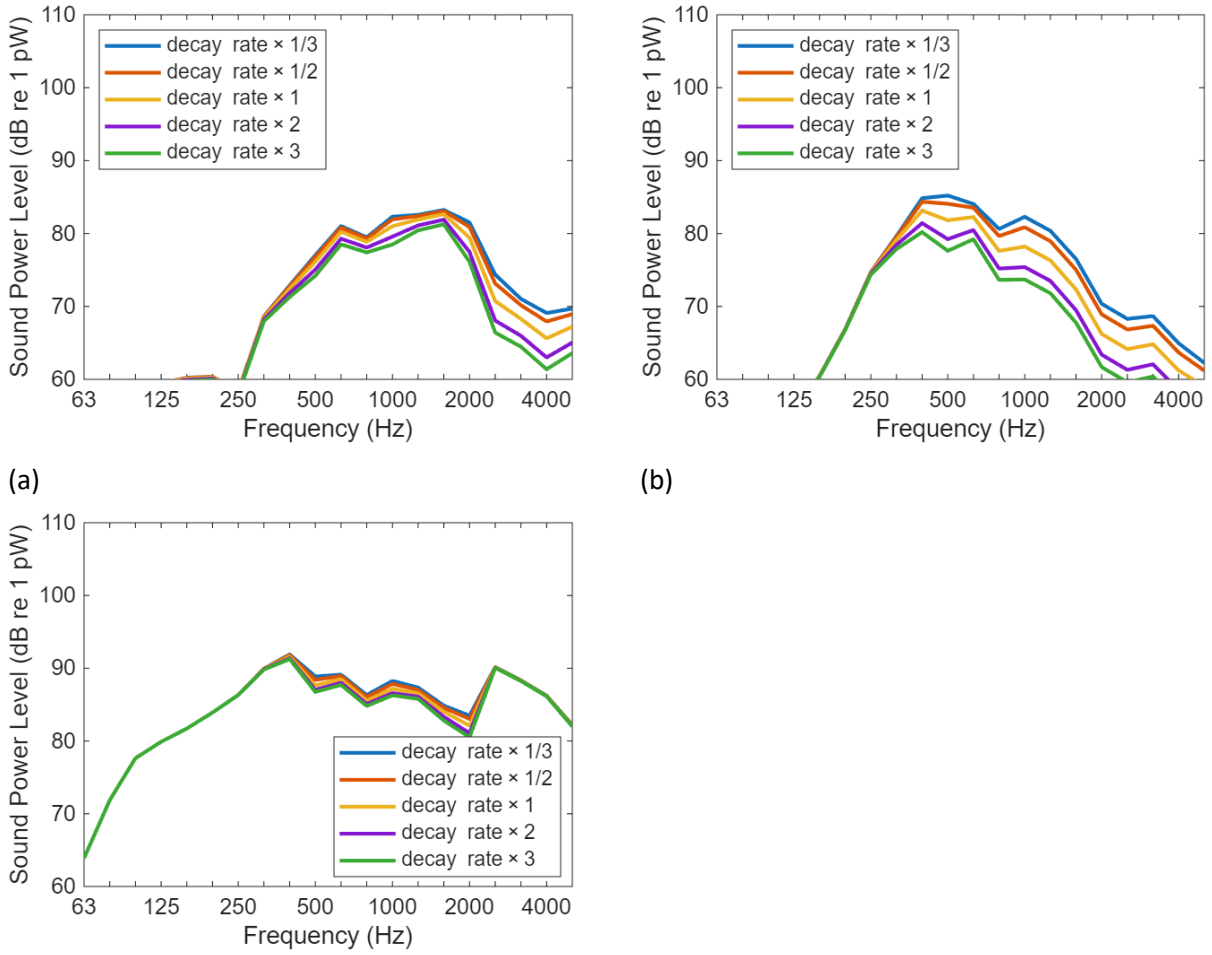

Figure 54. Influence of uncertainty of decay rate with rail damper on sound power levels, calculated with very stiff rail pad: (a) rail vertical, (b) rail lateral, (c) total.

Figure 55 shows the influence on the total A-weighted sound power levels for different rail pads. Figure 55(a) shows the variation of the mitigation effect, and Figure 55(b) shows the mitigation effect.

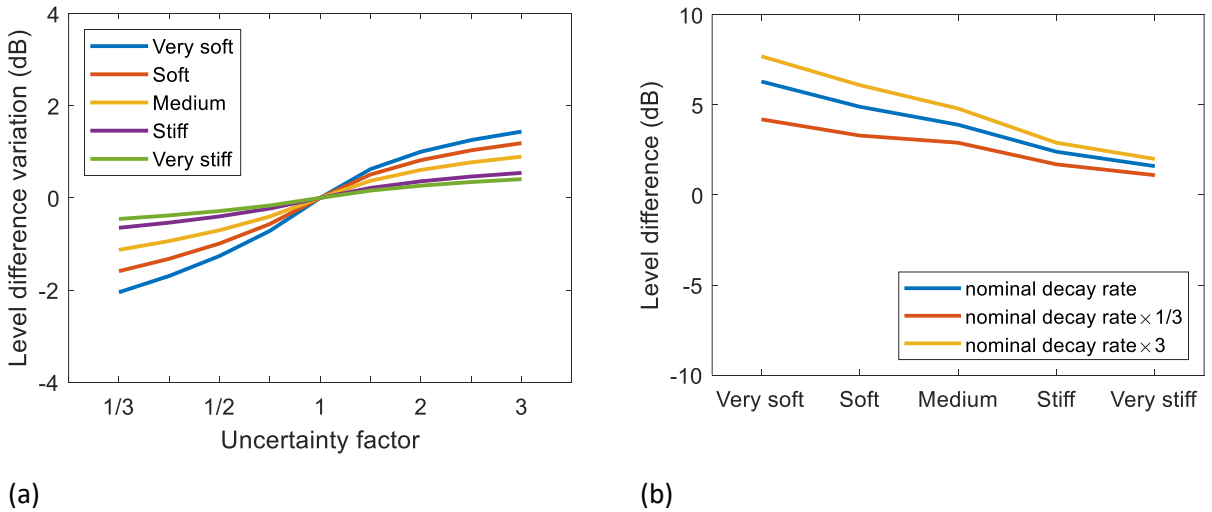

Figure 55. Influence of uncertainty of decay rate with rail damper: (a) variation of mitigation effect on total A-weighted sound power levels, (b) mitigation effect on total A-weighted sound power levels.

Co-funded by the European Union

The change in mitigation effect is smaller with increasing uncertainty factor than when it is reduced. For high decay rates, the rail noise in mid- and high-frequency ranges is reduced considerably, resulting in a higher importance of the wheel noise, and hence the mitigation effect on the total noise does not increase significantly with increasing uncertainty factor. On the contrary, for low decay rate, the TDR approaches that of the untreated track. Taking an uncertainty factor of 3, the mitigation effect increases by 1.4 dB for the very soft pad when the decay rate is higher than the nominal one and decreases by 2.1 dB when the decay rate is lower. The increase and decrease for the very stiff pad are 0.4 dB and 0.5 dB respectively.

5.1.2 Rail shields

Rail shields are characterised by the insertion loss of the rail noise. An uncertainty factor of 2 is applied to the insertion loss of the vertical and lateral rail noise components but only a reduction of the insertion loss values is considered, not an increase, as shown in Figure 56. This brings it more into line with the measurement data in [41]. The influence of the uncertainty on the mitigation effect on total A-weighted sound power level is shown in Figure 57. The mitigation effect decreases by 2.1 dB for the very soft pad and by 0.6 dB for the very stiff pad.

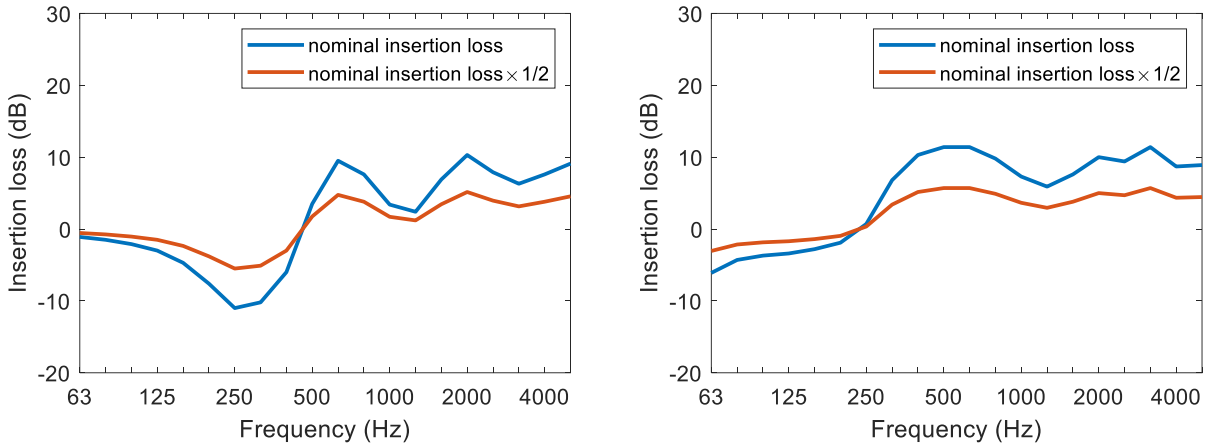

Figure 56. Insertion loss of a rail fitted with rail shield considering an uncertainty factor of 0.5: (a) vertical, (b) lateral.

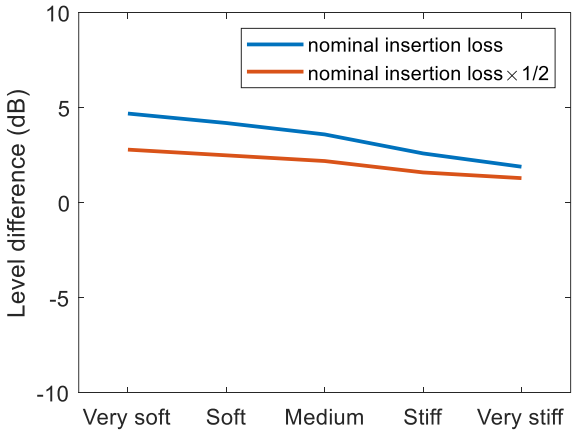

Figure 57. Influence of uncertainty of insertion loss with rail shield on mitigation effect on total A-weighted sound power levels.

Co-funded by the European Union

5.1.3 Optimised rail pads

The key feature of optimised rail pads is the high acoustic stiffness, which increases the TDR, and hence the uncertainty is applied to rail pad stiffness for the assessment. The effect of adopting optimised rail pads depends also on the stiffness of the original rail pad. Therefore, the uncertainty is applied to both the optimised and original rail pad.

Figure 58 shows the overall A-weighted levels of each component for the medium and very stiff rail pad, applying an uncertainty factor of 20% to the pad stiffness in both vertical and lateral directions.

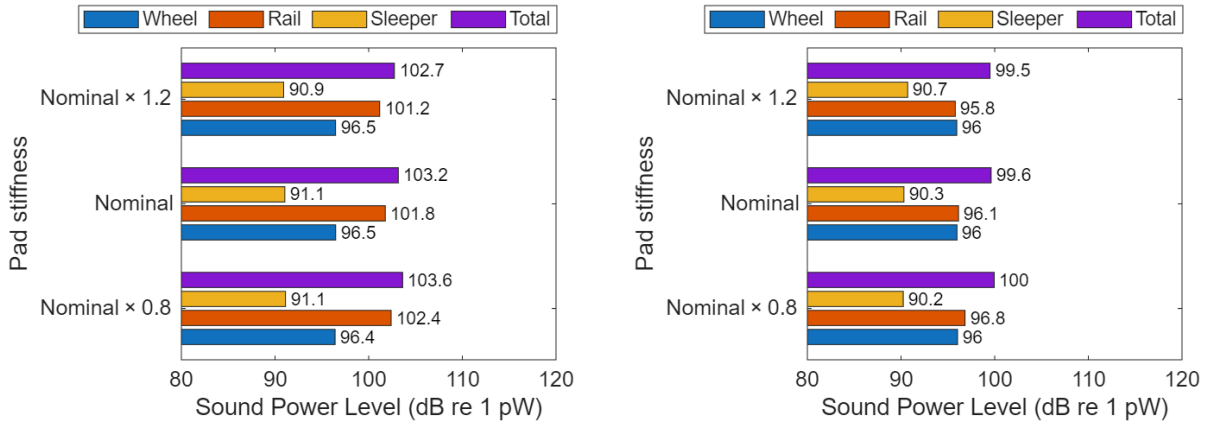

Figure 58. Influence of uncertainty of rail pad stiffness: (a) medium rail pad, (b) very stiff rail pad.

The uncertainty in the rail pad stiffness mainly influences the rail noise. A lower pad stiffness leads to an increase of 0.6 dB of the rail noise for the medium rail pad and 0.7 dB for the very stiff pad, and a higher pad stiffness results in a decrease of 0.6 dB and 0.3 dB for the two pads. The influence on total noise is almost the same for the medium pad but is much less pronounced for the very stiff pad, because the wheel noise is significantly lower than the rail noise for the medium pad (for the reference wheel) while the two contributions are comparable for the very stiff pad.

Given that the very stiff pad results in a TDR similar to optimised rail pads developed and tested in the UIC LOWNOISEPAD project [4], it is considered to represent an optimised rail pad while the other pads are taken as the original pads. Figure 59 shows the influence of the rail pad stiffness uncertainty on the mitigation effect in terms of the total A-weighted levels.

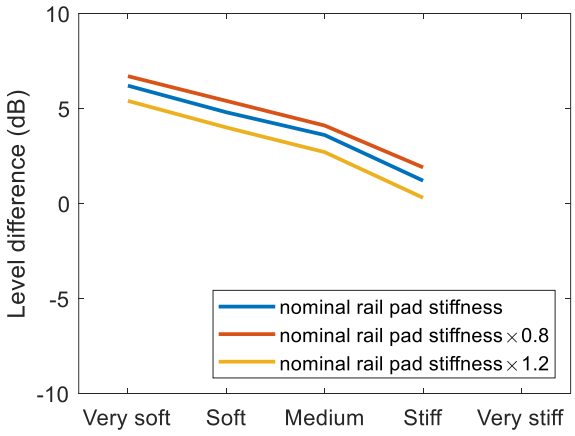

Figure 59. Influence of uncertainty of rail pad stiffness on mitigation effect of optimised rail pad.

Co-funded by the European Union

The influence is nearly independent on the stiffness of the original pads. The decrease of the mitigation effect is about 0.85 dB for all pads, and the increase is about 0.5 dB.

5.1.4 Acoustic rail grinding

Uncertainty in the effect of acoustic grinding is related to the estimates of rail roughness. In Appendix A, the effect is presented of using alternative assumptions for the reference rail roughness and the roughness two months after grinding. This leads to estimates of the effect of acoustic grinding, shown in Table A1, of between 1.5 and 3.8 dB(A), compared with the nominal estimate given in Section 3.3.4 of 3.7 dB(A). On the other hand, if the rail is initially rougher than average, due to corrugation or similar, the effect of acoustic grinding could be larger than these estimates.

An additional uncertainty arises from the development of rail roughness after grinding. The French study reported in Appendix A indicates that the rails continued to become smoother over a period of four years after grinding, leading to a further noise reduction of 1.5 dB(A), see Table A1. Conversely, results from Germany, Belgium and the Netherlands indicate that rail roughness grows again after grinding at a rate between 0.7 and 1 dB per year. The long-term average noise level reduction assumed in the German study of acoustic grinding is 3 dB, broadly consistent with the estimate given in Section 3.3.4.

As the reduction in rail roughness seen in Section 3.2.9 and Appendix A is largely independent of wavelength, the reductions stated above will be independent of train speed as well as train type or rail pad stiffness.

5.2 Vibration mitigation measures at the track

5.2.1 Under-sleeper pads

Uncertainty in the effect of under-sleeper pads is related to the value of dynamic stiffness of the USP and the ground stiffness. Results for different stiffness of USP are shown in Figure 41. So, for example, the difference between the medium and stiff USP is a halving of the values of insertion loss, from a peak of 7 dB to around 3 dB. However, the stiffness of the USP is fairly well known from information available from the manufacturers, so this source of uncertainty is not considered further here.

The stiffness of the ground can affect the insertion loss of the USP to some extent. The insertion loss of the three types of USP is shown in Figure 60 for the three types of ground. The ground type has only a small effect on the insertion loss of the stiff and medium USPs, whereas for the soft USP the effect is larger, especially for the stiff ground. However, it should be recognised that these three ground types represent quite large changes in stiffness. Apart from the soft USP, the insertion loss provided by the USP only varies in certain frequency bands and by mostly less than 3 dB when considering changes in ground stiffness.

Co-funded by the European Union

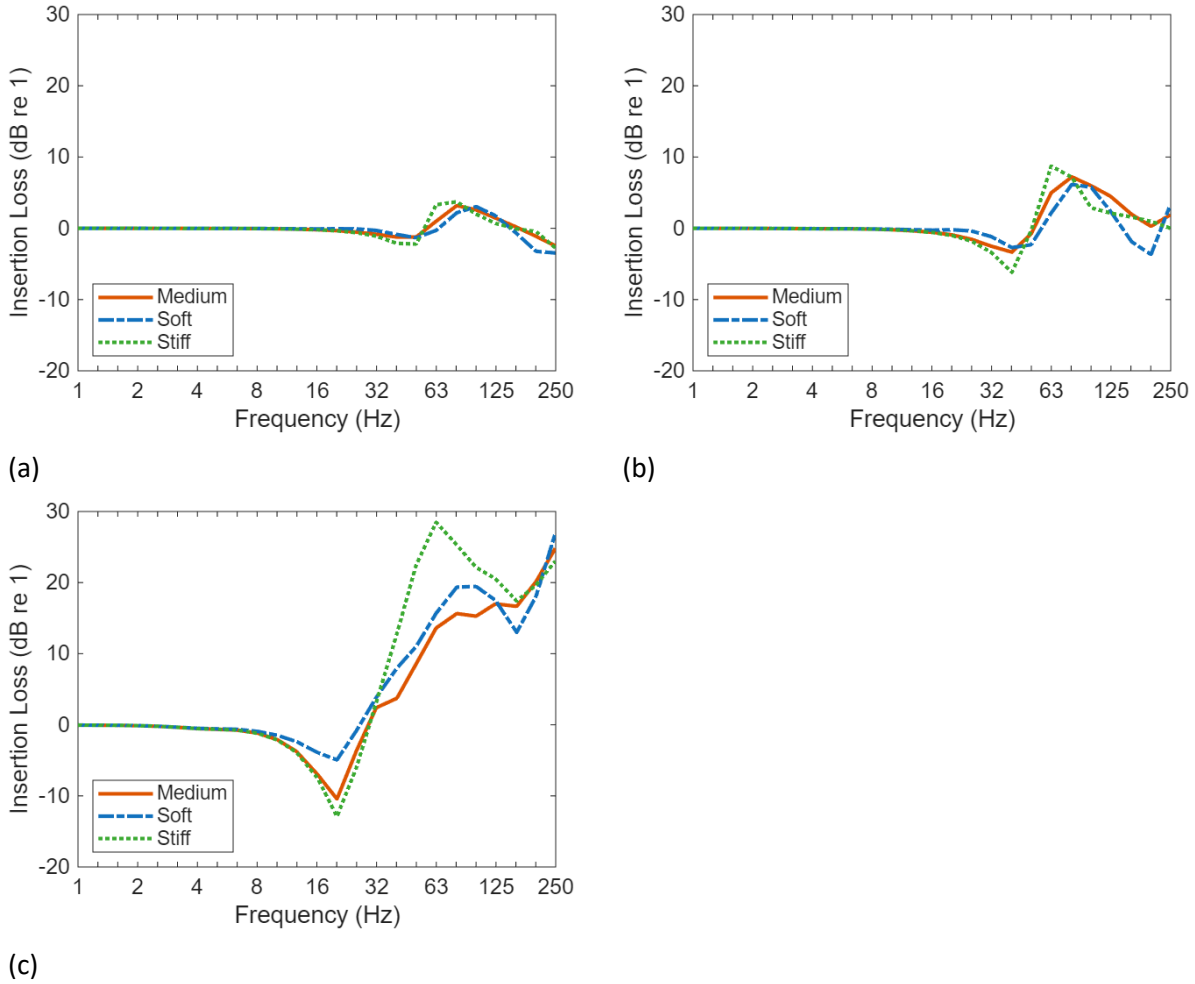

Figure 60. Uncertainty of insertion loss due to under-sleeper pads as a result of different ground stiffness: (a) stiff USP, (b) medium USP, (c) soft USP.

5.2.2 Under-ballast mats

Similar to under-sleeper pads, uncertainty in the effect of under-ballast mats is related to the value of dynamic stiffness of the UBM and the ground stiffness. Results for different stiffness of UBM are shown in Figure 42. There is a factor of 2 between the stiffness of these two UBMs. Apart from a shift in the frequencies of the dip and subsequent rise in the insertion loss, differences of around 6 dB occur at higher frequencies. However, the stiffness of the UBM is fairly well known from information available from the manufacturers, so this source of uncertainty is not considered further here.

The stiffness of the ground can affect the insertion loss of the UBM. The insertion loss of the two types of UBM is shown in Figure 61 for the three types of ground. The difference between the medium and soft ground is quite small, but for the stiffer ground larger differences are seen. Once more, it should be recognised that these three ground types represent quite large changes in stiffness.

Co-funded by the European Union

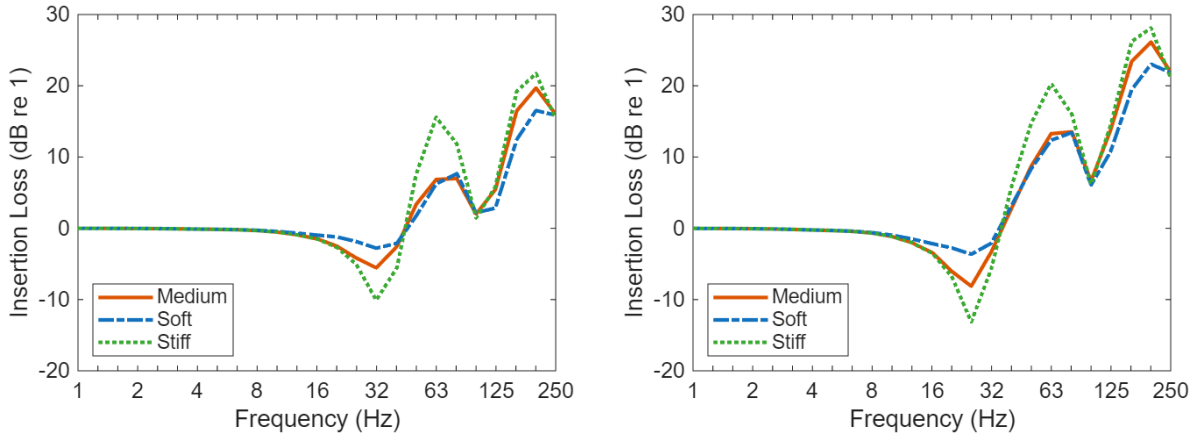

Figure 61. Uncertainty of insertion loss due to under-ballast mats as a result of different ground stiffness: (a) medium UBM, (b) soft UBM.

5.2.3 Rail pad stiffness

The insertion loss (vibration level difference) due to changes to rail pad stiffness relative to the reference case (medium rail pad stiffness) is shown in Figure 33(c) for the medium stiffness ground, which indicates that the effect is minimal unless a very soft rail fastener is introduced.

Figure 62 shows the insertion loss due to changing the rail pad stiffness from medium to soft or very soft. Results are shown for the three ground types. Uncertainty over the ground stiffness introduces only a small uncertainty in the insertion loss due to changing the rail pad stiffness, with the largest effects occurring above 100 Hz.

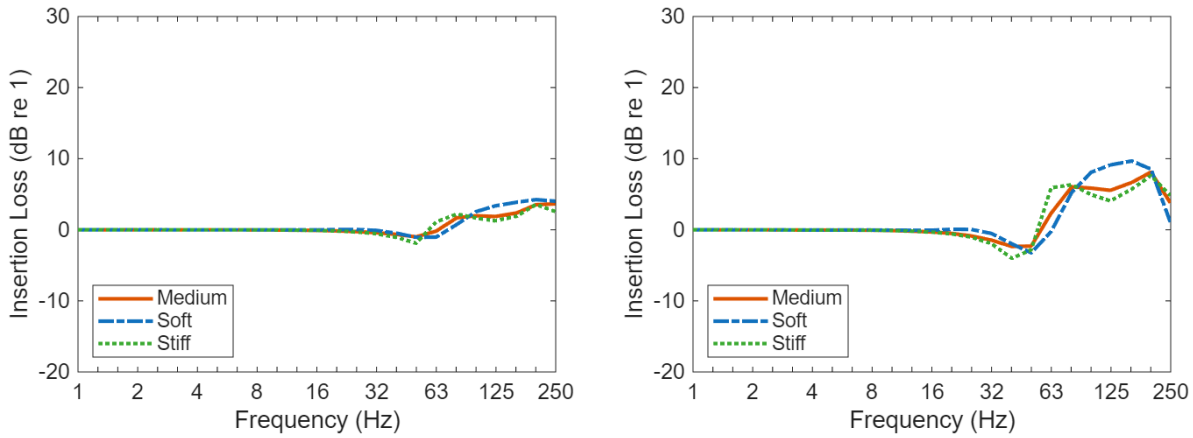

Figure 62. Uncertainty of insertion loss due to change in rail pad stiffness relative to medium rail pad as a result of different ground stiffness: (a) soft rail pad, (b) vert soft rail pad.

5.2.4 Unevenness

As shown in Section 4.2.9, a change in track unevenness can lead to significant reductions in vibration. The insertion losses plotted in Figure 43 indicate that changing from 'normally maintained' track to 'well maintained' track would lead to a reduction in vibration of between 4 and 8 dB. However, although these unevenness spectra are based on measured data for a typical mainline track, it is unclear whether the

Co-funded by the European Union

insertion loss represents the change in vibration that could be obtained due to maintenance activity, such as tamping. These estimates should therefore be seen as having a high degree of uncertainty.

5.3 Mitigation measures in the transmission path

Uncertainty in the estimates of mitigation measures in the transmission path are shown for two examples: heavy masses close to the track and subgrade stiffening.

5.3.1 Heavy masses beside the track

The effect of heavy masses close to the track has been shown for the three ground types in Section 4.4.1. The results for a receiver distance of 16 m are compared in Figure 63. This shows how the frequency content and level of the insertion loss shift considerably, with a higher insertion loss over a wider frequency range for the softer ground. There is likely to be considerable uncertainty in the effect unless the ground stiffness is well known.

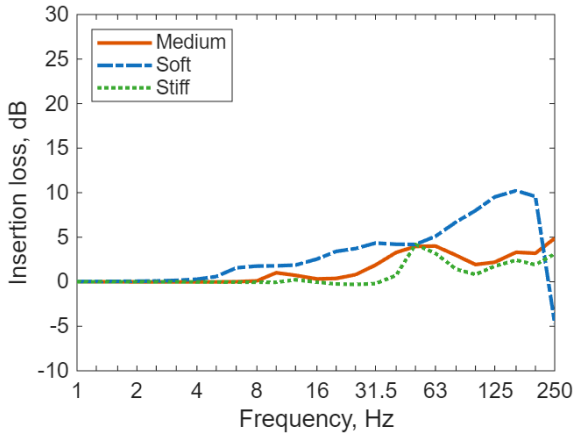

Figure 63. Insertion loss due to heavy masses beside the track for receivers at 16 m from the track for different soil types.

5.3.2 Subgrade stiffening beneath the track

The effect of subgrade stiffening beneath the track has been shown for the three ground types in Section 4.4.2. The results for a receiver distance of 16 m are compared in Figure 64. This shows how the cut-on frequency in the insertion loss shifts considerably, with a higher insertion loss starting from a lower frequency for the softer ground. There is likely to be a very large uncertainty in the effect unless the ground stiffness is well known.

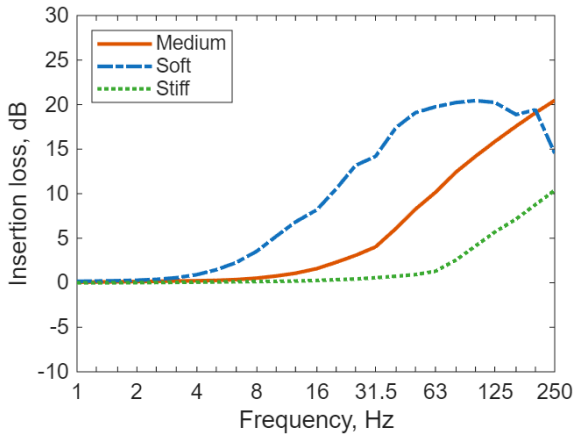

Figure 64. Insertion loss due to subgrade stiffening for receivers at 16 m from the track for different soil types.

Co-funded by the European Union

6. Conclusions

A web-based tool is being developed in WP4, which will allow track optimisation for noise, vibration and life cycle costs. To support this development, calculations have been carried out of noise and vibration source levels. These cover a range of abatement methods and different combinations of track components and will be stored in a database to be used by the tool. The calculations are performed using complementary physics-based models available to the project partners.

In correspondence with the Use Cases defined in Deliverable D4.1 [1], the calculated source levels for noise and vibration are limited to the most common situation of straight, plain track with trains passing at constant speed. This aligns with the available validated physics-based models. Passive provision will be allowed in the tool for other sources such as impact at switches and crossings, and curving (not squeal noise), for example on the basis of correction terms; however, these are not considered here.

Input parameters have been determined for the track in terms of rails, rail pads, sleepers, and ballast. Of these, the rail pad is expected to have the largest influence, so a wide range of stiffness and damping values is proposed, covering the range of expected values encountered in European tracks. For the trains, a more limited set of examples are included corresponding to typical cases.

Calculation results have been obtained for a large number of cases to quantify the effect of noise and vibration reduction measures. These results include rolling noise sound power spectra and both force densities and vibration velocity spectra for ground vibration. They have been obtained for a unit roughness (or unevenness) and will be combined in the online tool with roughness spectra, taking account of the train speed and contact filter. Example results, reflecting the final combined spectra, have been presented to illustrate the range of parameter variations covered. The uncertainty in the effect of each mitigation measure has been assessed.

The predicted results are broadly consistent with empirical evidence, but it is recognised that actual noise reductions in specific situations may differ from those obtained with the models. It will be the user's responsibility to check the applicability of the results. Although some mitigation measures affect both noise and vibration, the combined effect is not assessed here. This will be considered later in Deliverable D4.5 when the web-based tool is assessed and used for example case studies.

A benchmark study has been performed comparing the results of the TWINS and ToPNoise models for track dynamics and radiation. The effect of various track configurations on the stresses in the ballast has also been calculated, and the results can be used to give an indication of the effect on track settlement.

The planned objectives have been met. The calculation results illustrated here will be contained in a database to be used by the online tool, to be delivered and tested by the end of the project. These results will be reported in Deliverables D4.4 and D4.5.

Co-funded by the European Union

References

1. P. Yilmazer, R. Casquero, J. Oertli, A. Chalisey, M. Hosoda, D. Thompson, S. Blainey, C. Wan, T. Aasen, L. Véha, G. Dinhobl. *List of use cases and optimisation criteria*, QuieterRail Deliverable D4.1, July 2025.
2. D.J. Thompson, J.W. Verheij. *The dynamic behaviour of rail fasteners at high frequencies*. Applied Acoustics, 52 (1997) 1-17.
3. D.J. Thompson, W.J. van Vliet, J.W. Verheij. *Development of the indirect method for measuring the high frequency dynamic stiffness of resilient elements*. Journal of Sound and Vibration 213 (1998) 169-188.
4. International Union of Railways (UIC), Sustainability. *Optimised Rail Pad Performance for Noise Reduction: Outcomes and Recommendations (LOWNOISEPAD project)*, 2023.
5. D.J. Thompson, E. Ntotsios, G. Degrande, G. Lombaert, P. Reumers, B. Nélain, S. Barcet, and P. Bouvet. *Track-independent vehicle indicator and method for transposition of vibration emission data*. SILVARSTAR project GA 101015442, Deliverable D2.2, Report to the EC, April 2022.
6. D.J. Thompson, E. Ntotsios, G. Degrande, G. Lombaert, G. Herremans, T. Alexiou, B. Nélain, S. Barcet, P. Bouvet, B. Fröhling, A. Nuber. *Database for vibration emission, ground transmission and building transfer functions*. SILVARSTAR project GA 101015442, Deliverable D2.1, Report to the EC, revised, February 2023.
7. X. Zhang, D. Thompson, H. Jeong, M. Toward, D. Herron, C. Jones, N. Vincent. *Measurements of the high frequency dynamic stiffness of railway ballast and subgrade*. Journal of Sound and Vibration 468 (2020) 115081.
8. https://www.getzner.com/media/26404/download/Data Sheet Product Range Under Ballast Mats EN DE EN(2).pdf, accessed 21/02/2025.
9. E. Ntotsios, D. Thompson, M.F.M. Hussein. *A comparison of ground vibration due to ballasted and slab tracks*. Transportation Geotechnics 21 (2019) 100256.
10. X. Zhang, H. Jeong, D.J. Thompson, G. Squicciarini. *The noise radiated by ballasted and slab tracks*. Applied Acoustics 151 (2019) 193-205.
11. D.J. Thompson, E. Ntotsios, G. Degrande, G. Lombaert, P. Reumers, B. Nélain, S. Barcet, P. Bouvet. *Track-independent vehicle indicator and method for transposition of vibration emission data*. SILVARSTAR project GA 101015442, Deliverable D2.2, Report to the EC, November 2022.
12. D. Sehu, J.M. Wunderli, K. Heutschi, T. Thron, M. Hecht, A. Rohrbeck, T. Ledermann. *sonRail Projektdokumentation*, Schweizerische Eidgenossenschaft, October 2010, page I-177.
13. ISO 3095:2013. Acoustics – Railway applications – Measurements of noise emitted by railbound vehicles, International Organization for Standardization, Geneva, 2013.
14. CNOSSOS-EU_Rail_Input_Database_Tables_Final - 01April2014_revANNEXII v1.1 09April15.xlsx, accessed online November 2021 at: https://circabc.europa.eu
15. D. Thompson. *Railway noise and vibration. Mechanisms, Modelling and Means of Control*. Second edition, Elsevier, London, 2024.
16. A. Johansson, *Out-of-round railway wheels – assessment of wheel tread irregularities in train traffic*, Journal of Sound and Vibration 293 (2006) 795-806.
17. G. Squicciarini, M.G.R. Toward, D.J. Thompson. *Experimental procedures for testing the performance of rail dampers*. Journal of Sound and Vibration 359 (2015) 21-39.
18. X. Zhang, D. Thompson, J. Ryue, H. Jeong, G. Squicciarini. *The effect of rail shields on railway rolling noise*, International Journal of Rail Transportation 11 (2023) 552-572.
19. H.F. Ganji, P. Yılmazer, A. Kuijpers, L. Baeza, J. Carballeira. *State-of-the-art on on-board rail roughness measurement systems*. QuieterRail Deliverable D3.1, March 2026.

Europe's Rail
Co-funded by the European Union

20. P. Coulier, S. François, G. Degrande, G. Lombaert. *Subgrade stiffening next to the track as a wave impeding barrier for railway induced vibrations*. Soil Dynamics and Earthquake Engineering, 48 (2013) 119-131.
21. A. Dijckmans, A. Ekblad, A. Smekal, G. Degrande, G. Lombaert. *Efficacy of a sheet pile wall as a wave barrier for railway induced ground vibration*. Soil Dynamics and Earthquake Engineering, 84 (2016) 55-69.
22. D.J. Thompson, J. Jiang, M.G.R. Toward, M.F.M. Hussein, E. Ntotsios, A. Dijckmans, P. Coulier, G. Lombaert, G. Degrande. *Reducing railway–induced ground–borne vibration by using open trenches and soft–filled barriers*. Soil Dynamics and Earthquake Engineering, 88 (2016) 45-59.
23. A. Dijckmans, P. Coulier, J. Jiang, M.G.R. Toward, D.J. Thompson, G. Degrande, G. Lombaert. *Mitigation of railway induced ground vibration by heavy masses next to the track*. Soil Dynamics and Earthquake Engineering, 75 (2015) 158-170.
24. D.J. Thompson, J. Jiang, M.G.R. Toward, M.F.M. Hussein, A. Dijckmans, P. Coulier, G. Degrande, G. Lombaert. *Mitigation of railway-induced vibration by using subgrade stiffening*. Soil Dynamics and Earthquake Engineering 79 (2015) 89-103.
25. D.J. Thompson, B. Hemsworth, N. Vincent. *Experimental validation of the TWINS prediction program for rolling noise, part 1: description of the model and method*. Journal of Sound and Vibration, 193 (1996) 123-135.
26. D.J. Thompson, P. Fodiman, H. Mahé. *Experimental validation of the TWINS prediction program for rolling noise, part 2: results*. Journal of Sound and Vibration, 193 (1996) 137-147.
27. X. Zhang, D.J. Thompson, E. Ntotsios, B. Hima, G. Squicciarini. *Effect of baseplate flexibility and rail pad stiffness on slab track dynamics*. Engineering Structures 334 (2025) 120296.
28. X. Zhang, H. Jeong, D.J. Thompson, G. Squicciarini. *The noise radiated by ballasted and slab tracks*. Applied Acoustics 151 (2019) 193-205.
29. E. Ntotsios, M. Toward, D. Thompson, P. Insley, G. Sica, S. Koroma, J. Rothhämel. *Validation of rolling noise predictions of in-service high-speed trains on ballastless track*. In: Proceedings of 15th International Workshop on Railway Noise, Isla de la Toja, Spain, 15-19 September 2025.
30. EN 15461:2008+A1:2010, Railway applications – Noise emission – Characterization of the dynamic properties of track selections for pass by noise, European Committee for Standardization, Brussels, 2010.
31. D. Thompson, W. Sun, M. Toward, G. Squicciarini, E. Cierco, A. Isnardo, M. Rissmann, P. Bouvet, M. Dittrich. *Comparison of methods for estimating track decay rate*. In: Proceedings of 15th International Workshop on Railway Noise, Isla de la Toja, Spain, 15-19 September 2025.
32. B. Asmussen, D. Stiebel, P. Kitson, D. Farrington, D. Benton. *Reducing the noise emission by increasing the damping of the rail: results of a field test*. In: B. Schulte-Werning, et al. (Eds.) Proceedings of 9th International Workshop on Railway Noise, Munich, Germany, 4-8 September 2007, Notes on Numerical Fluid Mechanics & Multidisciplinary Design 99 (2008) 229-235.
33. F. Margiocchi, F. Poisson, C. Gramowski, J. P. Tartary. *A 8-years complete assessment of rail damper performances on an operated track in France*. Proceedings of 11th World Congress on Railway Research, Milan, 2016.
34. D.J. Thompson, C.J.C. Jones, T.P. Waters, D. Farrington. *A tuned damping device for reducing noise from railway track*. Applied Acoustics 68 (2007) 43-57.
35. J. Oertli. *Erprobung von Schienendämpfern, Schlussbericht* (Testing of rail dampers, Final Report), SBB, April 2016.
36. N. Isert, S. Lutzenberger. *Jahresbericht 2024 Fahrbahnlabor*, Müller-BBM report, 2025, https://www.fahrbahnlabor.ch/de/berichte/jahr/Jahresbericht_2024_Fahrbahnlabor_V2.pdf

Europe's Rail
Co-funded by the European Union

37. G. Lombaert, S. François, and G. Degrande. *TRAFFIC Matlab toolbox for traffic induced vibrations*. Report BWM-2012-10, Department of Civil Engineering, KU Leuven, November 2012. User's Guide Traffic 5.2.
38. D.R.M. Milne, L.M. Le Pen, D.J. Thompson, W. Powrie. *Properties of train load frequencies and their applications*. Journal of Sound and Vibration 397 (2017) 123-140.
39. P. Reumers, G. Degrande, G. Lombaert, F. Seyfaddini, G. Herremans, E. Ntotsios, D.J. Thompson, B. Nélain, P. Bouvet, B. Fröhling, A. Nuber. *Validation of the prototype vibration prediction tool against documented cases*. SILVARSTAR, GA 101015442, Deliverable D1.3, June 2022.
40. G. Degrande, G. Lombaert, E. Ntotsios, D. Thompson, B. Nélain, P. Bouvet, S. Grabau, J. Blaul, A. Nuber. *State-of-the-art and concept of the vibration prediction tool*. SILVARSTAR, GA 101015442, Deliverable D1.1, May 2021.
41. M. Dittrich, E. Jansen, C. Czolbe. *Characterisation of the effect of rail web shielding*. In: Proceedings of 13th International Workshop on Railway Noise, Ghent, Belgium, 16-20 September 2019.
42. J. Florentin, S. De Bock. *Railway noise control through preventive rail grinding: setting the right objectives*. In: Proceedings of 15th International Workshop on Railway Noise, Isla de la Toja, Spain, 15-19 September 2025.
43. *Rapportage bepaling gemiddelde Nederlandse railruwheid* (Reporting of determination of average Netherlands rail roughness), Dekra Rail report 22/220391/003, 2023.
44. J. Wilkes, D.J. Thompson, *A study of the effect of grinding machine parameters on acoustic rail roughness and surface quality*. Proceedings of the Institution of Mechanical Engineers, Part F: Journal of Rail and Rapid Transit 239(5), 443-450, 2025.
45. P. Fodiman, B. Trolle, F. Létourneaux, M. Ribourg. *Optimisation of rail grinding parameters to improve the acoustic track performance and its durability: towards an acoustic maintenance of the rail on the French network*. Proceedings of 11th World Congress on Railway Research, Milan, 2016.
46. F. Létourneaux, M. Ribourg, P. Fodiman, B. Trolle. *A new metrics to assess the acoustic performance of rail grinding processes*. In: Proceedings of 12th International Workshop on Railway Noise, Terrigal, Australia, 2016.
47. A.H.W.M. Kuijpers, W. Schwanen, B.H.C.A. van Dijck, *Beheersing railruwheid als geluidsmaatregel* (Control of rail roughness as a noise control measure), M+P Report M+P.RAIL.06.15.11, 2009.
48. B. Asmussen, H. Onnich, R. Strube, L. M. Greven, S. Schroder, K. Jager, K. G. Degen. *Status and perspectives of the "Specially Monitored Track"*. Journal of Sound and Vibration 293(3-5): 1070-1077, 2006.
49. E. Verheijen. *A survey on roughness measurements*. Journal of Sound and Vibration 293, 784–794 (2006).
50. RailTrackModellingToolbox: Open source Rail Track Modelling Toolbox, 2025. [Online]. Available: https://github.com/jcugnoni-heig/RailTrackModellingToolbox.
51. Train Noise Expert. https://trainnoiseexpert.com/
52. T. Dahlberg. *Some railroad settlement models – a critical review*. Proc Inst Mech Eng, Part F: J Rail Rapid Transit. 2001;215(F4):289–300.
53. Y. Sato. *Japanese studies on deterioration of ballasted track*. Vehicle System Dynamics, 1995, 24(Suppl.), 197–208.
54. Y. Sato. *Optimization of track maintenance work on ballasted track*. In Proceedings of the World Congress on Railway Research (WCRR '97), Florence, Italy, 16–19 November, 1997, Vol. B, pp. 405–411.
55. K. Demharter. *Setzungsverhalten des Gleisrostes unter vertikaler Lasteinwirkung*. Mitteilungen des Prüfamtes für Bau von Landverkehrswegen, Technischen Universität München, Part 36, 1982.

Co-funded by the European Union

56. N. Guérin. *Approche expérimentale et numérique du comportement du ballast des voies ferrées*. PhD thesis, Ecole Nationale des Pont et Chaussées, Paris, 1996.
57. A. Hecke. *Effects of future mixed traffic on track deterioration*. Report TRITA-FKT 1998:30, Railway Technology, Department of Vehicle Engineering, Royal Institute of Technology, Stockholm, 1998.

Co-funded by the European Union

Appendices

Appendix A. Alternative rail roughness spectra

In this appendix, various measured rail roughness spectra are considered as alternatives to the sonRail spectra listed in Table 13. In particular, to account for the effect of acoustic rail grinding, typical spectra after such grinding are required, as well as typical network average spectra.

Network average spectra are provided for Belgium in [42] and for the Netherlands in [43]. The average roughness over a range of sites in the UK is presented in [15]. In Figure A1 these three average roughness spectra are compared with the sonRail spectra used in the main report.

There is strong agreement between the three results for the most important wavelength range between 63 and 10 mm. All three have a small peak at 63 mm, which is likely to be due to the use of preventive grinding and/or the presence of mild corrugation [44]. The sonRail 'average' curve is higher than these measurements in the mid wavelength range, and lower than the Belgian and UK results at short wavelengths.

At wavelengths longer than 80 mm, the Belgian and Netherlands results are much lower than the UK results, whereas the UK results follow the ISO3095 limit curve more closely. This difference may be a feature of the measurement system used (m|rail in the first two cases, CAT in the UK measurements); this deserves further investigation but is beyond the scope of the current project.

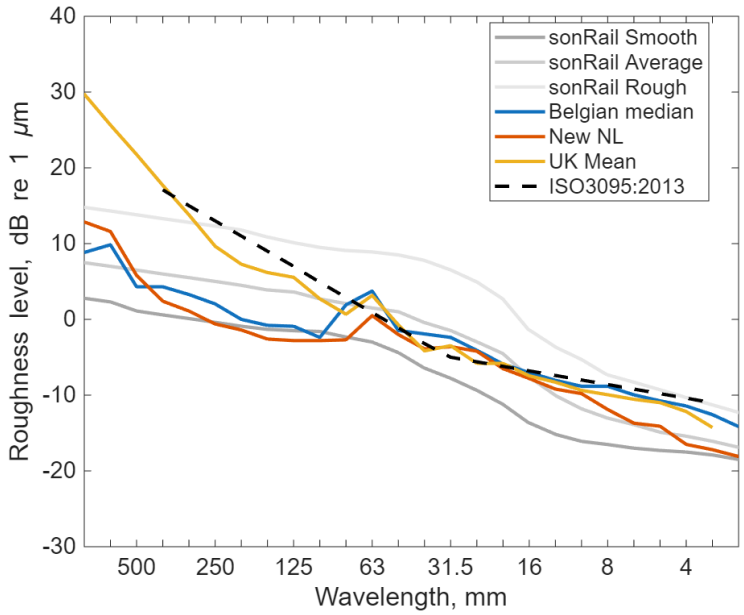

Figure A1. Examples of measured rail roughness: average spectra from UK [15], Belgium [42], and Netherlands [43], compared with sonRail spectra [12].

The effect of using the Belgian and UK average spectra in the noise predictions for the reference case is shown in Figure A2. The large differences at low frequency in Figure A2(a) are a consequence of the different trends seen in Figure A1. Nevertheless the overall levels in Figure A2(b) contain only small differences, and they are consistent with the reference results for the sonRail average roughness from Figure 22.

Co-funded by the European Union

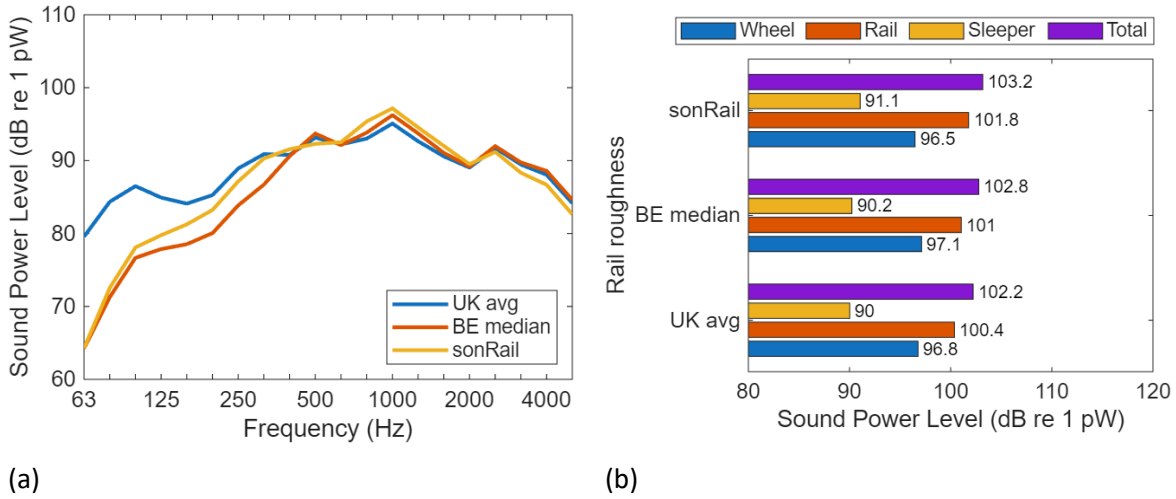

(a) (b)

Figure A2. Effect of alternative rail roughness spectra: (a) total sound power spectra, (b) overall A-weighted sound power levels.

Immediately after rail grinding, the rail surface may be significantly rougher due to the presence of grinding marks. The corresponding wavelengths depend on the speed of the grinding train and the rotational speed of the stones, whereas the magnitude is affected by the choice of stones, the applied pressure and the use of a combination of speeds [44, 45, 46]. The aim of 'acoustic grinding' is to minimise this initial roughness. As well as grinding, milling can also be used.

In [47] rail roughness was measured at a number of sites 53 days after grinding or milling. The average spectra of the sites subjected to grinding and milling are shown in Figure A3. The milling operation was combined with grinding using oscillating stones and a finishing step and shows a lower roughness spectrum than the grinding. In a study in France [45, 46] the rail roughness was monitored at five sites after grinding, testing several sets of grinding parameters. The spectra directly after grinding showed large variability, and in some cases large tonal roughness levels. However, the roughness generally reduced with the passing of traffic. An example of good practice, which used cuts at 5.5 and 6.0 km/h using 'soft' stones, is included in Figure A3; this was measured two months after grinding. It shows very similar levels to the result of milling from [47]. Also shown is the spectrum from the same site 48 months after grinding which is considerably lower.

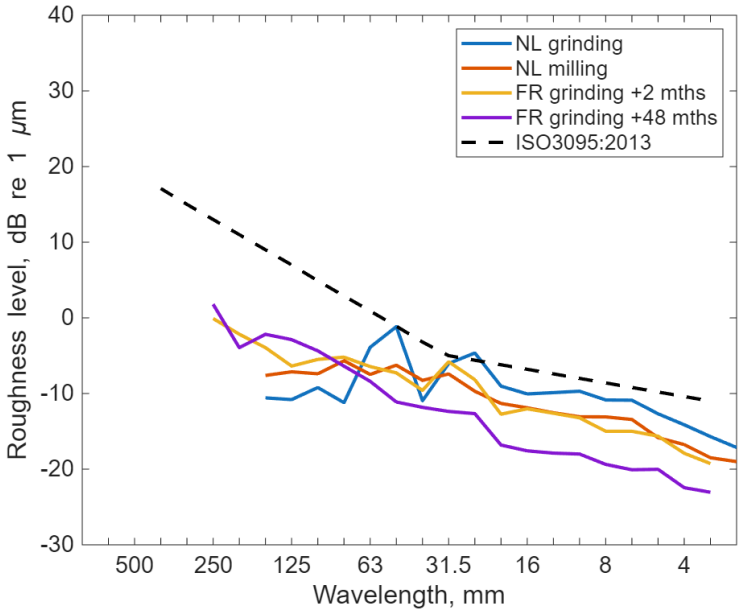

Figure A3. Examples of measured rail roughness spectra after acoustic grinding or milling [45, 47].

Co-funded by the European Union

Introducing these roughness spectra into the calculations, the sound power levels obtained are shown in Figure A4. Although there are differences in roughness spectra of up to 10 dB, the differences in noise levels between these cases are much more modest (less than 3 dB) due to the influence of the wheel roughness.

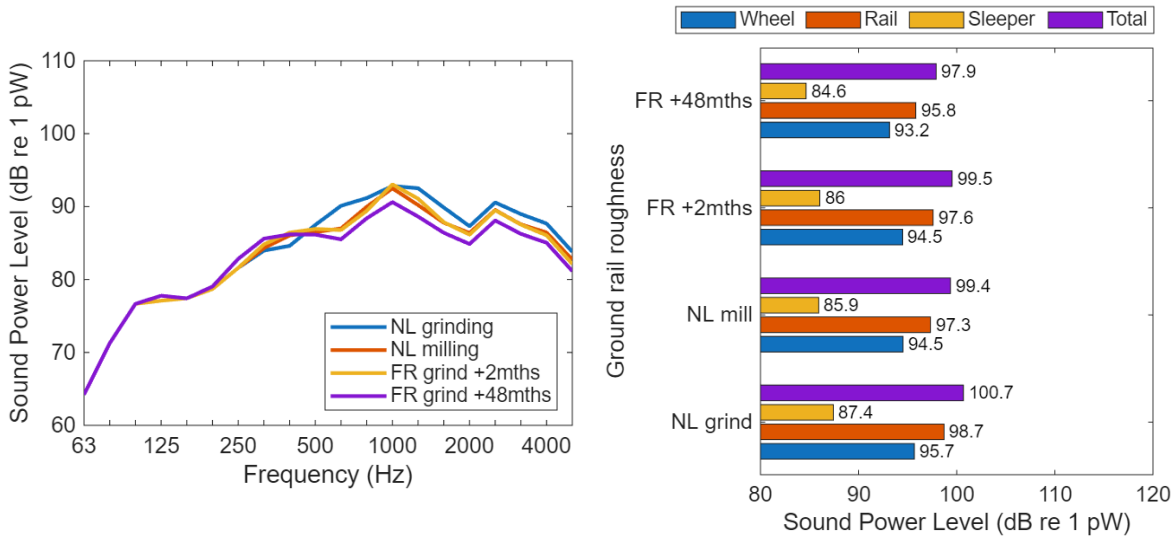

(a) (b)

Figure A4. Effect of rail roughness after acoustic rail grinding or milling: (a) total sound power spectra, (b) overall A-weighted sound power levels.

To predict the effect of rail grinding on noise emissions, the results for a 'normal' roughness spectrum should be compared with the results after acoustic grinding. The various permutations considered here are listed in Table A1. These indicate that the noise level is predicted to reduce by between 2 and 4 dB after acoustic grinding, considering the level after two months. The sonRail 'smooth' curve gives results that are closely compatible with the Netherlands milling study or the French grinding study, and for simplicity this can be used in the tool. The alternative spectra can also be used if required, and are listed in Table A2.

Table A1. Predicted effect of rail grinding on A-weighted sound power levels, dB(A).

		sonRail average	UK average	BE median
		103.2	102.2	102.8
sonRail smooth	99.5	3.7	2.7	3.3
NL grinding	100.7	2.5	1.5	2.1
NL milling	99.4	3.8	2.8	3.4
FR grinding +2 mths	99.5	3.7	2.7	3.3
FR grinding +48 mths	97.9	5.3	4.3	4.9

There is a lack of consistency between results reported from different networks about the long-term effects of rail grinding. One of the first studies of the use of grinding to control noise was reported by Asmussen et al. [48]. They indicated that the monitored noise levels grew at a rate of approximately 0.7 dB per year, so that repeat grinding, triggered by a noise level increase of 6 dB, was usually required after 8 years. Florentin [42] reported that roughness levels also grow after grinding in Belgium and the Netherlands [49]. However, as seen above, the results from France [45, 46] indicate that the rail continues to become smoother. This is an area requiring further research to understand the reasons for these differences.

Co-funded by the European Union

Table A2. Alterative rail roughness spectra for noise calculations, dB ref. 10^{-6} m (values in italics are extrapolated).

Wavelength, m	UK average	Belgian median	NL grinding	NL milling	France grinding +2 mths	France grinding +48 mths
1.25	33.5	*14.0*	*14.0*	*14.0*	*14.0*	*14.0*
1.0	30.3	*12.0*	*12.0*	*12.0*	*12.0*	*12.0*
0.8	29.7	8.8	*8.8*	*8.8*	*8.8*	*8.8*
0.63	25.7	9.9	*9.9*	*9.9*	*9.9*	*9.9*
0.5	21.8	4.3	*4.3*	*4.3*	*4.3*	*4.3*
0.4	17.7	4.3	*4.3*	*4.3*	*4.3*	*4.3*
0.31	13.8	3.3	*3.3*	*3.3*	*3.3*	*3.3*
0.25	9.7	2.0	*-0.1*	*-0.1*	-0.1	1.8
0.2	7.3	0.0	*-2.2*	*-2.2*	-2.2	-3.9
0.16	6.2	-0.8	*-3.9*	*-3.9*	-3.9	-2.2
0.12	5.6	-0.9	*-6.4*	*-6.4*	-6.4	-2.9
0.1	2.7	-2.4	-9.2	-7.4	-5.5	-4.4
0.08	0.7	1.9	-11.2	-5.7	-5.2	-6.4
0.063	3.2	3.7	-3.9	-7.5	-6.4	-8.4
0.05	-0.7	-1.5	-1.2	-6.3	-7.3	-11.1
0.04	-4.2	-1.9	-11.0	-8.3	-9.6	-11.8
0.0315	-3.5	-2.4	-6.0	-7.4	-5.8	-12.4
0.025	-5.8	-4.1	-4.6	-9.7	-8.2	-12.7
0.02	-5.8	-5.9	-9.0	-11.3	-12.7	-16.8
0.016	-7.5	-7.0	-10.1	-11.9	-12.0	-17.6
0.012	-8.3	-8.0	-9.9	-12.5	-12.6	-17.9
0.01	-9.4	-8.8	-9.7	-13.1	-13.2	-18.0
0.008	-9.9	-8.8	-10.9	-13.1	-15.0	-19.4
0.0063	-10.5	-10.0	-10.9	-13.4	-15.0	-20.1
0.005	-11.0	-10.8	-12.7	-15.8	-15.6	-20.0
0.004	-12.2	-11.4	-14.1	-16.8	-17.9	-22.5
0.00315	-14.3	-12.6	-15.7	-18.5	-19.3	-23.1
0.0025	*-16.0*	-14.2	-17.1	-19.5	*-20.5*	*-24.0*
0.002	*-18.0*	*-16.0*	*-19.0*	*-21.0*	*-22.0*	*-25.0*

Co-funded by the European Union

Appendix B. Benchmark study of ToPNoise and TWINS for track dynamics and sound power

B1 Introduction

Within WP4 complementary tools are available to the project partners for the calculation of the dynamic and acoustic response of wheels and tracks. An extensive benchmarking study has been performed between the TWINS model for rolling noise [25, 26] and the ToPNoise (Tool for the Prediction of Railway Noise) Modelling Toolbox [50] which uses finite element models (FEM) and boundary element models (BEM). The dynamic and acoustic response for different track types is calculated using these different tools. This appendix shows the equivalence of both tools for four calculation scenarios.

A description of the models is provided, detailing the type of modelling carried out. The compared results are the point mobilities, wheel-rail contact force for unit roughness, track decay rate (TDR), and sound power for unit roughness. For each model, the components and material properties used are listed, followed by a spectral comparison of the relevant results.

The objective of this work is to compare the predictions of the ToPNoise Toolbox with those of TWINS and assess their equivalence. While TWINS predicts rolling noise efficiently using simplified beam-based track models and modal wheel models, the Rail Track Modelling Toolbox employs a reduced-order 3D finite-element model that includes most track components explicitly.

B2 Model Description

B2.1 TWINS

The TWINS (Track-Wheel Interaction Noise Software) model [25, 26] consists of a number of modules to calculate the frequency responses of the wheel and track, the interaction forces between them, their responses to roughness interaction and their noise radiation:

- The wheel mobility is calculated from the modal basis obtained from an axisymmetric finite element model.
- The track mobility is calculated using an analytical Timoshenko beam model. In the current comparisons a discretely supported track model is used, with the calculations averaged over five excitation positions within a sleeper span.
- The wheel/rail interaction is calculated using analytical formulae.
- The sound radiation of the wheel is calculated using analytical formulae that have been derived from the results of axisymmetric boundary element models.
- The rail sound radiation is calculated using a 2D boundary element model with corrections applied to allow for 3D effects.
- The sleeper sound radiation is calculated using an analytical model.

Further details of the theoretical models are available in [15]. The TWINS models as incorporated into the TNE software [51] are used here but are referred to as ‘TWINS’ throughout this appendix.

B2.2 ToPNoise

The proposed approach relies on a detailed numerical model of the track and wheel, using a full 3D representation of all components except the ballast and the clamps, which are represented by springs. The main objective of this modelling strategy is to efficiently capture the effect of individual components such as rail pads or wheel/rail geometry. Since accurate predictions of the track dynamics demand the absence of boundary effects and wave reflections, considering a long section (in this case, 400 sleepers) is required. This can be achieved through the application of dynamic substructuring. The contact force between the track and wheel is implemented similar to TWINS, taking the contact patch, the train speed, the axle load, and potentially the combined roughness into account. The rolling noise is subsequently predicted through

Co-funded by the European Union

boundary element models (BEM), which allow the inclusion of the complex shape of all components.

The structural model runs in the following steps:

1. Modal analysis of the track unit cell shown in Figure B1 with free boundary conditions. This represents one half of a sleeper section.
2. Selection of modes for the Craig-Bampton substructuring approach.
3. Calculation of the forced harmonic response of a 400-sleeper section, both for lateral and vertical point-force excitation. The point force is applied at mid-span (A), quarter-span (B), and above the sleeper (C) to allow spatial averaging.
4. Modal analysis of the wheelset with free boundary conditions.
5. Calculation of the forced harmonic response of the wheelset using modal superposition.

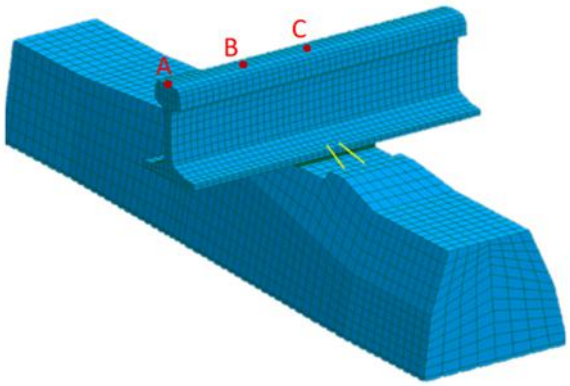

Figure B1. Mesh of the track unit cell.

B2.3 Considered scenarios

Both modelling approaches are compared for four scenarios. The wheels are axisymmetric and double-curved with a diameter of 960 mm, as shown in Figure B2. The track parameters are selected to represent a wide variety of practical situations:

1. A standard ballasted track with B91 concrete sleepers, 60E2 rails, and very stiff pads (similar to a typical Swiss superstructure).
2. A standard ballasted track with B91 concrete sleepers, 60E2 rails, and medium-soft pads (similar to a typical UK superstructure).
3. A ballasted track with wooden sleepers, 60E2 rails, and medium pads.
4. A ballasted track with steel sleepers, 60E2 rails, and stiff pads.

The corresponding material proprieties are reported in Table B1. For the calculation of the contact force and sound power, an axle load of 54 kN and a train speed of 100 km/h was used.

Co-funded by the European Union

Table B1. Material properties of the track for the different benchmark scenarios.

		Scenario 1 (stiff pad)	Scenario 2 (soft pad)	Scenario 3 (wood slp)	Scenario 4 (steel slp)
Rail pad	Vertical acoustic stiffness (MN/m)	4425	169	500	1000
	Lateral acoustic stiffness (MN/m)	175	46	177	120
	Vertical damping loss factor	0.159	0.059	0.5	0.15
	Lateral damping loss factor	0.16	0.061	0.5	0.15
Sleeper	Mass density (kg/m³)	2436	2436	800	7850
	Total mass (kg)	280	280	78	76
	Young's modulus (GPa)	42	42	15	210
	Poisson's ratio	0.2	0.2	0.2	0.3
Ballast	Vertical stiffness (MN/m)	120	120	140	107
	Lateral stiffness (MN/m)	35	35	140	105
	Vertical viscous damping (kN.s/m)	160	160	180	70
	Lateral viscous damping (kN.s/m)	600	600	180	31.18

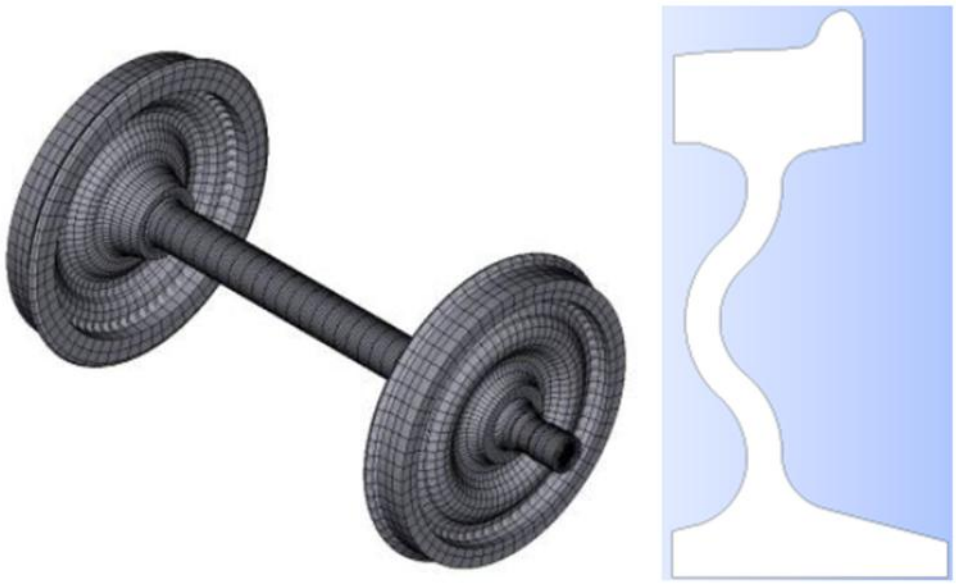

Figure B2. Mesh of the full wheelset, and cross-section geometry of the double-curved wheel.

The following spectra are compared:

1. Point mobilities in vertical and lateral direction, and cross-mobility in the excitation point (narrow band, magnitude and phase).
2. Track decay rate (one-third octave bands).
3. Contact force for a speed of 100 km/h and unit roughness (narrow band, magnitude and phase).
4. Velocity responses.
5. Sound power level of the wheel, track, and the total system (one-third octave bands, only scenarios 1 and 2).

Co-funded by the European Union

B2.4 Notable differences between the models

1. The rail pads are defined as springs with vertical and lateral spring-damper systems in TWINS, whereas they are 3D meshed bodies in ToPNoise. This has two repercussions. The first is obvious: an equivalent complex Young's modulus E and Poisson's ratio ν must be found to represent the frequency-dependent stiffness and damping of the spring elements. Tabular values of E were used to approximate the viscoelastic pad representation in TWINS. The second is the finite extent of the contact area between the rails and the pads in the FEM, which could lead to an increased effective stiffness due to a non-negligible rotational stiffness along the rail.
2. The ballast properties in TWINS are defined as a spring-damper system with viscoelastic properties, and as a frequency-dependent stiffness with hysteretic damping in ToPNoise. The latter values were adapted to match the visco-elastic values in the desired frequency range.
3. The rail modelling approach also differs. In TWINS, the rail is represented by Timoshenko beam elements, i.e. as a one-dimensional model with equivalent sectional properties, whereas ToPNoise uses a three-dimensional finite element representation. This is particularly important for the lateral point mobility, since the bending moment on the cross-section yields higher-order deformation shapes.

B3 Results

The compared results focus on the key indicators of the track and wheel dynamic responses, with different track scenarios (as reported in Table B1) combined with double-curved wheels with a diameter of 960 mm.

B3.1 Structural response

Although different points on the rail span were considered in this study, only the mid-span results are presented to maintain clarity and avoid redundancy, since the results and trends are consistent and converge across other span location. In the figures, blue and orange are used for ToPNoise and TWINS, respectively.

B3.1.1 Point mobility

- Rail point mobility

Figure B3 presents the vertical point mobilities for the four investigated scenarios, as predicted by ToPNoise and TWINS. Overall, a good agreement is observed, particularly in the vertical direction. Yet, ToPNoise consistently shows a slightly stiffer prediction, as indicated by the shift to higher frequencies.

This discrepancy is more pronounced in the cases with stiffer rail pads (Scenario 1, 3 and 4), where the shift is clearly visible, whereas for Scenario 2, which includes softer pads, the predictions of the two models are nearly coincident.

These differences can be attributed to the different modelling approaches used for the rail pads. In TopNoise, the rail pads are modelled using a three-dimensional mesh, whereas in TWINS they are represented as discrete springs (as described in Section B2.4). Consistent with this interpretation, reducing the contact area in the ToPNoise model shifts the results toward lower frequencies, leading to improved agreement between the two models.

Co-funded by the European Union

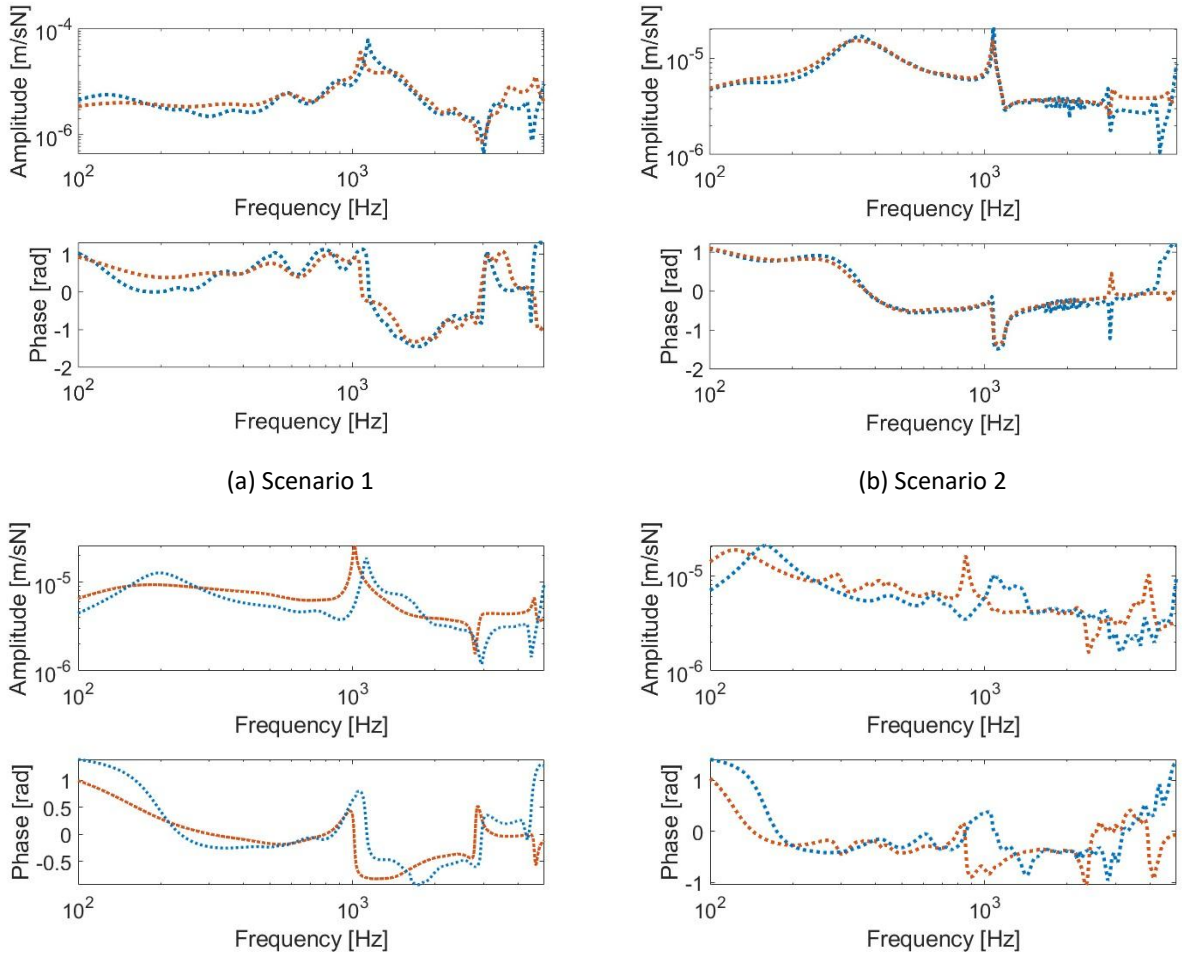

(a) Scenario 1

(b) Scenario 2

(c) Scenario 3

(d) Scenario 4

Figure B3. Vertical point mobility of the rail at mid-span (ToPNoise in blue and TWINS in orange).

On the other hand, as expected the differences are more pronounced for the rail lateral point mobilities (Figure B4) and rail cross mobilities (Figure B5). These differences arise from the modelling assumptions for the rail. In TWINS, the rail is simplified using Timoshenko beam theory (as described in Section B2.4). Additional compliance mechanisms are captured in the 3D ToPNoise model and can reduce effective lateral stiffness. Consequently, TWINS predicts lower lateral point mobility, especially at higher frequencies, as can be seen for all Scenarios in Figure B4. This assumption affects also the cross mobilities, for which the TWINS model gives higher estimates, as reported in Figure B5.

Co-funded by the European Union

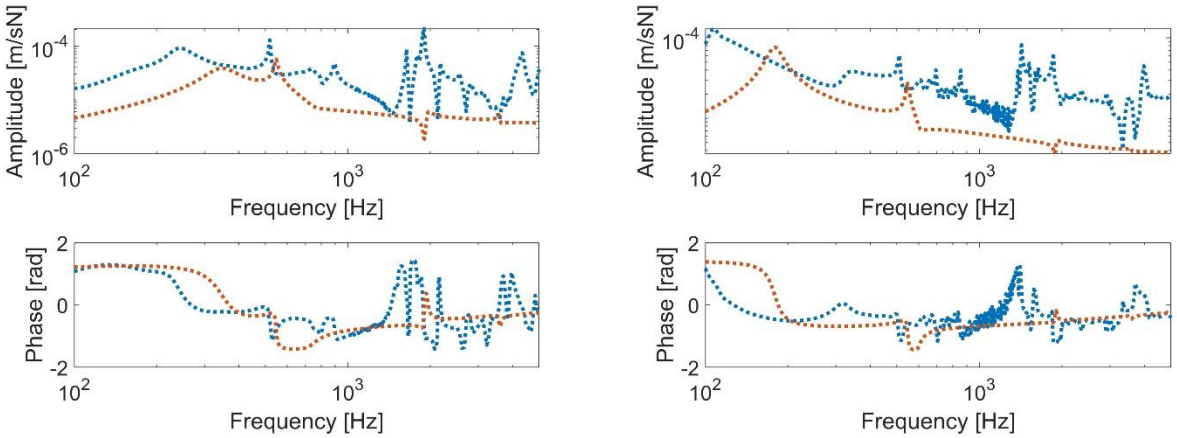

(a) Scenario 1

(b) Scenario 2

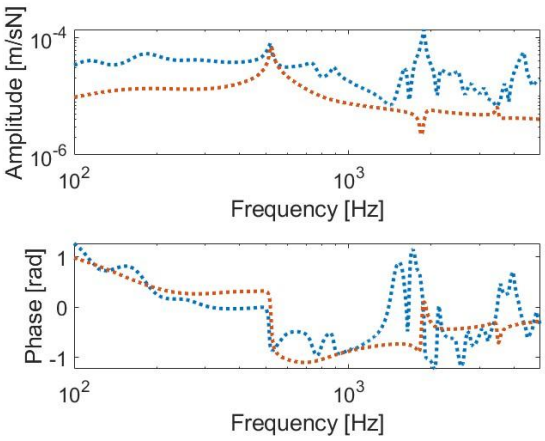

(c) Scenario 3

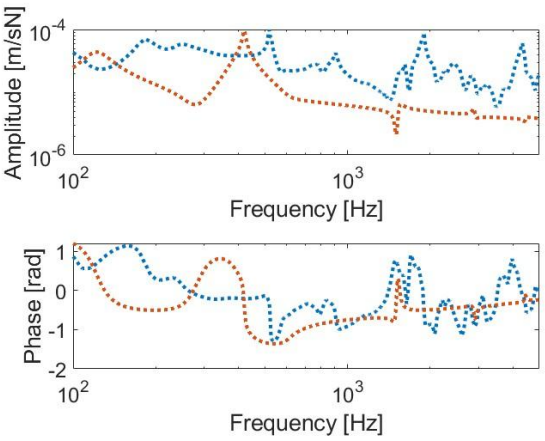

(d) Scenario 4

Figure B4. Lateral point mobility of the rail at mid-span (ToPNoise in blue and TWINS in orange).

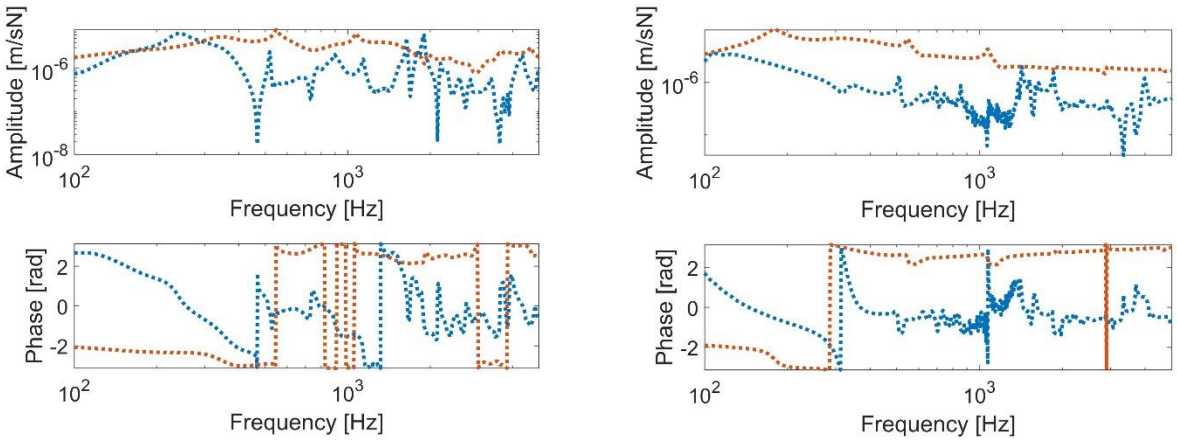

(a) Scenario 1

(b) Scenario 2

Figure B5. Cross mobility of the rail at mid-span (ToPNoise in blue and TWINS in orange).

- Wheelset point mobility

The point mobility of the wheelset calculated with the two models is compared in Figure B6. The frequency response of the wheelset is evaluated in two directions: vertical (radial) and lateral (axial). The damping ratios are adopted from [15]. The resonance peaks correspond to structural modes at different harmonics.

Differences between the two models are observed in the low-frequency region, below about 500 Hz. These

Co-funded by the European Union

discrepancies arise from differences in the modelling approaches. In the TWINS approach, a wheel model constrained at the hub is used, and the rigid-body motion is superimposed on the flexible wheel vibration to approximate the dynamic behaviour of the complete wheelset. In contrast, ToPNoise uses a finite element (FE) model of the full, unconstrained wheelset.

Nevertheless, very good agreement is observed between the predicted frequency responses for the vertical, lateral, and cross mobilities over the remaining frequency range above 500 Hz.

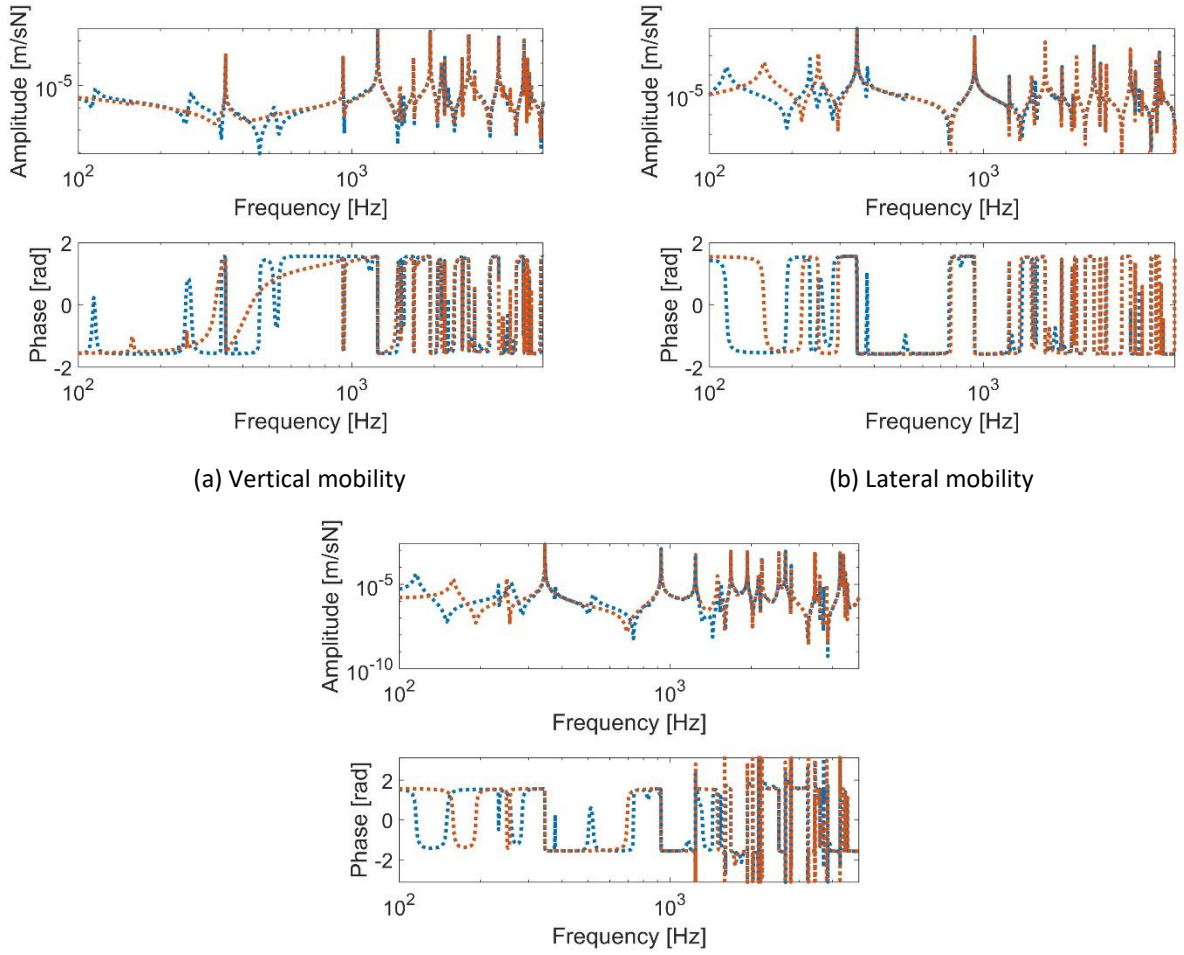

(a) Vertical mobility

(b) Lateral mobility

(c) Cross mobility

Figure B6. Wheel point mobilities (ToPNoise in blue and TWINS in orange).

B3.1.2 Contact force

The contact force comparison follows directly the mobility formulation given by [15], where the contact force is obtained as a ratio between the acoustic combined roughness and the sum of the wheel, rail and contact mobilities. Since the force is inversely proportional to the sum of the total mobility, the lower lateral rail mobility predicted by TWINS leads to higher contact force values.

The contact forces are compared for Scenarios 1 and 2 in Figure B7. The contact forces obtained by the two models have a good agreement in the vertical direction whereas, in the lateral direction, the spectra predicted by TWINS are clearly higher compared to ToPNoise.

Co-funded by the European Union

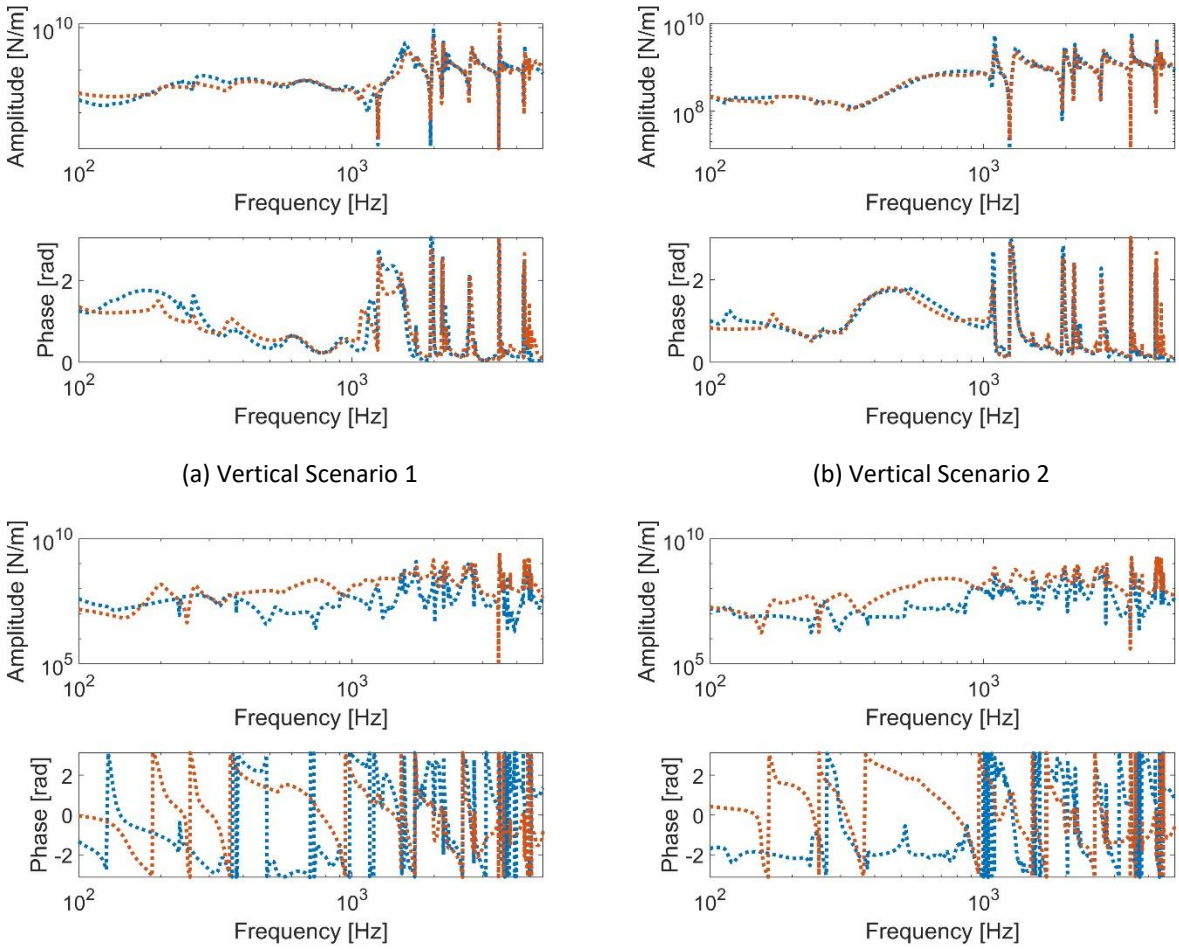

(a) Vertical Scenario 1

(b) Vertical Scenario 2

(c) Lateral Scenario 1

(d) Lateral Scenario 2

Figure B7. Contact force (ToPNoise in blue and TWINS in orange).

B3.1.3 Velocity response

The velocity response at the contact point is obtained by multiplying the contact force by the respective mobility. Since the contact force is inversely proportional to the total mobility, the differences seen in the point mobility and contact force partially compensate when evaluating the response.

- Rail response

For the rail velocity response presented in Figure B8, the vertical response shows a strong agreement for Scenario 1 and 2, reflecting the consistency of the vertical mobility and contact force. At the same time the modelling assumptions lead to a deviation in the lateral direction. Yet, the overestimation of contact force and the underestimation of mobility in TWINS partly offset each other, reducing the overall discrepancy in the predicted rail velocity between the two models.

Co-funded by the European Union

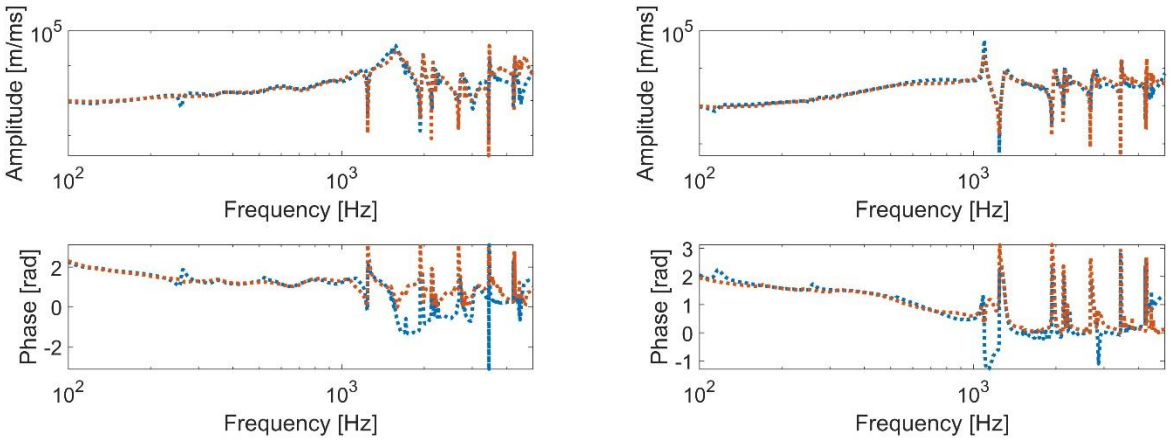

(a) Vertical Scenario 1

(b) Vertical Scenario 2

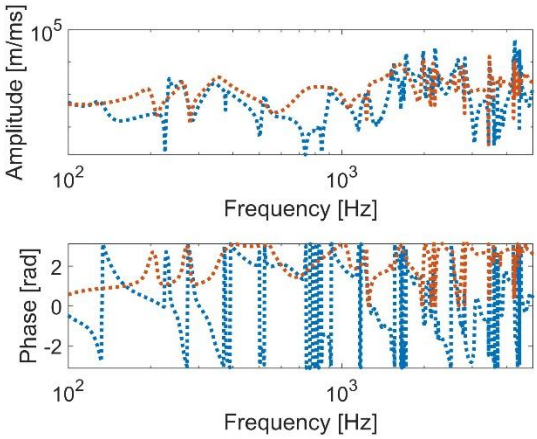

(c) Lateral Scenario 1

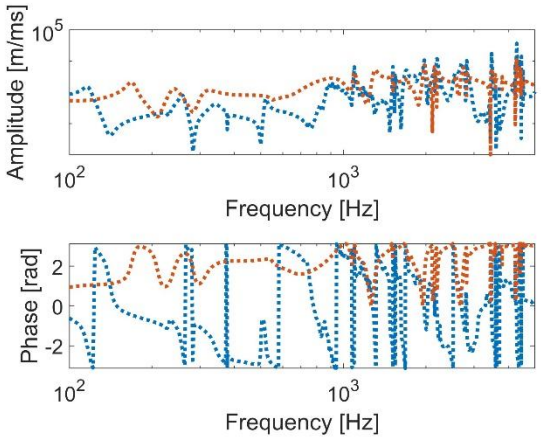

(d) Lateral Scenario 2

Figure B8. Rail response at mid-span (ToPNoise in blue and TWINS in orange).

- Wheel response

As for the rail, the wheel velocity response shown in Figure B9 has a similarly good agreement in the vertical direction for Scenarios 1 and 2, consistent with the close correspondence in vertical dynamics between the two models. In the lateral direction, some deviations remain due to the different modelling assumptions.

Co-funded by the European Union

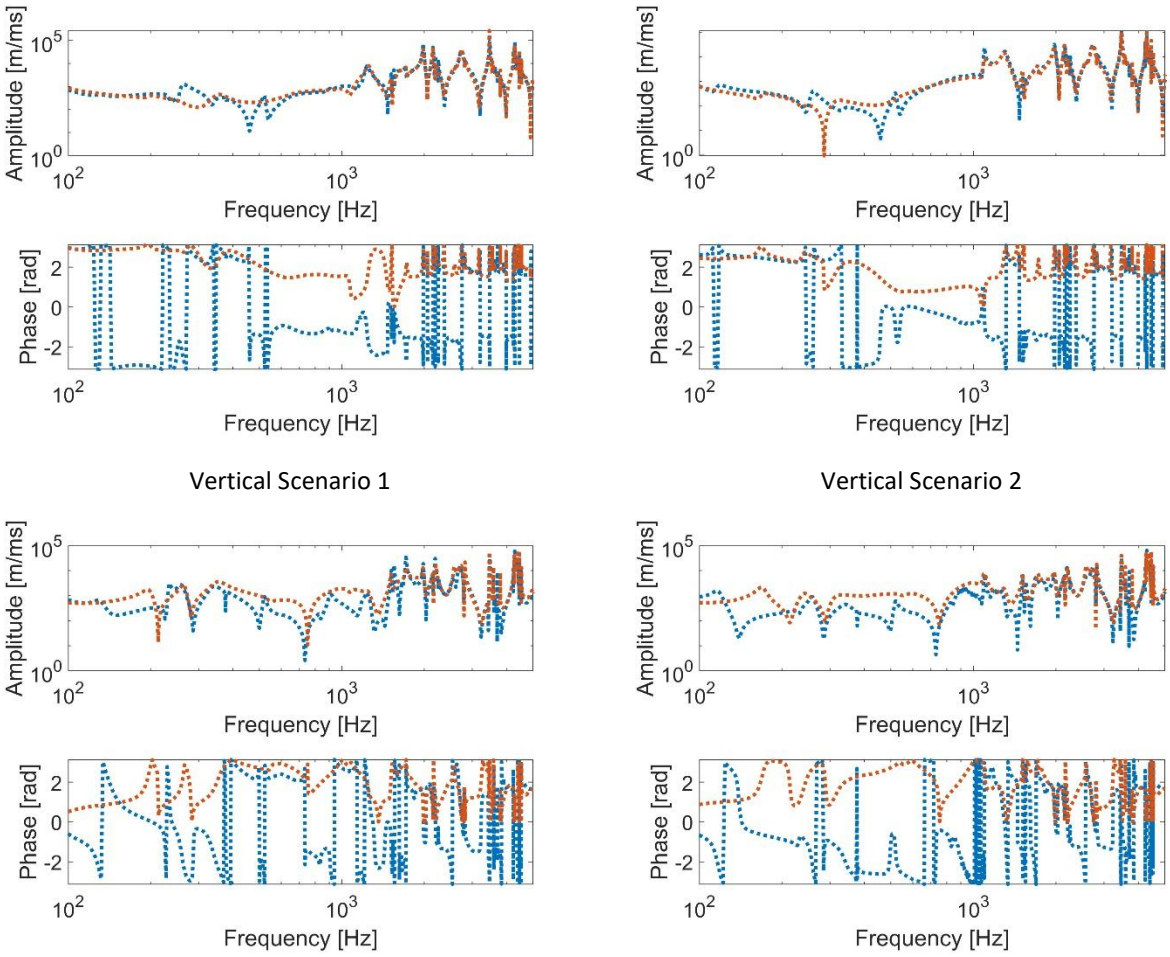

Figure B9. Wheel response (ToPNoise in blue and TWINS in orange).

B3.1.4 Track decay rate (TDR)

Track decay rates (TDRs) were obtained according to EN 15461 [30] and thus include modelled frequency response functions at successive positions along the rail.

In Figure B10 a consistent trend between TWINS and ToPNoise across the four scenarios can be seen. In the vertical direction, the agreement is good over the full frequency range, with only minor differences. On the other hand, in the lateral direction, slightly larger deviations appear at high frequencies, mainly due to the different modelling approaches for rail pads and ballast.

These results confirm that, despite the different structural assumptions of the two models, both approaches provide a consistent prediction of wave amplitude decay along the rail.

Co-funded by the European Union

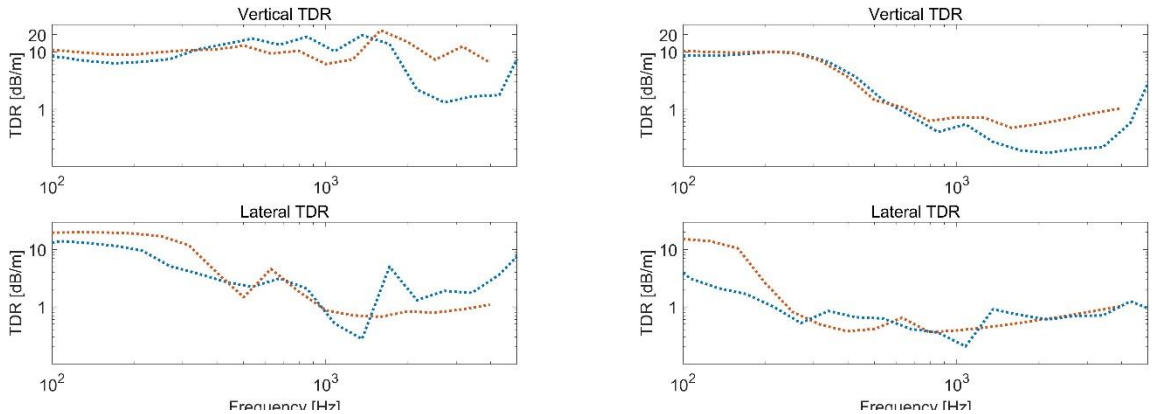

(a) Scenario 1

(b) Scenario 2

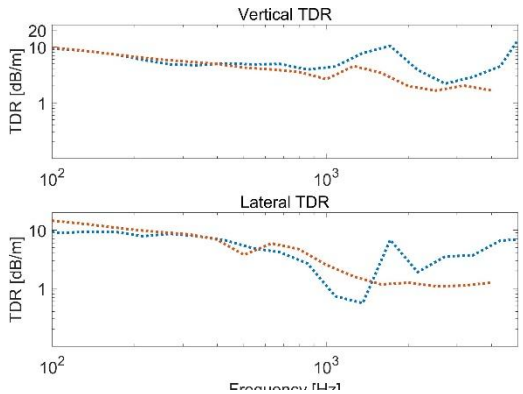

(c) Scenario 3

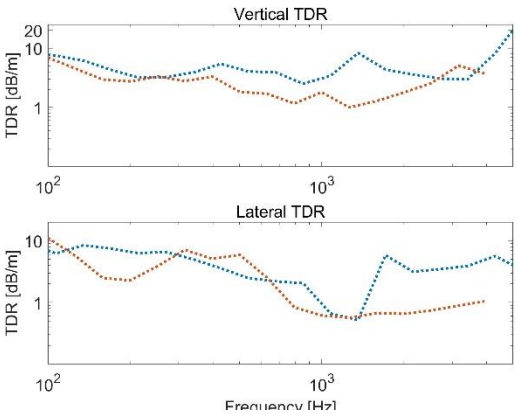

(d) Scenario 4

Figure B10. Track Decay Rate (ToPNoise in blue and TWINS in orange).

B3.2 Noise Radiation

The sound power levels predicted by the two models are compared in Figures B11 to B13. One-third octave band noise spectra are evaluated separately for the wheel and the rail, as well as for the complete system including the contribution of the sleepers. The sound radiation of each structure is computed in free space. Only the radiation of a single wheel is considered in the calculations. The estimated sound power levels correspond to unit roughness. The vibroacoustic frequency response functions (FRFs) for unit force are multiplied by the contact force for unit roughness. The comparison is based on the track properties of Scenario 1 (stiff pads) and Scenario 2 (soft pads).

B3.2.1 Wheel

Sound power level spectra of the wheel for unit roughness are shown in Figure B11. The TWINS approach predicts higher levels over almost the entire frequency range compared to ToPNoise. This trend is consistent for both track configurations: stiff pads (Figure B11(a)) and soft pads (Figure B11(b)).

These differences are related to the predicted wheel–rail interaction forces. As shown in Figure B4, ToPNoise predicts a higher lateral driving-point mobility of the rail than the TWINS approach. The higher rail mobility contributes to a reduction in the lateral contact force component (see Figure B7), which in turn results in lower radiated sound power from the wheel.

Co-funded by the European Union

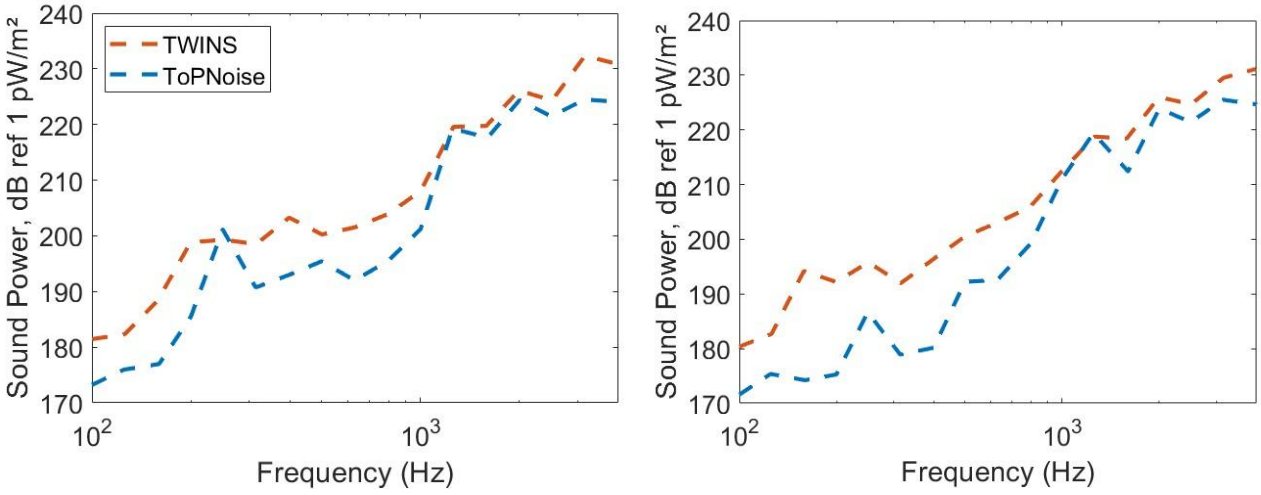

(a) Scenario 1

(b) Scenario 2

Figure B11. Sound power for unit roughness radiated by the wheel (ToPNoise in blue and TWINS in orange).

B3.2.2 Rail

The rail sound power results are obtained by averaging the radiation over multiple excitation points (A-B-C) distributed along half a span between two sleepers. In ToPNoise, three excitation points are considered, whereas the TWINS approach uses five points within the same interval. Figure B12 shows the rail sound power level spectra for unit roughness predicted by the two models.

For the track with stiff pads (Figure B12(a)), differences are observed over the entire frequency range. Below 1.6 kHz, the TWINS approach consistently predicts higher sound power levels than ToPNoise, with deviations ranging from approximately 2 dB to 10 dB. Above 1.6 kHz, the trend reverses, and ToPNoise yields higher levels, with differences up to about 7 dB. A similar trend is observed for the track with soft pads (Figure B12(b)). In this case, TWINS predicts higher **sound** power levels up to 800 Hz, whereas at higher frequencies ToPNoise generally predicts larger values.

These discrepancies originate from differences in the predicted lateral dynamic behaviour of the rail. As shown in Figure B4, the lateral driving-point mobility calculated with ToPNoise is consistently higher than that obtained with the TWINS approach. For unit roughness, the resulting reduction in lateral contact force leads to lower radiated sound power in the corresponding frequency ranges.

Co-funded by the European Union

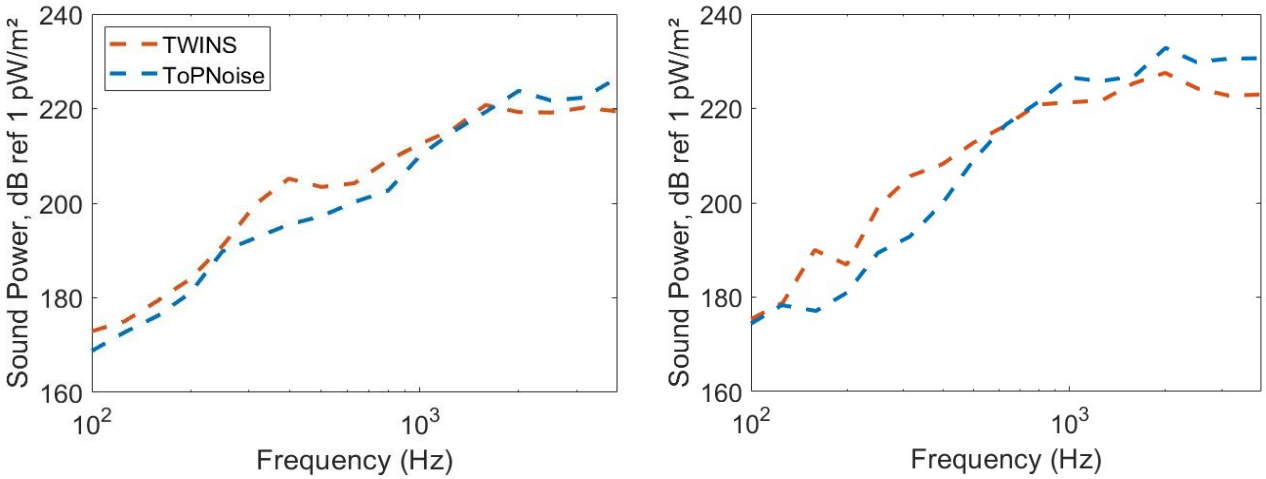

(a) Scenario 1 (b) Scenario 2

Figure B12. Sound power for unit roughness radiated by the rail (ToPNoise in blue and TWINS in orange).

B3.2.3 Total

The overall noise emissions include the contributions from the wheel, rail, and sleepers. The comparison results are shown in Figure B13. For the track configuration with stiff pads (Figure B13(a)), good agreement between the two models is observed up to 2.5 kHz. In the 3.15 kHz and 4 kHz one-third octave bands, ToPNoise predicts higher levels, with differences of approximately 6 dB and 3 dB, respectively. Below 800 Hz, the sleeper contribution is dominant. In this frequency range, the total sound power levels predicted by ToPNoise increase relative to the wheel and rail contributions alone, leading to closer agreement with the TWINS results.

For the configuration with soft pads (Figure B13(b)), the levels estimated using the TWINS approach are higher than those predicted by ToPNoise in the frequency range between 160 Hz and 500 Hz. The two models yield equal levels at the centre frequencies of 630 Hz and 800 Hz. At higher frequencies, ToPNoise generally predicts higher sound power levels, with the exception of the 4 kHz centre frequency.

Both models also predict an overall increase in noise levels when soft rail pads are used.

The differences observed in the total sound power levels reflect the trends identified in the individual component contributions. As discussed previously, the lower lateral contact forces predicted by ToPNoise result in lower overall sound power levels compared to the TWINS approach up to approximately 1.6 kHz for stiff pads and 800 Hz for soft pads.

For the configuration with stiff pads, the wheel becomes dominant at higher frequencies in both models. Consequently, the differences in total sound power levels in this range follow the differences previously observed in the wheel radiation results. For the configuration with soft pads, the dominance behaviour differs between the two approaches. In the TWINS model, the wheel contribution becomes dominant only at very high frequencies, whereas in ToPNoise the rail contribution remains dominant over a wider frequency range. As a result, the higher rail vibration levels predicted by ToPNoise at higher frequencies lead to increased total sound power levels relative to the TWINS results.

Overall, the differences between the two models remain within a reasonable range, considering the different modelling assumptions adopted in each approach.

Co-funded by the European Union

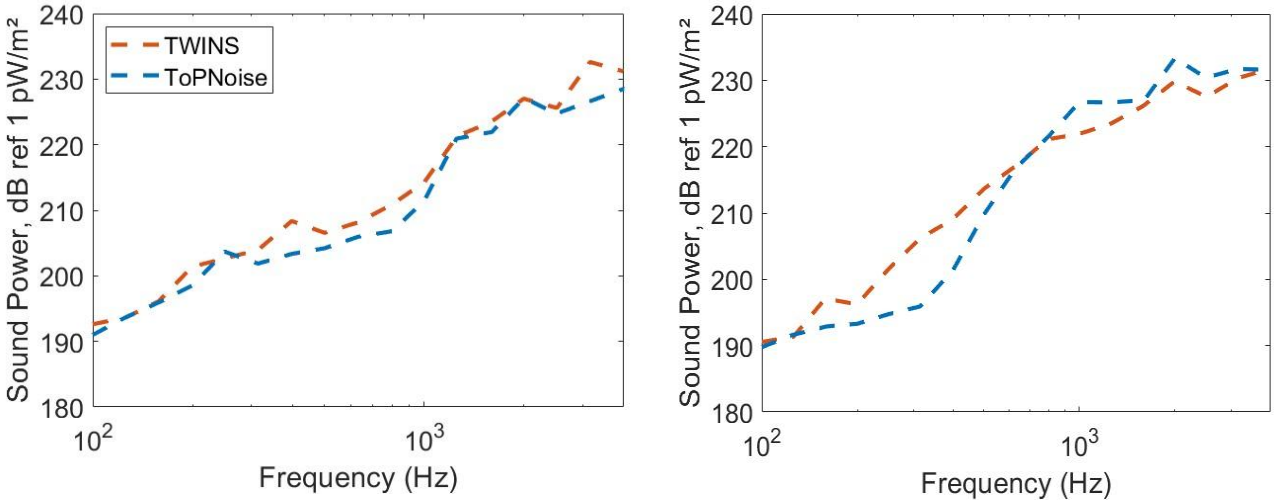

(a) Scenario 1

(b) Scenario 2

Figure B13. Sound power for unit roughness radiated by rail, wheel and sleepers (ToPNoise in blue and TWINS in orange).

Co-funded by the European Union

Appendix C. Calculation of ballast stresses

C1 Introduction

To study the variations in stress generated on the ballast, a finite element calculation model was used based on the TopNoise / open source Railtrack Modelling Toolbox [50]. A description of the model is provided in this report, detailing the type of modelling carried out, the behaviour of the materials and the type of mechanical load used. The objective of this study was to observe the evolution of stresses as a function of the type of rail pads, sleepers or rails used. The model takes into account the presence of Under Sleeper Pads (USP). A total of 170 simulations were carried out. The results of these simulations are presented in this appendix, and a summary is provided at the end of the document.

C2 Model description

C2.1 Geometry

The proposed approach relies on a hybrid numerical model. It combines three-dimensional solid elements in the central zone with discrete and beam elements at the extremities. The main objective of this modelling strategy is to efficiently capture the distribution of stresses in the ballast layer during the passage of a train, while keeping the computational cost reasonable.

High accuracy is required near the wheel-rail contact area, where stress gradients are the highest. For this reason, the region close to the contact point is modelled using 3D solid elements. Outside this area, the track structure is represented using discrete elements to maintain rigidity and load transfer effects at the boundaries of the 3D area without unnecessary refinement.

The considered portion of track is therefore represented as shown in Figure C1.

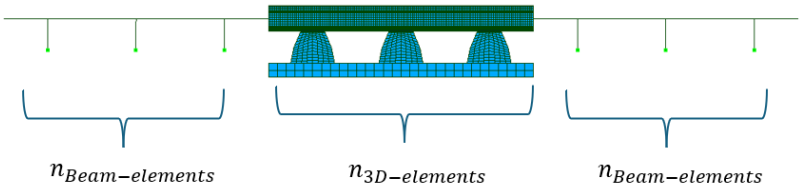

Figure C1. Illustration of the elements used in the mesh.

A preliminary sensitivity study was conducted to optimize the number of elements and reduce the overall size of the model. The results showed that most of the applied load is transmitted by a limited number of sleepers. Consequently, the model retains three sleepers modelled with full 3D solid elements in the central area. In addition, it was observed that six beam-type sleepers are sufficient to account for the effects of stiffness near the edges of the modelled domain.

To further simplify the numerical model and reduce computational time, symmetry conditions were applied, and only half of the track section was finally retained for the simulations, as indicated in Figure C2.

Co-funded by the European Union

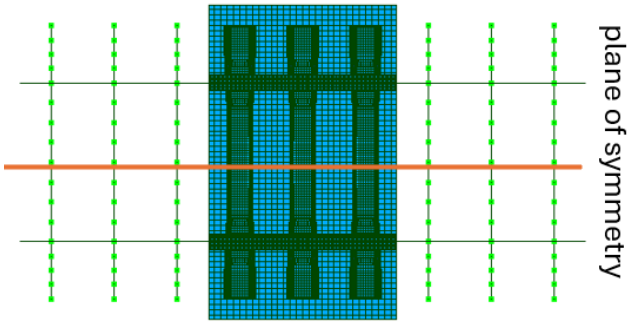

Figure C2. Plane of symmetry used for the model.

C2.2 Element description

The track model is divided into two parts. One part of the track is composed of 3D elements, while the other part is simplified, composed of discrete elements and Timoshenko beam elements. The railway track consists of a section of rail, ballast, sleepers and may include the USP. However, a different model is proposed for each part of the structure, as shown in Figure C3.

- In the 3D section, volume elements are used that are predominantly linear hexahedra.
- In the simplified part, the rails and sleepers are modelled using Timoshenko beams, while the pads, ballast and USPs are modelled using a mass-spring-damper system.

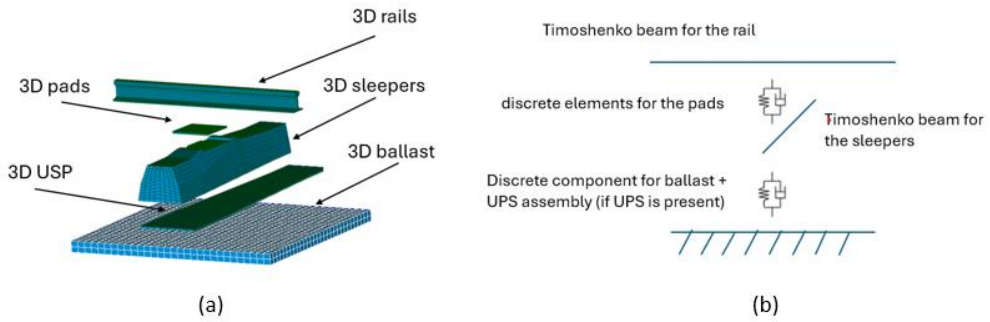

Figure C3. Parts of the models: (a) 3D parts, (b) simplified parts.

C3 Material properties

This paragraph describes all the material parameters used in this study. Most of these parameters have already been detailed in other sections.

C3.1 Mechanical behaviour

The material behaviour considered in the model depends on the type of elements used. Given that a large portion of the load is transmitted through only three sleepers, and since most of the pads exhibit significant relaxation effects, a detailed description of the material response is required in this zone. For this reason, a generalized Maxwell model is adopted to accurately capture the viscoelastic behaviour of the rail pads. However, it was observed that the excitation induced in the track by the passage of a train is mainly located in the low-frequency range. Consequently, only one Prony term is retained in the model. The excitation frequency generated by a moving train can be estimated as

$$f = \frac{v}{4L} \tag{C1}$$

Co-funded by the European Union

where *L* is the sleeper spacing and *v* the train speed (see Section C4.2).

Since the material behaviour of the pads is defined based on a generalised Maxwell behaviour with a single term, the Young's modulus is expressed as follows:

$$E^*(t) = E_0 + E_1 e^{-\frac{t}{\tau_1}} \tag{C2}$$

After conversion to the frequency domain:

$$E^*(\omega) = E_0 + \frac{E_1(i\omega\tau_1)}{1 + i\omega\tau_1} \tag{C3}$$

From this expression, it is possible to extract the imaginary and real parts:

$$\begin{cases} E'(\omega) = E_0 + \dfrac{E_1(\omega\tau_1)^2}{1 + (\omega\tau_1)^2} \\ E''(\omega) = \dfrac{E_1(\omega\tau_1)}{1 + (\omega\tau_1)^2} \end{cases} \tag{C4}$$

Using this system, E_0 can be estimated using the static stiffness, and E_1 and τ_1 can be estimated using low-frequency stiffness and loss factor values. Outside the 3D zone, the properties of the pads are determined with discrete elements using low-frequency material properties, and the damping is modelled as Rayleigh-type.

In addition to the pads, the other material properties are assumed to be isotropic elastic or orthotropic elastic with Rayleigh-type damping. In the case of Rayleigh damping, the damping matrix is assumed to be proportional to both the mass matrix and the stiffness matrix. In the following, the coefficients α and β will denote the proportionality factors associated with the mass and stiffness contributions, respectively.

Table C1 provides a summary of all properties in the model based on the type of element used.

Table C1. Material behaviour used.

	3D elements	Beams and discrete elements
Rail	Elastic properties	Elastic properties
Pads	Viscoelastic properties. Generalised Maxwell model defined in a Prony series	Equivalent stiffness at low frequency and Rayleigh damping
Sleepers	Orthotropic elastic and Rayleigh damping	Orthotropic elastic and Rayleigh damping
Ballast	Elastic and Rayleigh damping	Equivalent stiffness at low frequency and Rayleigh damping
USP	Elastic and Rayleigh damping	Equivalent stiffness at low frequency and Rayleigh damping

C3.2 Values used for simulations

The material parameters used to calculate stresses in the ballast are summarized in this section.

Co-funded by the European Union

C3.2.1 Rail

Two types of rails were considered in our study. These are the 60E2 and 54E2 rails. Their material properties are summarized in Table C2.

Table C2. Rail parameters.

Rail Type		60E2	54E2
Masse density (kg/m³)		7850	7850
Poisson's ratio (-)		0.3	0.3
Damping loss factor	tan(delta)	0.02	0.02
	Rayleigh Coeff α, β	17.42, 8.24e-6	17.42, 8.24e-6

C3.2.2 Rail pads

Based on the material properties previously defined in the context of acoustic and vibration calculations, Table C3 shows how these parameters are used to assess the stresses exerted on the ballast. For the ballast stress calculations, the low frequency stiffness (under load) of the rail pad is to be considered. As with the acoustic calculation, five pads were considered and listed according to their rigidity.

Table C3. Rail pads.

Rail pad type		Very soft	Soft	Medium	Stiff	Very stiff
Static stiffness (MN/m)		50	100	150	250	700
Low-frequency stiffness (MN/m)		60	120	200	350	1000
Vertical static Young's Modulus, E_0 (MPa)		14.40	28.81	43.21	72.02	201.65
First Young's Modulus term, E_1 (MPa)		5.21	10.428	19.59	36.75	108.03
First characteristic time term, τ_1 (s)		0.0059	0.0059	0.0088	0.0101	0.0106
Damping loss factor	tan(delta)	0.15	0.15	0.15	0.15	0.15
	Rayleigh Coeff α, β	130.65, 6.18e-05	130.65, 6.18e-05	130.65, 6.18e-05	130.65, 6.18e-05	130.65, 6.18e-05

C3.2.3 Sleepers

Five sleeper configurations were initially examined for the stress analysis. To keep the number of case studies limited, the investigation was narrowed down to a single concrete sleeper. The final selection therefore includes one concrete, one wooden, and three composite sleepers. Steel sleepers were not considered because of the difficulties involved in representing accurately the ballast-sleeper interaction in the numerical model. Table C4 summarises the parameters of the sleepers used for the simulation.

Co-funded by the European Union

Table C4. Sleeper parameters.

Sleeper type		Concrete (B91)	Wood	Composite 1 (Sicut, recycled plastic)	Composite 2 (KLP, steel-reinforced polymer)	Composite 3 (Fibre-reinforced foamed urethane)
Mass density (kg/m^3)		2436	800	825	1004	747
Total mass (kg)		280	38.89	65.4	95.8	76.8
Length (m)		2.6	2.5	2.6	2.6	2.5
Young's modulus (longitudinal) (GPa)		46.3	15.0	2.6	7.7	11.2
Young's modulus (transverse) (GPa)		20.0	7.0	n/a	n/a	n/a
Total support surface (m^2)		0.68	0.65	0.66	0.65	0.64
Poisson's ratio (-)		0.2	0.2	0.3	0.35	0.4
Sleeper spacing (m)		0.6	0.6	0.6	0.6	0.6
Damping loss factor	tan(delta)	0.016	0.04	0.038	0.064	0.029
	Rayleigh Coeff α, β	13.94, 6.59e-06	34.84, 1.65e-05	33.10, 1.57e-05	55.75, 2.64e-05	25.26, 1.19e-05

For concrete, wood, and composite sleepers, under-sleeper pads (USPs) may be included as an option. The properties of three examples are listed in Table C5.

Table C5. USP parameters.

USP type		Soft	Medium	Stiff
Type		SLN220G	SLB2210G	Used on SBB
Thickness		20 mm	10 mm	8.5 mm
Vertical low-frequency stiffness (MN/m)		14	150	420
Young modulus (MPa)		4.42	2.21	5.26
Damping loss factor	tan(delta) (-)	0.1	0.2	0.25
	Rayleigh Coeff α, β	87.103, 4.12e-5	174.21, 8.24e-5	217.76, 1.03e-4

C3.2.4 Ballast

The ballast properties adopted in this study are summarized in Table C6. A single ballast type and one nominal layer thickness are considered. The parameters used for the stress analysis are the same as those employed in the acoustic calculations.

Co-funded by the European Union

Table C6. Ballast parameters used for calculating stresses on the ballast.

Thickness beneath sleeper (m)		0.3
Young's modulus (MPa)		141.34
Ballast density (kg/m³)		1933
Damping loss factor	tan(delta)	0.1
	Rayleigh Coeff α, β	87.103, 4.12e-5

C4 Mechanical load

This section provides a brief description of the type of load used to assess the passage of the train over the rails. It also indicates the type of vehicle associated with the load.

C4.1 Vehicle parameters

The proposed study was carried out using a single type of train. The parameters of the train used are summarised in Table C7. This data is reused in the various simulations proposed.

Table C7. Train parameters.

	Passenger (unpowered)
Car body	
Mass (kg)	32,000
Overall vehicle length (m)	25.0
Bogie	
Mass (kg)	2,500
Distance between bogie centres (m)	17.0
Wheelset	
Mass (kg)	1,200
Total axle load (kN)	108
Distance between axles (m)	2.5

C4.2 Load description

During the passage of a train, the rail bends and the applied load is distributed over a characteristic length l. As modelling moving loads is too time consuming for a large-scale parametric study with detailed 3D description of track components, it was chosen to model the loading as a fixed load applied on top of the rail, aligned with the sleeper, as in a simulated laboratory test.

To take the velocity into account and loading profile during pass by, a simplified time varying force model is implemented as follows:

$$F(t) = F \sum_{i=1}^{n} \varphi(v(t - t_i)) \qquad \text{(C5)}$$

where:

- $\varphi(x)$ is an influence function centred at $x = 0$ and defined over a characteristic length l,
- F is the load per wheel (total axle load divided by 2),

Co-funded by the European Union

- n is the number of axles,
- v is the train speed, set to 100 km/h,
- t_i denotes the time at which the i-th axle reaches the considered position

The influence function φ is chosen as a half-sinusoidal shape and is defined as:

$$\varphi(x) = \begin{cases} \sin\left(\frac{\pi x}{l}\right) & if \quad 0 < x \leq l \\ 0 & otherwise \end{cases} \tag{C6}$$

For an axle load of 108 kN, most of the load is distributed over three sleepers. Consequently, the characteristic length is taken as twice the sleeper spacing, leading to a value of l = 2L = 1.2m.

Since the spacing between two consecutive axles is approximately 2.5 m, which is significantly larger than the characteristic length l, the interaction between axle loads is assumed to be negligible. The loading function can therefore be reduced to a single term for simplification purpose. With the axle position expressed as a function of time, $x = vt$, equations (C5) and (C6) yield the time domain loading function:

$$F(t) = \begin{cases} F\ \sin\left(\frac{\pi v t}{2\,L}\right) & if \quad 0 < t \leq 2L/v \\ 0 & otherwise \end{cases} \tag{C7}$$

where *L* denotes the sleeper spacing. The shape of the half-sinusoidal load is illustrated in Figure C4.

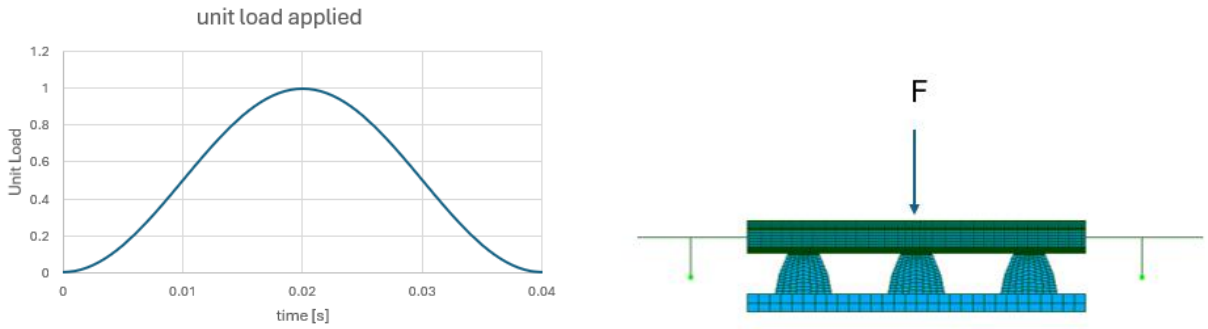

(a) (b)

Figure C4. Time history (a) and position (b) of the mechanical load.

C4.3 Numerical simulation

The finite element models are built automatically in the open-source Salome-Meca / Code-Aster platform by combining predefined finite element meshes using a set of Python scripts. The finite element computations are carried out using Code-Aster's non-linear dynamics solver with Newton-Raphson / MUMPS parallel solver and a custom MFront material subroutine for the generalized Maxwell constitutive law. An adaptive time stepping strategy is used with a characteristic time step of 0.5 ms for a total duration of 40 ms.

C5 Results

C5.1 Indicators used to compare the stress field in the ballast

Following the simulations, it was observed that the stress fields on the ballast varied significantly depending on the simulation case. Three types of indicators were established in order to compare the stresses in the ballast obtained from the different simulations. These indicators are as follows (see Figure C5):

Co-funded by the European Union

- The maximum compressive stress observed on the ballast throughout the simulation. In parallel with this maximum stress, we also extract the time at which the maximum value is reached. It is also possible that stress concentrations may occur in the ballast at the edge of the sleepers due to idealized bonded contact and 3D continuum modelling hypotheses. These stress concentrations can make it difficult to compare the results. This is why two other criteria are considered as well.
- The average vertical compressive stress over the rails centre line. This criterion is much less sensitive to stress concentrations and makes it easier to compare different fields.
- The compressive stress observed at the centre of the area described above. This point is also aligned with the applied load.

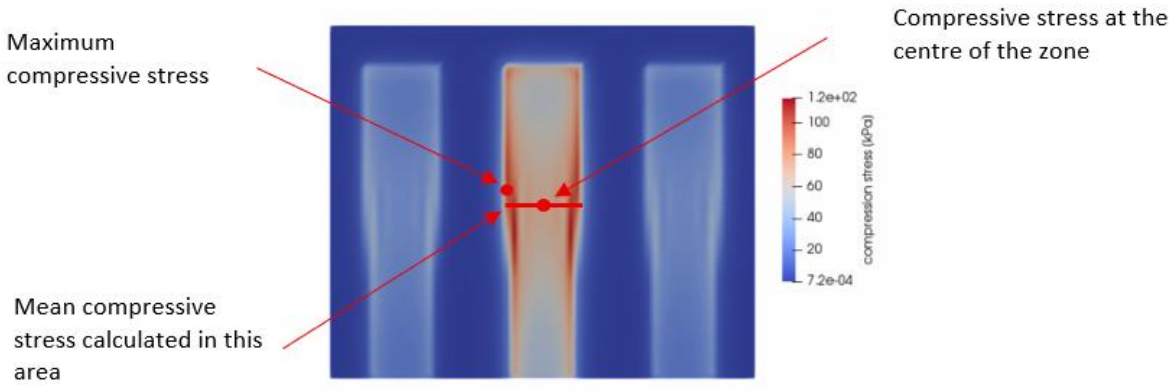

Figure C5. Description of indicators.

C5.2 Influence of rail pads, USP and rail type on results

By observing the indicators defined above and the stress field in the various simulations, an initial difference can be seen in the results when changing the type of rail, see Figure C6 and Figure C7. The stress field in the ballast appears to be greater when using 54E2 rails. Furthermore, the results also show that using more flexible rail pads and USPs also leads to a better stress state in the ballast.

Co-funded by the European Union

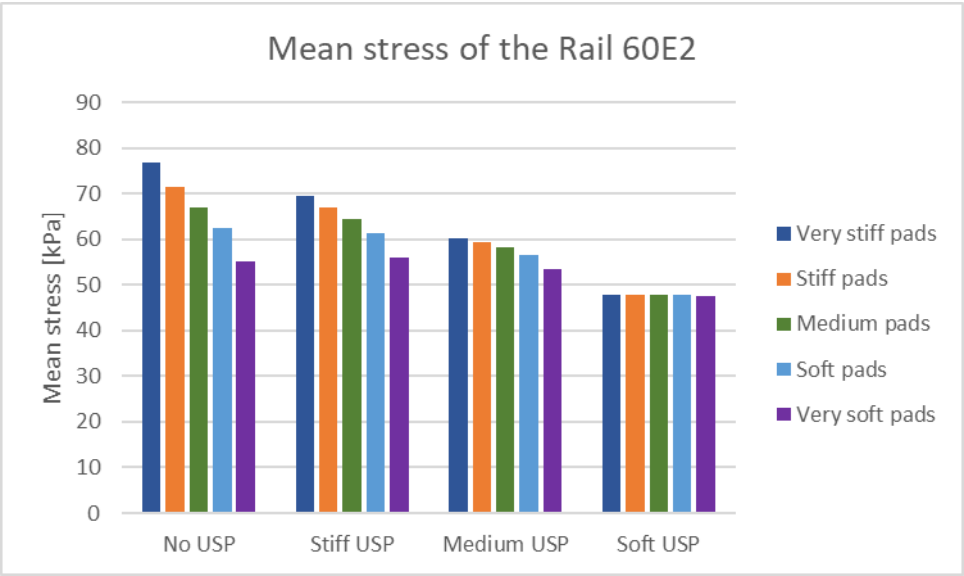

Figure C6. Mean stress evolution for 60E2 rails with concrete sleepers.

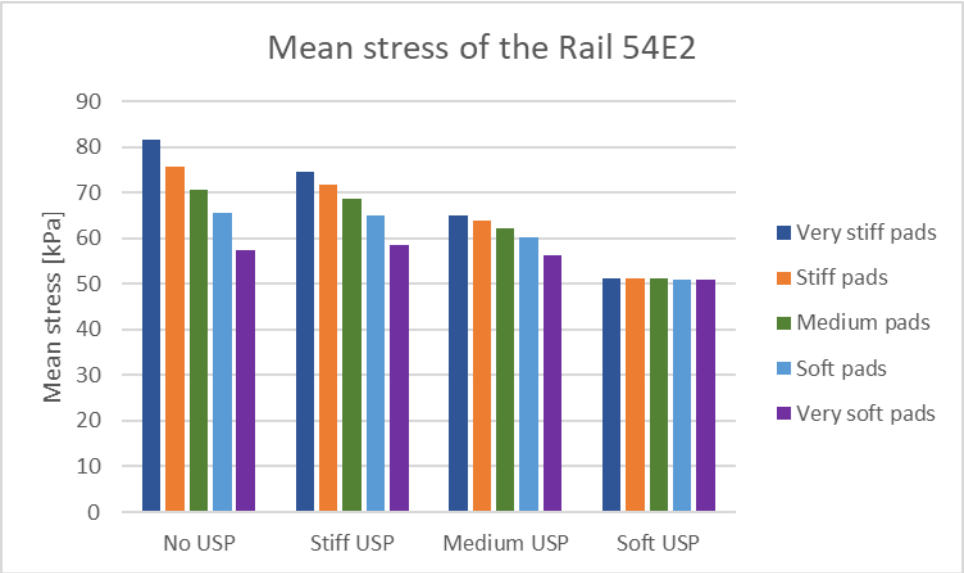

Figure C7. Mean stress evolution for 54E2 rails with concrete sleepers.

Looking at Figure C6 and Figure C7, the ballast stresses with softer rail pads and USPs are significantly reduced compared to stiffer rail pads and hard USP (or no USP). Indeed, as the overall rail support stiffness decreases, the stress is more uniformly distributed among sleepers (but rails are more solicited in bending as they carry away the load in the redistribution paths). In these examples, limit values of approximately 47 and 50 kPa of average compressive stress are obtained for the 60E2 and 54E2 rails. On the other hand, it was also observed that taking USPs into account allowed for a more homogeneous distribution of stresses in the ballast under the sleepers.

Co-funded by the European Union

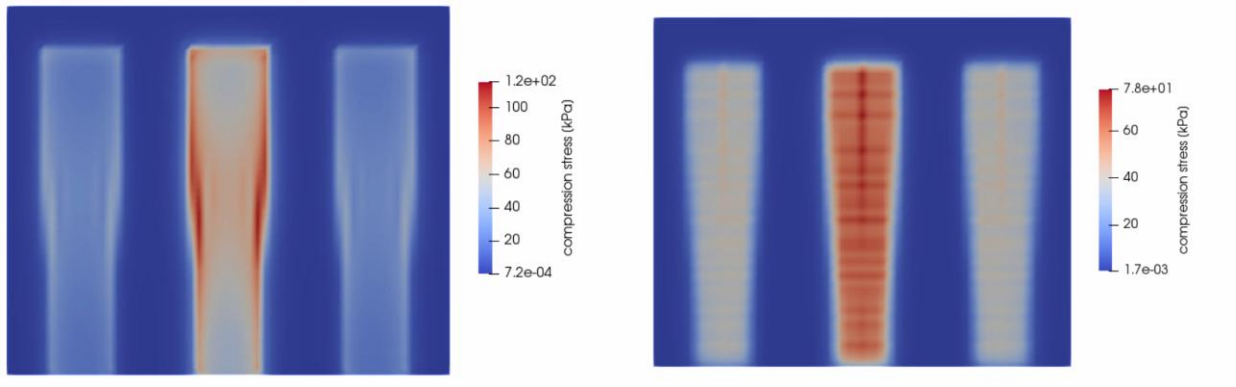

Figure C8. Variation in compression stress fields in ballast for concrete sleepers with (b) or without (a) stiff USP.

Indeed, as can be seen in Figure C8, the stress field appears to be less concentrated at the edges (on the sleeper's footprint) after implementation of the USPs. This observation is also visible in the data when comparing maximum stresses and average stresses.

C5.3 Influence of sleepers on results

Finally, different types of sleepers also affect how the stresses are redistributed in the ballast. The results in Figure C9 show that composite sleepers tend to transfer significantly more stress in the ballast than wooden and concrete sleepers. These composite sleepers have been modelled assuming isotropic material properties corresponding to their reported longitudinal modulus. However, those sleepers exhibit a relatively low Young's modulus of about 2 GPa to 11 GPa, which, when combined with their relatively small beam section, leads to a low bending stiffness.

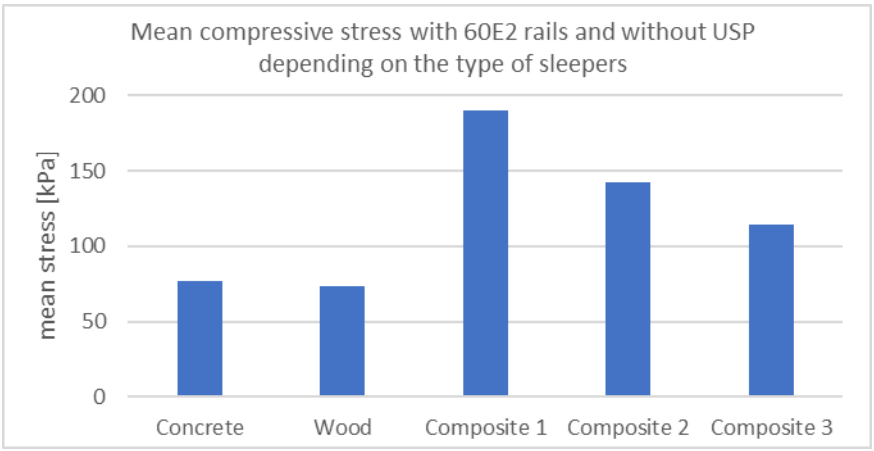

Figure C9. Mean compressive stress depending on the type of sleepers.

Due to this low bending stiffness, stresses are not redistributed as efficiently along the length of the sleeper and stress concentrations on a small section below the rail occur. As shown in Figure C10, the ballast stress distribution along the sleepers is completely different for concrete B91 sleepers (high bending stiffness) and composite 1 sleeper (low bending stiffness).

Co-funded by the European Union

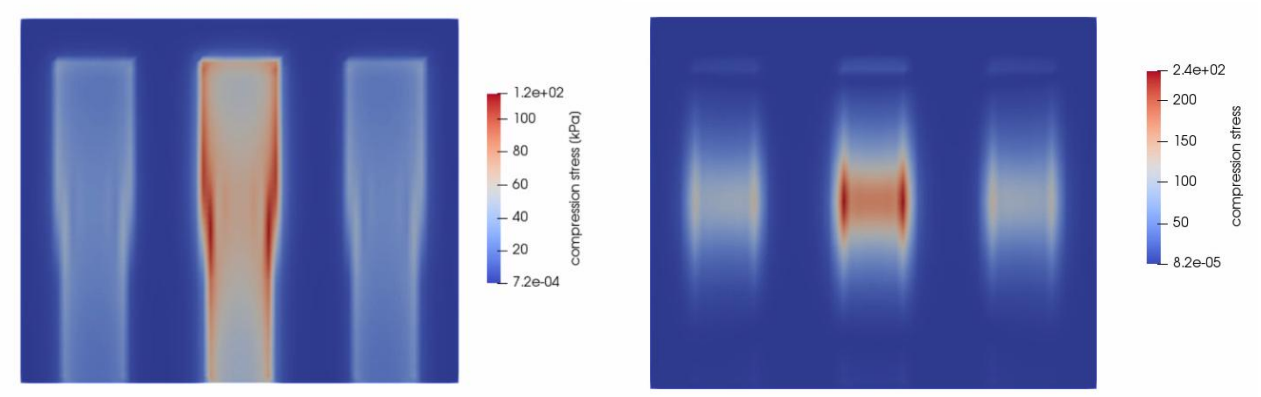

Figure C10. Comparison of stress fields on ballast obtained with concrete and composite 1 sleepers. Both cases are without USP with stiff rail pads.

C5.4 Effect of ballast stress on track settlement and degradation rate

The ballast stresses calculated in this work can be used to derive a comparative, first order approximation of the track deterioration due to ballast settlement and degradation.

Several track settlement models have been proposed in literature to predict the progressive settlement of the track in the ballast bed over time (e.g. [52] for a detailed overview). Each model has been developed and adapted on actual track measurements for specific types of track construction and traffic and environmental conditions. Due to the complexity of the mechanisms at play, there is no generally accepted track degradation model and associated parameter set that can cover the full range of actual conditions, track construction methods and types of ballast and soil.

However, most of the track settlement models consider that the track settlement depends non-linearly on the number of loading cycles and ballast loading.

The model of Sato [53] considers a first rapid evolution of the settlement modelled as an exponential decay term combined with a slower, long term, linear settlement (constant settlement rate for high number of cycles) as:

$$s(N) = \gamma\left(1 - e^{-\alpha N}\right) + \beta N \qquad \text{(C8)}$$

where s denotes the track settlement (typically in mm) and N the number of loading cycles, α, β, γ are constants of the model depending on train speed, axle load, ballast type etc. For normal operation and estimation of long-term track degradation, the second term βN is dominant, thus the value of β represents a constant long term settlement rate. Sato notes that β depends on track construction, subgrade and ballast type but also on train speed and loading. However, this model does not account explicitly for the loading amplitude (axle load or peak ballast contact pressure).

In another work, Sato [54] proposed that the track settlement rate r (expressed as mm / cycle) is linked directly to the sleeper-ballast pressure p. Two power law forms for the settlement rate r are proposed, one with a threshold value and the other without:

$$r = \frac{ds}{dN} = a\,(p - b)^2 \quad for\ p > b \qquad \text{(C9)}$$

$$r = \frac{ds}{dN} = a\,p^n \qquad \text{(C10)}$$

Based on the analysis in [52], the exponent n of equation (C10) can reach values in the order of 4 or above, showing thus a very strong dependence of track settlement rate on the ballast loading (or contact pressure).

Other models based on German data proposed a settlement rate law [55] which shows much lower dependency on the ballast load, with an exponent of only 1.21. This may be explained by the higher overall

Co-funded by the European Union

ballast and soil quality (crushed rocks + sand) or different track construction technique compared to the study in Japan.

$$r = \frac{ds}{dN} = c_1 + c_2\, p + c_3\, p^{1.21}\, \ln N \tag{C11}$$

Guérin [56] proposed the following settlement rate model for the ballast as a power law of the maximum elastic track deflection *d* over one loading cycle. Track deflection typically has a non-linear dependency on applied force due to the soil and ballast compaction mechanisms. However, for moderate variation of the applied load *P*, it might be reasonable to assume an approximately linear response of the track deflection versus load with an equivalent stiffness *k*. In this case, Guérin's model can also be converted to an equivalent load (or pressure) dependent power law as shown below:

$$r = \frac{ds}{dN} = c_1\, d^{\,n} \;\; = c_1 \left(\frac{P}{k}\right)^n = c_2\, P^{\,n} \tag{C12}$$

Guérin identified an exponent $n = 2.51$, which sits in the middle of the values found in German and Japanese studies.

Finally, the ORE (Office for Research and Experiments of the International Union of Railways, UIC) has proposed the following model to estimate track deterioration [57]:

$$s = s_0 + hT^{\alpha} P^n v^{\gamma} \tag{C13}$$

where s_0 is the initial settlement after tamping, *T* is the traffic volume, *P* the axle load and *v* the speed. The proposed values of the exponents for traffic volume (cumulative tonnage) are $\alpha = 1$ and for axle load (hence ballast loading), $n = 3$. With these values, this degradation model closely resembles the power law settlement model proposed by Sato.

Based on this short review, the long-term ballast settlement rate *r* can be generally approximated as a power law of the applied load, or even better, of the peak ballast compressive stress *p* as follows:

$$r = \frac{ds}{dN} \cong c\, p^{\,n} \implies s \;\cong r\, N = c\, p^n\, N \tag{C14}$$

To compare the effect of different track constructions, for example by changing track components, it is reasonable to consider that, in a first order approximation, the track maintenance would occur at a similar track settlement level s_{max} (similar geometric degradation of the track). With this assumption, the maintenance interval is inversely proportional to the track settlement rate *r*, i.e. a track construction leading to a faster ballast settlement will require earlier maintenance due to geometry degradation, for example.

Considering a known track maintenance interval for a track construction A (given by number of loading cycles N_a), and assuming a known power law dependency of the settlement rate on ballast contact stress (power exponent *n*), it is possible to estimate roughly the maintenance interval of another track construction B based on the ratio of ballast pressure p_a/p_b for the two respective conditions:

$$s_{max} = c\, p_a^n\, N_a = c\, p_b^n N_b \implies \frac{N_b}{N_a} = \left(\frac{p_a}{p_b}\right)^n \tag{C15}$$

As an example, if track configuration B shows a reduction of 10% in ballast pressure compared to configuration A, $p_a/p_b \cong 1.1$, and assuming a power exponent of $n = 3$, we can estimate that the maintenance interval would increase approximately by a factor $N_b/N_a = 1.1^3 = 1.33$. Thus, a reduction of ballast pressure of 10% would lead to an approximate increase of 33% of the maintenance interval. The reported power exponents for track settlement rate found in this review range from 1.21 [55] to 4 and above [52], with a middle ground value of 2.5 to 3.

This simplified approach is based on many assumptions and obviously requires experimental validation based on real observations as there are many different causes for track deterioration and thus reducing this phenomenon to just track settlement is inherently limited.

Co-funded by the European Union

Nevertheless, this simple method, combined with the calculated ballast stress results of this study, can help in the selection of optimal components considering both the impact of noise and vibration, but also the potential economic aspects by providing first order estimates of relative maintenance intervals for life cycle analysis.

C6 Conclusion

The results of this study indicate that the ballast pressure strongly depends on the track construction and component selection. Overall, using sleepers with high bending stiffness, large contact surface combined with soft rail pads and / or soft USP significantly reduces the ballast loading by providing a better stress redistribution between (and along) the sleepers.

The use of softer rail pads and USP systems leads to a reduction in compressive stresses within the ballast. However, the differences between configurations tend to decrease as the overall track structure becomes more flexible. As expected, tracks with USP promote a more uniform load distribution in the ballast and help limit local stress concentrations.

In the case of concrete B91 sleepers / 60E2 rail, the change from very hard rail pads to very soft pads correspond to a potential reduction of 27% of ballast pressure without under sleeper pads. The effect of under sleeper pads is also very significant, i.e. leading to a reduction of 37% of peak ballast stress for B91 / 60E2 case with very hard rail pads. Regarding rail configurations, stiffer 60E2 rails appear to generate lower stress levels in the ballast than 54E2 rails due to a better redistribution effect.

Finally, with the properties of the composite sleepers considered in this study, the simulations show that their overall bending stiffness is generally too low to redistribute the contact pressure efficiently along the length of the sleeper, leading to a stress concentration directly below the rail.

A database of 170 simulated cases, with different stress indicators, has been generated. Combined with the track degradation estimation method described in Section C5.4, these data can be used to calculate a first order estimate of the relative maintenance intervals for different track component selections.

Europe's Rail
Co-funded by the European Union